DEPARTMENT OF THE AIR FORCE

AIR UNIVERSITY

AIR FORCE INSTITUTE OF TECHNOLOGY

Wright-Patterson Air Force Base, Ohio

AFIT/GE/ENG/90D-55

CHARACTERIZATION OF AN AIR-TO-AIR OPTICAL HETERODYNE COMMUNICATION SYSTEM

THESIS

Rebecca N. Seeger
Captain, USAF

AFIT/GE/ENG/90D-55

AFIT/GE/ENG/90D-55

CHARACTERIZATION OF AN AIR-TO-AIR OPTICAL HETERODYNE COMMUNICATION SYSTEM

THESIS

Presented to the Faculty of the School of Engineering
of the Air Force Institute of Technology
Air University
In Partial Fulfillment of the
Requirements for the Degree of
Master of Science in Electrical Engineering

Rebecca N. Seeger, B.S., B.S.E.E.
Captain, USAF

December, 1990

Preface

Throughout the process of developing the theoretical model and evaluating the results of this effort, I received both help and support from many sources. First, I'd like to thank my advisor, Capt Byron Welsh, for his continued support and guidance throughout my research. In addition, I would like to express my gratitude to Lt Col David Norman and Maj Steven Rogers (who both expects and demands only the best) for providing me the educational tools in optical communication necessary to tackle this topic.

Finally, I'd like to thank my classmates, especially Scott, Vance and Joe, for their continuing encouragement and support. Thanks guys.

Rebecca N. Seeger

Table of Contents

List of Figures

List of Tables

List of Symbols

Symbol

α	- Signal-to-noise ratio efficiency factor
η	- Quantum efficiency of the receiver photodetector
$\frac{\eta}{e}$	- Quantum efficiency in electrons per unit energy
κ	- Wave number (with respect to eddy size) (m^{-1})
λ	- Wavelength (m)
ρ_o	- Transverse separation for which the spherical wave coherence is reduced by e^{-1} (m)
Σ	- Infinite surface upon which a wave is incident
$\Phi_n(\kappa)$	- Power spectral density of the refractive index fluctuations (m^3)
$\chi(\theta)$	- Obliquity factor
$\psi(\underline{r},\underline{p})$	- Nonlinear phase perturbations on the spherical wave due to propagation through an inhomogeneous medium
θ	- Angle between the normal to Σ and the line joining $\underline{r}$ and $\underline{p}$ (rad)
AM	- Amplitude modulation
A_R	- Amplitude of the local oscillator signal (W)
AWGN	- Additive white Gaussian noise
BER	- Bit error rate
bps	- Bits per second
BPSK	- Binary phase shift keying
C_n^2	- Structure constant of the refractive index fluctuations $(m^{-2/3})$
cw	- Continuous wave
dB	- Decibels
D	- Aperture dimension (m)
D	- Wave structure function
D_n	- Refractive index fluctuations structure function

Symbol

D_χ	- Log-amplitude structure function
D_s	- Phase structure function
$\underline{\varepsilon}$	- Unit vector (m)
E_{min}	- Minimum pulse energy (J)
erfc	- Complementary error function
$F(\underline{p})$	- Transmitter aperture field
g	- Gain of the current amplifier (dB)
$G(\underline{r},\underline{p})$	- Green's function
h	- Aircraft altitude (m)
$H(\underline{p},\underline{r},z)$	- Two point correlation function
IF	- Intermediate frequency
J_o	- Bessel function of the first kind
k	- Optical wave number (equal to $2\pi/\lambda$) (m^{-1})
L	- Eddy size (m)
MCF	- Mutual coherence function
n_1	- Deviation of the refractive index fluctuations from the free-space value
N	- Noise power (W)
$\underline{p}$	- Point in the observation plane
P_t	- Transmitter laser power (W)
PDF	- Probability density function
PSD	- Power spectral density
$Q(y)$	- Complementary error function
r_o	- Efficiency saturation dimension (m)
$\underline{r}$	- Point in the aperture (source) plane
R	- Resistance of the load $(ohms)$
S	- Signal power (W)
SNR	- Signal-to-noise ratio
u	- Optical wave

Symbol

$U_A(\underline{r})$	- Receiver aperture weighting
U_o	- Field at the center of the transmitting aperture
V	- Aircraft (relative wind) velocity (m/s)
W_A	- Normalization factor which represents the intensity of the transmitter field integrated over the transmitting aperture (power density) $(W \cdot m^2)$
$W(y)$	- Uniform weighting function
WRDC	- Wright Research and Development Center
Δx	- Difference variable
Σx	- Sum variable
y	- Argument of an arbitrary function
z	- Propagation path length (m)
z_c	- Mean field-decay length (m)
$< \cdot >$	- Ensemble average

AFIT/GE/ENG/90D-55

Abstract

The primary goal of this research was to determine the feasibility of air-to-air optical communication systems using coherent detection in a turbulent environment. Secondary goals were to determine (1) the signal-to-noise ratio (SNR) degradation due to turbulence and (2) the effect of varying the wavelength (1.5, 830, 904 nm), altitude (5000-12500 m), path length (40-160 km) and aperture side length (1-15 cm) on the turbulence affected SNR.

The research was conducted under the following assumptions: (1) ideal transmitter and receiver, (2) equally sized, uniformly weighted, square transmitter and receiver apertures, (3) ideal tracking by the receiver, and (4) zero losses due to beam steering, beam spreading and scintillation.

It was shown that the SNR efficiency (defined as the ratio of the turbulence affected SNR to the non-turbulence affected SNR) ranged from 0.16 to 67.2 percent. The 67.2 percent efficiency was achieved for a wavelength of 904 nm, path length of 40 km, altitude of 5000 m and aperture side length of 1 cm.

The feasibility analysis showed that, depending on the transmitter power and data rate, path lengths in excess of 160 km could be achieved for bit error rates of both 10^{-5} and 10^{-10}.

CHARACTERIZATION OF AN AIR-TO-AIR OPTICAL HETERODYNE COMMUNICATION SYSTEM

I. Introduction

1.1 Background

In air-to-air applications, optical communication systems have shown promise as a means of covert communications with high data rate capability. Experiments, such as HAVE LACE (Laser Airborne Communications Experiment) conducted by the United States Air Force, have shown that air-to-air optical communication systems employing incoherent (direct) detection are feasible with acceptable signal-to-noise ratio (SNR), and thus probability of error, performance. However, the SNR achievable in incoherent detection systems is quantum limited; that is, there is a "... minimum pulse energy E_{min} required to maintain a given bit error rate (BER) which any practical receiver must satisfy ..." (33:356).

Coherent (heterodyne) detection systems, on the other hand, offer a significant improvement in SNR performance on the order of 10-20 decibels (dB) (25, 26, 32). Greater SNR performance, in turn, leads to higher data rate capability and better probability of error (or BER) performance.

Both incoherent and coherent detection systems, however, are adversely affected by the effects of atmospheric turbulence on the propagating optical wave. The resulting amplitude fluctuations of the optical wave due to turbulence affect both incoherent and coherent detection. The effect is reduced power (or SNR) at the receiving aperture. In addition, coherent detection is further affected by the

optical wave's phase fluctuations due to turbulence. In coherent detection, a locally generated wave (local oscillator) is combined with the received wave. The portions of the received wave that are out of phase, due to phase fluctuations, with the detector's local oscillator will combine destructively resulting in an even further reduction in the received SNR.

The Communications Technology Branch of the Wright Research and Development Center (WRDC), Wright-Patterson AFB, OH is presently sponsoring research to determine the effects of atmospheric turbulence on optical communication systems employing coherent detection systems.

1.2 Problem

The basic problem facing WRDC is to determine the feasibility of air-to-air optical communication systems using coherent detection in a turbulent environment. This study will characterize the performance of an optical heterodyne communication link between aircraft in the presence of atmospheric turbulence. If optical heterodyne communication systems prove to be feasible in air-to-air applications, these systems will provide a means of covert communications with higher data rate capability than conventional radio frequency and microwave communication systems currently employed in aircraft, as well as incoherent optical communication systems.

1.3 Definitions

Before the scope and assumptions of this study can be presented, several terms and concepts must be defined.

Power spectral density of turbulence ($\Phi_n(\kappa)$): The power spectral density (PSD) of turbulence is a measure of the number of eddies of different sizes making up the turbulence (18:388). The PSD is designated as $\Phi_n(\kappa)$ where κ is the wave number ($\kappa = 2\pi/L$ where L is the eddy size). Eddies are packets of air in which the refractive index of each of the packets varies with respect

to the average index of refraction (10, 18). The spectrum, $\Phi_n(\kappa)$, consists of three regions determined by the inner and outer scales of the turbulence which are directly related to the eddy sizes. In the region consisting of eddy sizes greater than the outer scale, $\Phi_n(\kappa)$ may be described by either the von Kármán spectrum or the Kolmogorov spectrum. In the region consisting of eddy sizes between the inner and outer scales, $\Phi_n(\kappa)$ is described by the inertial subrange of the Kolmogorov spectrum. Finally, in the region consisting of eddy sizes less than the inner scale, $\Phi_n(\kappa)$ is again described by the Kolmogorov spectrum. Chapter II contains a complete discussion of $\Phi_n(\kappa)$ as well as an illustration of the regions (Figure 2) (18:388-389).

Receiver fundamental limits: Receiving optical systems are fundamentally limited in performance capability due to the basic laws of nature (that is, quantum mechanics) (30:262-263).

Isotropic and homogeneous turbulence: When the refractive index fluctuations of the turbulence have a spherically symmetric autocorrelation function, the turbulence is statistically isotropic. Similarly, when the refractive index fluctuations are stationary from a three-dimensional spatial standpoint, the turbulence is statistically homogeneous (18:386).

Frozen atmosphere: Under the assumption of a frozen atmosphere (or frozen turbulence), the atmospheric refractive index fluctuations do not vary with time, but rather drift across the channel with constant velocity due to wind (18:386).

Refractive index fluctuations structure constant (C_n^2): The refractive index fluctuations structure constant, C_n^2 ($m^{-2/3}$), is a measure of the strength of the fluctuations and depends on both the atmospheric conditions and the altitude of the turbulence.

Mutual Coherence Function (MCF): The MCF describes the loss of coherence of a coherently transmitted wave (29:482). Of special interest to this research effort is the loss of coherence caused by propagation through turbulence.

Cross-Correlation Function ($H(\underline{p},\underline{r},z)$): $H(\underline{p},\underline{r},z)$ is the two point correlation function. For finite optical beam propagation, all of the propagation properties needed to determine the MCF are contained in $H(\underline{p},\underline{r},z)$ (28:2154). The terms $\underline{p}$ and $\underline{r}$ represent points in the transmitter and receiver planes, respectively; while z represents the distance between the two planes.

1.4 Scope

This study investigates the feasibility of an air-to-air optical heterodyne communication link from a probability of error, or BER, performance standpoint. The communication system parameters to be varied are transmitter/receiver aperture sizes, aircraft separation, aircraft altitudes and data rate.

The turbulence is modeled based on Gaussian cross-correlation statistics for the turbulence induced phase fluctuations. The turbulence strength, C_n^2, described in Chapter II, is modeled using the Hufnagel model (23:6-14).

This study only considers the turbulence losses due to phase fluctuations resulting from propagation through turbulence. Losses due to beam spreading, beam steering and scintillation are not addressed. This study also does not consider aircraft skin turbulence caused by aircraft motion.

1.5 Standards

For this research effort, a BER of 10^{-5} is considered acceptable for feasibility. This value is commensurate with similar research and experimental efforts. For example, HAVE LACE required a BER of 10^{-6} at 160 km (22:6), while Kanavos required a BER of 10^{-5} during a study of air-to-air direct detection optical communciation systems (24:58,63).

1.6 Assumptions

This study is conducted with the following assumptions:

1. An ideal transmitter and receiver.
2. Equal transmitter and receiver dimensions.
3. Ideal tracking by the receiver.
4. Locally isotropic and locally homogeneous turbulence. Note that, according to Davis, turbulence consisting of eddy sizes between the inner and outer scales of turbulence is both isotropic and homogeneous (9:140). However, as discussed by Goodman, turbulence consisting of eddy sizes greater than the outer scale is both nonisotropic and nonhomogeneous, but the refractive index fluctuations may still possess an isotropic and homogeneous structure function (18:391).
5. "Frozen" atmospheric turbulence. This assumption, also known as Taylor's hypothesis, follows from the fact that the "fluctuation time" of the turbulence is much longer than the time required for the optical wave to propagate through the atmospheric communication channel (18:386).
6. A Gaussian probability density function (PDF) is used to characterize the statistics of the phase fluctuations resulting from the optical wave propagating through the atmospheric turbulence. This characterization is discussed further in Chapter II.
7. Square transmitter and receiver apertures. The SNR equation, developed in Chapter III, can be reduced to a four-fold integral using circular apertures, and 2 two-fold integrals using square apertures. Due to the limited processing capability of even today's computers, current numerical integration methods perform best on only three-fold or less integrals, thus discouraging their use for the circular aperture SNR equation.
8. A Gaussian cross-correlation function, $H(\underline{p}, \underline{r}, z)$. The use of the Gaussian cross-correlation function allows the SNR equation to be reduced to the 2 two-fold integrals for the square apertures discussed above.

9. Zero losses due to beam steering, beam spreading and scintillation. This was discussed in Section 1.4.

1.7 General Approach

To determine the feasibility of an optical heterodyne communication link in the presence of atmospheric turbulence, the following approach is taken:

1. Investigate the relationship between aperture dimensions and SNR.
2. Develop a theoretical model of the SNR both with and without the effects of atmospheric turbulence considered.
3. Determine a SNR efficiency factor, α, which is the ratio of the turbulence affected SNR to the non-turbulence affected SNR.
4. Once the SNR model is developed, calculate the SNRs (with and without turbulence effects considered) while varying the following parameters:
   (a) Transmitting and receiving aperture sizes. The side lengths (of the square apertures) considered range between 1.0 and 15.0 cm.
   (b) Aircraft separation. Separations, or path lengths, considered range from 40 to 160 km.
   (c) Aircraft altitude. Altitudes considered range from 5000 to 12500 m.
   (d) Wavelength. Wavelengths considered are 1.5, 830, and 904 nm.
   (e) Aircraft velocity. Velocities considered range from 141.0 to 244.6 m/s, although the majority of the analysis uses 218.0 m/s.
   (f) Data rate. Data rates considered are 20000, 40000, 100000 and 1000000 bps.
5. Calculate the BERs from the associated SNRs.
6. Evaluate the BERs to determine the feasibility of optical heterodyne communication systems in the presence of atmospheric turbulence.

1.8 Sequence of Presentation

This research report is organized as follows:

1. Chapter II, the Literature Review, presents a summary of the current knowledge in the areas of optical communication systems and coherent detection systems in the presence of atmospheric turbulence.
2. Chapter III presents the theory and methodology applied in developing the models outlined in the General Approach.
3. Chapter IV contains the analysis and evaluation of the calculated SNRs and BERs. From the BERs, feasibility is determined.
4. Chapter V contains the conclusions of the feasibility evaluation and recommendations for further research.

In addition, this report contains several appendices.

1. Appendix A contains a discussion of the different nomenclature and mathematical expressions used to describe the phase coherence length.
2. Appendix B contains the development of the SNR for circular apertures.
3. Appendix C contains the development of the computer code which models the SNRs. This appendix also contains a copy of the computer code.

II. Literature Review

2.1 Introduction

Since the development of the laser, there has been a resurgence of interest in the use of optical communication systems. Guided optical (or fiber optic) systems, for example, are being used extensively in telephone and data communications. In the area of unguided systems, earth-to-space and space-to-space optical communication systems for high data rate transfer have been developed (16:22–3). Also, air-to-ground (Air Force 405B project) and air-to-air (HAVE LACE) optical communication experiments have been conducted by the United States Air Force (10:1). This research effort focuses on unguided optical systems operating in the atmosphere.

Both the Air Force HAVE LACE program and theoretical research have shown that optical communications can be conducted through the earth's atmosphere with acceptable signal-to-noise ratio (SNR) performance (9, 10, 11, 16, 24). The use of optical communications systems in the role of air-to-air communications between aircraft offers many advantages, as well as several disadvantages, with respect to radio frequency (RF) and microwave communications. Table 1 lists several of these advantages and disadvantages.

Three of the advantages listed are of particular interest to the Air Force:

1. Small receiver/transmitter apertures: small receiver and transmitter aperture sizes are desirable due to the weight and size limitations aboard strategic and tactical aircraft.
2. High data rate capability: Feldmann states that communications systems performing "Strategic Data Exchange" (for example, intelligence collection or command and control missions) will be required to transmit data at rates ranging from 19.2 kilobits per second up to several megabits per second (10:1–2).

Table 1. Advantages and Disadvantages of Optical Communications Over Radio Frequency and Microwave Communications in the Atmosphere (10, 19, 24)

Advantages	Disadvantages
- Higher Received Power to Transmitted Power Ratio	- Atmospheric Effects
- Small Receiver/Transmitter Apertures	- Less Suited to Broadcasting Due to Narrow Beam
- High Data Rate Capability	- Accurate Pointing and Tracking Required
- Low Probability of Intercept/ Increased Jam Resistance	- Higher Level of Noise in Receiver Due to Quantum Limited Nature of Detection Process
- Better Directional Resolution With Smaller Apertures	-Low Generation Efficiency in Optical Carrier
- Exploitation of the Unused Portion of the Electromagnetic Spectrum	- Possible Hazard (Due to Laser Beam)
- No Communication License Required	

3. Low probability of intercept/ increased jam resistance: in both strategic and tactical environments, covert communications may be necessary to accomplish the mission, thus the need for communications systems with low probability of intercept. In the command and control role, communication is paramount, thus calling for jam resistant systems.

On the other hand, the primary disadvantage listed in Table 1, with respect to air-to-air communications between aircraft, is the atmospheric effects. The atmospheric effects on an optical communication link may severely limit the range and the probability of error performance of an optical communication system.

The following sections of this literature review address the effects of the atmosphere on an optical communication system. Section 2.2 covers atmospheric turbulence to include observable effects on an optical wave propagating through turbulence. Section 2.3 addresses detection of an optical wave, and the effects of turbulence on the detection process. Section 2.4 then discusses current research efforts in model-

ing both the MCF and SNR with respect to coherent detection. Section 2.5 addresses BER with respect to direct detection systems. Finally, Section 2.6 presents a short summary.

2.2 Atmospheric Turbulence

Atmospheric turbulence can be viewed as packets of air, called eddies, in which the refractive index of each of the eddies varies with respect to the average index of refraction (10, 18). Figure 1 illustrates an optical beam propagating through the eddies. As the optical beam propagates, it experiences both phase and amplitude fluctuations. The phase and amplitude fluctuations result in several observable effects on the propagating wave front (9:139):

1. *Beam Steering:* the entire beam may be deviated from the line of sight, giving rise to a loss of power at the receiving aperture.
2. *Beam Spreading:* small-angle scattering by the inhomogeneities spreads the signal energy over a large region, resulting in a reduced energy density at the receiver.
3. *Scintillation:* destructive interference within the beam produces local fluctuations in the amplitude, so that over the beam there appear areas brighter and darker when compared to the average. This leads to fluctuations in received power which are strongly dependent on the dimensions of the receiver aperture. The time variations of these fluctuations must be considered in amplitude modulation (AM) signals.
4. *Phase Fluctuations:* the time variation in phase produces a spurious modulation which interferes with the signal modulation, and the spatial variation tends to destroy the signal modulation in AM signals.

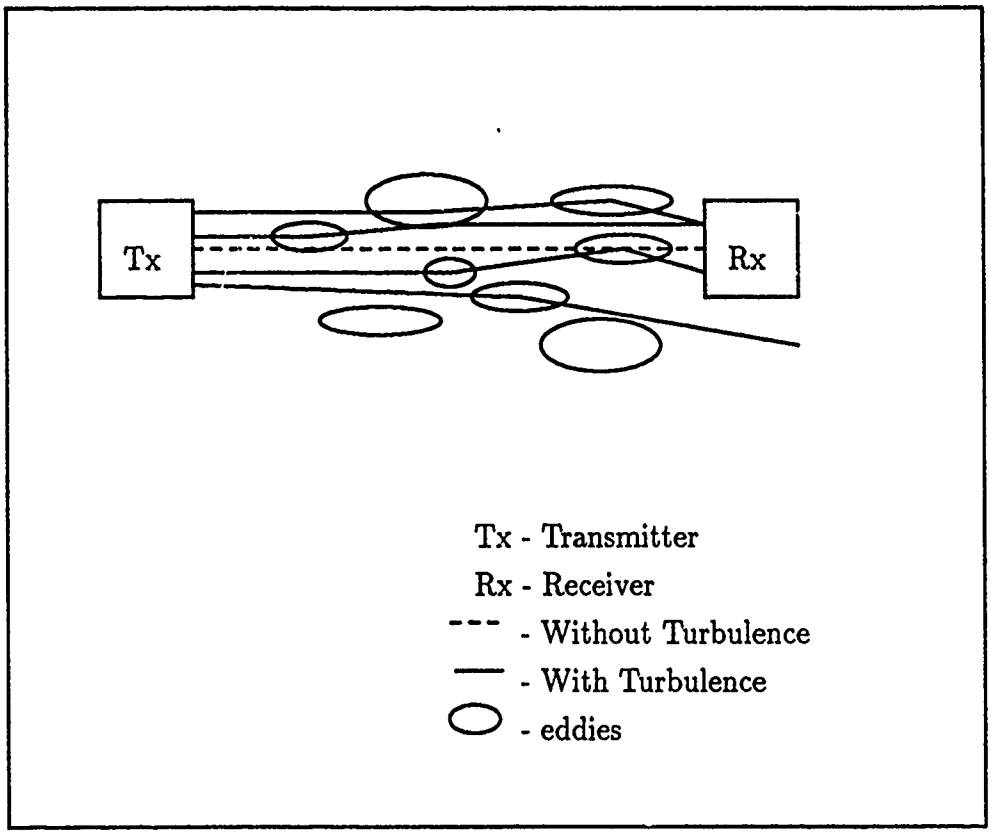

Figure 1. Optical Beam Propagation Through Atmospheric Turbulence

With respect to coherent detection systems, beam steering and phase fluctuations are of primary interest. This research effort concentrates on the latter, phase fluctuations, caused by atmospheric turbulence.

2.2.1 **Atmospheric Turbulence Description** The refractive index of air at optical frequencies is dependent on the optical beam wavelength, atmospheric pressure, and temperature (8, 18). Many authors define n_1 as a measure of the deviation of the refractive index from the free space value. The free space value is approximately equal to unity (8, 18).

According to Goodman, the variations on the refractive index due to pressure are small and can be ignored (18:388). Therefore, the refractive index variations are primarily due to temperature variations. How the temperature variations result in refractive index inhomogeneities is best explained by Goodman:

> The random fluctuations n_1 of the refractive index are caused predominantly by random microstructure in the spatial distribution of temperature. The origin of this microstructure lies in extremely large scale temperature inhomogeneities caused by differential heating of different portions of the Earth's surface by the sun. These large-scale temperature inhomogeneities, in turn, cause large-scale refractive index inhomogeneities, which are eventually broken up by turbulent wind flow and convection, spreading the scale of the inhomogeneities to smaller and smaller sizes. (18:388)

The refractive index inhomogeneities affect an optical wave in two distinct ways: distortion of the phase front such that the isophase surface of the wave front is no longer plane, and fluctuations in the amplitude or intensity across the wave front (3, 9, 11, 12). Recall, it is the phase and amplitude fluctuations that cause the observable effects listed in the previous section.

2.2.2 **Atmospheric Turbulence Models** Because of the random nature of the refractive index fluctuations, a deterministic model of the atmospheric effects is

not possible. That is, the refractive index eddies vary randomly not only in size and location, as illustrated in Figure 1, but also with time. Thus, statistical methods based on the probabilistic behavior of the refractive index fluctuations must be used to model the effects of the turbulence.

Much has been written on modeling the effects of optical wave propagation through atmospheric turbulence. However, as Goodman states, "... without a doubt the most influential work on the subject is that of V.I. Tatarski" (18:385). This influence is readily apparent from all the recent literature on the subject that reference Tatarski's work (2, 3, 6, 7, 8, 9, 10, 11, 13, 15, 18, 24, 27, 37). In his book, Tatarski assumed a Kolmogorov spectrum (discussed shortly) for $\Phi_n(\kappa)$ and then derived a structure function for the refractive index fluctuations, D_n, as well as the amplitude and phase fluctuation's probability density functions (PDFs) (35).

The spectrum, $\Phi_n(\kappa)$, is a measure of the number of eddies of different sizes making up the turbulence where the independent variable, κ, is the wave number. The wave number, κ, is inversely related to eddy size, L, by $\kappa = 2\pi/L$ (recall Figure 1 which illustrates the different eddy sizes) (18:388). Based on Kolmogorov's classic work on turbulence, as described by Coodman, $\Phi_n(\kappa)$ is believed to consist of three regions defined by the inner and outer scales of turbulence. Figure 2 shows the Kolmogorov spectrum and its relationship to the inner, κ_m, and outer, κ_o, scales and $\Phi_n(\kappa)$. Refering to Figure 2, $\Phi_n(\kappa)$ has units of m^3, C_n^2 has units of $m^{-2/3}$ and κ has units of m^{-1}. Also note that the von Kármán spectrum is often used to overcome the known defects in the $\Phi_n(\kappa)$ model for very small wavenumbers (18:388-390).

According to Goodman, the three regions of turbulence can be described as follows. The first region consists of the very large eddy (or refractive index) inhomogeneities ($\kappa < \kappa_o$) before they are broken up by the turbulent wind flow and convection. The second region is the inertial subrange of the spectrum. This region is bounded by the outer and inner scales of the turbulence ($\kappa_o < \kappa < \kappa_m$). It is in the inertial subrange that "... the shape of the PSD is determined by the

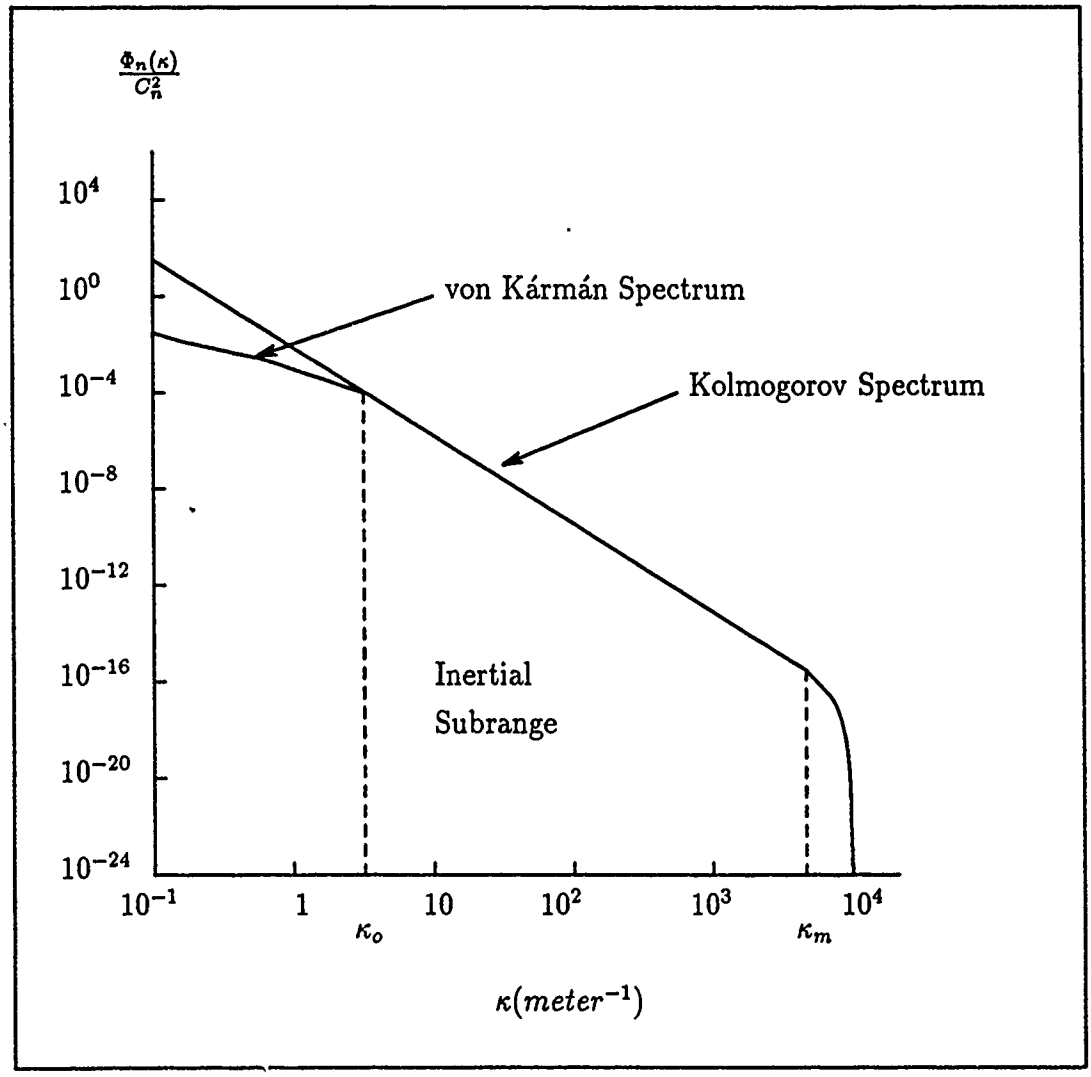

Figure 2. Power Spectral Density of Refractive Index Fluctuations (18:390)

physical laws that govern the breakup of large turbulent eddies into smaller ones" (18:389). Finally, the third region is the region outside the inner scale of the turbulence ($\kappa > \kappa_m$) in which the eddies dissipate their energy due to the viscous forces of the atmosphere. In this region $\Phi_n(\kappa)$ drops rapidly (18:388-389).

The structure function, D_n, is derived from $\Phi_n(\kappa)$ and describes the statistical behavior of the refractive index fluctuations at two points in space by the equation (18:391)

$$D_n = E\{[n_1(\underline{r}_1) - n_1(\underline{r}_2)]^2\} \tag{1}$$

where

$\underline{r}_i$ = a point in space

n_1 = random fluctuations of the refractive index

E = expected value operator

(The dependence of $D_n(\underline{r}_1, \underline{r}_2)$ on $\Phi_n(\kappa)$ follows from the fact that $\Phi_n(\kappa)$ is the three-dimensional PSD of n_1.) Goodman, by assuming homogeneous turbulence, solves Equation (1) to yield (18:392)

$$D_n = C_n^2 \, |\underline{r}|^{2/3} \tag{2}$$

where $\underline{r} = \underline{r}_1 - \underline{r}_2$.

The structure function, D_n, determines the wave structure function, D. (The wave structure function describes the statistics of the optical fluctuations which result from propagation through the randomly inhomogeneous turbulence.) The wave structure function, D, in turn, describes the behavior of the propagating optical wave at two points in the turbulent medium. The relationship between D_n and D is defined by (18:426)

$$D = 2.91 k^2 \, |\underline{r}| \, D_n \tag{3}$$

where k is the optical wave number ($k = 2\pi/\lambda$, λ = wavelength). The wave structure function can also be described in terms of the log-amplitude structure function, D_χ,

and the phase structure function, D_S, by (18:404-407)

$$D(\underline{r}_1, \underline{r}_2) = D_\chi(\chi_1(\underline{r}_1), \chi_2(\underline{r}_2)) + D_S(S_1(\underline{r}_1), S_2(\underline{r}_2))$$

where

$\chi_i(\underline{r}_i)$ = log-amplitude of the propagating optical wave at a point in space

$S_i(\underline{r}_i)$ = phase of the propagating optical wave at a point in space

$D_\chi(\chi_1(\underline{r}_1), \chi_2(\underline{r}_2)) = E[(\chi_1(\underline{r}_1) - \chi_2(\underline{r}_2))^2]$

$D_S(S_1(\underline{r}_1), S_2(\underline{r}_2)) = E[(S_1(\underline{r}_1) - S_2(\underline{r}_2))^2]$

(Note that, when considering coherent detection systems, it is the phase structure function, D_S, that is of primary interest.)

The wave structure function is also related to the MCF of an optical wave propagating through turbulence. The MCF is defined as the cross-correlation of the optical wave at two points in the observation plane. According to Lutomirski and Yura, the MCF describes the loss of coherence of a coherently transmitted wave propagating through turbulence (29:482). In addition, Yura stated that the MCF determines the SNR of an optical communication system that uses coherent detection (37:1399). Lutomirski and Yura concluded by stating that, under the conditions of atmospheric turbulence, the MCF is directly related to the wave structure function by (29:482)

$$MCF = \exp(-D/2)$$

The final quantity of interest is the PDF of the complex amplitude fluctuations, and in particular, the phase fluctuations of the propagating optical wave at a point in space. In his work, Tatarski characterized the statistics of the amplitude fluctuations using a log-normal PDF and the phase fluctuations using a Gaussian PDF (35:Ch 6,7).

With respect to the amplitude fluctuations, current literature refines and limits Tatarski's work (6, 9, 7, 29). For example, Churnside and Clifford predict a log-normal Rician PDF (6), as do Churnside and Frehlich (7). However, since this analysis is concerned with coherent detection, the amplitude fluctuations do not play a major role in modeling the optical communication system. Rather, it is the phase fluctuations that dominate the optical communication system model. With respect to the phase fluctuations, the reviewed literature agrees with Tatarski's results of a Gaussian PDF (2, 9, 11, 13).

2.3 Optical Communication Detection Systems

Optical communication detection systems fall into two categories: incoherent or direct detection receivers, and coherent (including heterodyne and homodyne) detection receivers. Direct detection receivers respond to the intensity of the optical wave, while coherent receivers respond to the amplitude and phase.

2.3.1 **Direct Detection Systems** In a direct detection system, the signal current is proportional to the received intensity at the receiver aperture (2, 26). The direct detection operation is based on "photon counting" (25:39). Its primary advantage is the simplicity of design and operation.

2.3.2 **Coherent Detection Systems** Coherent receiver systems, on the other hand, are more complex in design and operation. In coherent systems, a locally generated optical wave is added (or mixed) with the received optical wave before photodetection (14, 15). This locally generated optical wave is equivalent to a local oscillator generated waveform in RF operation. However, there is a distinction made between RF and optical coherent detection. In RF, the difference between coherent and incoherent detection of the intermediate frequency (IF) signal depends on whether or not the phase of the signal is used. In optical systems, coherent detection is defined as any detection process that uses a local oscillator (26:36).

2.3.3 **Coherent Versus Direct Detection Systems** Coherent detection systems have several advantages over direct detection systems. First, coherent detection systems offer a significant improvement in receiver sensitivity (or SNR) (4, 25, 26, 32). The SNR improvements stated in the literature range from 10 dB (25, 26) to (theoretically) 20 dB (26, 32). Second, coherent detection systems offer greater frequency selectivity for the transmitters and receivers (25, 26, 32). Third, they provide for conveniently tunable receivers (25:1). And finally, coherent detection allows for the use of alternative modulation formats (since they respond to both the phase and amplitude of the received optical wave) (25:1). However, both direct detection and coherent detection systems are affected by propagation of the received wave through the atmosphere.

2.3.4 **Atmospheric Effects on Optical Communications Detection Systems** Both direct detection and coherent detection systems are adversely affected by the optical wave amplitude and phase fluctuations caused by atmospheric turbulence. The random amplitude fluctuations result in reduced gain and fading in both the direct detection and coherent detection systems (16:13), as well as an overall signal power loss due to propagation through the turbulence (3:33).

However, the coherent detection system is most affected by the random phase fluctuations of the optical wave. The areas of the optical wave that are out of phase with the detector local oscillator will add destructively resulting in a reduced IF amplitude (that is, after mixing) and thus reduce the SNR at the IF stage of the detector (16:19). Stated another way, since the turbulence reduces the coherence of the optical wave (as described by the MCF), the effective area of the receiver aperture is reduced to the size of the phase coherence length (11, 16). According to Fried, when assuming an infinite, uniform amplitude plane wave, the phase coherence length is the minimum aperture diameter which gives (approximately) the maximum possible SNR (11:62). Fried (11) and Chen (5) showed that, by increasing the aperture size beyond the phase coherence length, the SNR will only increase by about 3 dB.

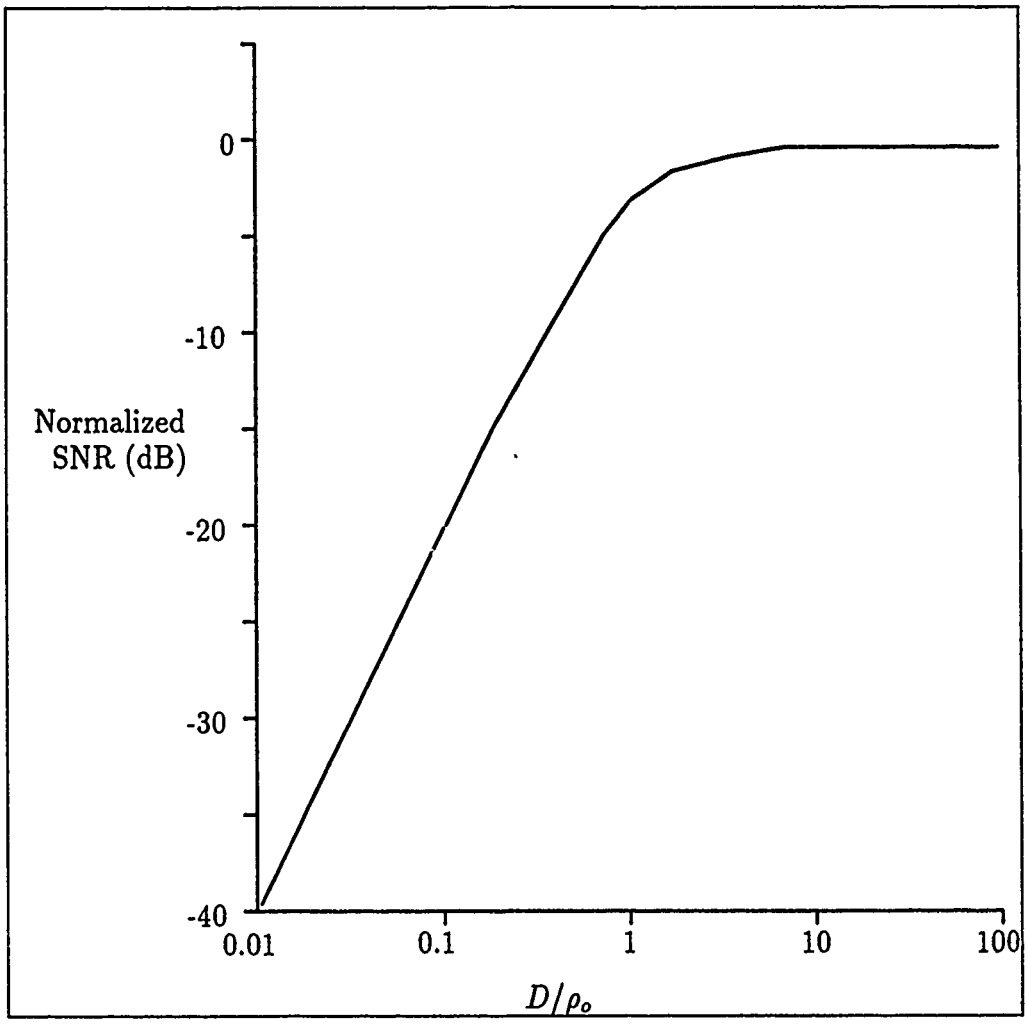

Figure 3. Normalized Signal-to-Noise Ratio Versus Normalized Aperture Size

That is, as Chen states, when an aperture diameter is equal to the phase coherence length, the SNR is only 3 dB below what can be achieved as the aperture diameter approaches infinity (5:1017). The relationship between the phase coherence length, denoted ρ_o, and a circular aperture diameter, denoted D, was shown graphically by both Fried (11:62) and Chen (5:1017). Chen's particular representation is shown in Figure 3.

Lutomirski and Yura, however, found that Fried's results for a maximum useful receiver diameter are not valid for all ranges (29:483). While also assuming an

infinite, uniform amplitude plane wave, they showed that the SNR increases with increasing receiver aperture sizes for path lengths small when compared to the mean field-decay length, z_c (29:487). However, when the path lengths are greater than z_c (where z_c is typically less than 10 km), Lutomirski and Yura showed that their results agree with Fried (29:487).

Lutomirski and Buser extended Fried's results to the case of a finite transmitting aperture. Their results can be summarized as follows:

> 1. The largest useful receiver diameter is the smaller of $(z/k)^{1/2}$ and the transverse coherence length, p_o, of the field at the receiver due to the field $U_A(\underline{r})$ on the transmitter plane.
> 2. The largest useful transmitter diameter is the smaller of $(z/k)^{1/2}$ and the transverse coherence length, ρ_o, of the field at the transmitter due to the field $F(\underline{p})$ in the receiver plane. (28:2159)

The transverse (phase) coherence lengths, p_o and ρ_o, are defined as the transverse separations for which the correlation of the propagating optical wave at two points in space is reduced by e^{-1}, and where the wave is emitted from the transmitter and receiver, respectively. The term $(z/k)^{1/2}$ defines the Fresnel zone, where z is the propagation path length (m) and k is the optical wave number (m^{-1}) (28:2158-2159).

The implications of Fried's, as well as Lutomirski and Buser's, results are that, when the aperture diameters are larger than both the Fresnel zone and the applicable transverse coherence length, the SNR saturates due to turbulence (28:2159).

It is interesting to note here the varied nomenclature and mathematical expressions used to describe the phase coherence length. For example, Fried calls it the "efficiency saturation dimension" and denotes it r_o (11:57), while Lutomirski and Buser refer to it as the "turbulence-induced coherence length" or "transverse coherence length" and denote it ρ_o (28:2153,2159). Appendix A presents a brief discussion concerning the various nomenclature and mathematical expressions found

in the reviewed literature to describe the phase coherence length. For this study, Yura's expression is used (37:1403):

$$\rho_o = \left(0.545k^2C_n^2z\right)^{-\frac{3}{5}} \tag{4}$$

where

k = optical wave number (m^{-1})

C_n^2 = structure constant of the refractive index fluctuations (turbulence strength) $(m^{-2/3})$

z = propagation path length (m)

(Note that the terms will be addressed in more detail in Chapter III.)

2.3.5 **Noncoherently Combined Large Aperture Optical Heterodyne Receiver** Chen studied the use of combining multiple receivers as a means of overcoming the phase coherence length limit of the receiving aperture. His analysis addressed noncoherently combining the output signals from an array of smaller receivers, and comparing the results to a monolithic heterodyne receiver of equivalent aperture size. He showed that, in the absence of turbulence, the monolithic receiver performed better than the noncoherently combined small receivers array when viewed from a SNR aspect. However, once turbulence was introduced into the analysis, Chen found that the noncoherently combined small receivers array performed significantly better than the monolithic receiver. The monolithic receiver was now severely limited by the phase coherence length. Chen concluded by stating that the optimal situation occurred when the receiver diameter of each of the small receivers in the combined aperture was on the order of the phase coherence length (5:1013).

2.4 Mutual Coherence Function and Signal-to-Noise Ratio Development

As stated previously, the MCF determines the SNR of an optical heterodyne communication system. Thus, much research has been conducted investigating the MCF in the presence of turbulence.

Lutomirski and Yura, by extending the Huygens-Fresnel principle, derived an expression for the MCF of an optical wave propagating in an inhomogeneous medium, such as atmospheric turbulence (29:1653). According to Lutomirski and Yura

> The principle as applied to propagation in a vacuum states that every point of a wavefront may be considered as a center of a secondary disturbance which gives rise to spherical wavelets, and the wavefront at a later instant may be regarded as the envelope of these wavelets...for a refractive medium, the extended principle is that the secondary wavefront will again be determined by the envelope of spherical wavelets from the primary wavefront, but each wavelet will now be determined by the propagation of a spherical wave through the refractive medium. (29:1653)

First, Lutomirski and Yura proved that the Huygens-Fresnel principle could be extended to optical wave propagation in a weakly inhomogeneous medium, such as atmospheric turbulence. From the extended Huygens-Fresnel principle, they showed that the field due to a disturbance across an aperture can be calculated. By applying the reciprocity theorem of Helmholtz to the field and averaging, the MCF of the propagating optical wave results (29:1653-1654). The reciprocity theorem of Helmholtz states that, given two points in space, P_o and P_1, a point source located at P_o will produce the same effect on P_1 as an identical point source at P_1 will produce on P_o. That is, symmetry exists with respect to the source plane and the observation plane (17:41).

Yura used Lutomirski and Yura's extended Huygens-Fresnel principle and applied it to a finite optical beam. Yura showed that the resulting finite beam MCF is valid for an arbitrary complex disturbance in the transmitting aperture (37:1400).

Lutomirski and Buser, like Yura, also applied the extended Huygens-Fresnel principle to a finite optical beam. However, Lutomirski and Buser then went further to apply the resulting finite beam MCF to coherent detection (28). First, they showed that "a necessary and sufficient condition for instantaneous reciprocity is that the transmitter aperture field and the receiver weighting be identical" (28:2157). (Lutomirski and Buser define instantaneous to mean for each realization of the refractive index field (28:2157).) They presented a special case that fulfills this condition: a uniform plane wave in a circular aperture transmitted to a uniformly weighted, circular receiver when the transmitting and receiving apertures are of equal diameter (28:2157). (The importance of reciprocity will become apparent when the MCF is derived in Chapter III.)

Lutomirski and Buser then developed the normalized, average SNR for coherent detection. Starting with the signal power as developed by Fried (11), Lutomirski and Buser introduced the cross-correlation of the complex fields at two points in the observation plane, $\underline{p}_1$ and $\underline{p}_2$, due to spherical wave sources at two points in the transmitting aperture plane, $\underline{r}_1$ and $\underline{r}_2$. They used a geometric optics approach to derive an expression for the cross-correlation function, $H(\underline{p}, \underline{r}, z)$, where z is the propagation path length, and $\underline{p}$ and $\underline{r}$ again represent points in the observation plane and transmitting aperture, respectively. Note that, for isotropic and homogeneous turbulence, $\underline{p} = \underline{p}_1 - \underline{p}_2$ and $\underline{r} = \underline{r}_1 - \underline{r}_2$ (28:2154). Lutomirski and Buser showed that the propagation properties required to determine the MCF (for a finite transmitter source) are contained in $H(\underline{p}, \underline{r}, z)$. The derived signal power is then averaged, and the normalized, average SNR expression is developed (28:2154-2159).

Assuming infinite Gaussian apertures, Lutomirski and Buser solved the normalized SNR to a get closed form solution for two cases: propagation in a vacuum ($H(\underline{p}, \underline{r}, z) = 1$) and propagation in turbulence (28:2158-2159).

The derived MCF and SNR expressions of Lutomirski and Yura, Yura, Fried, and Lutomirski and Buser are presented and discussed further in Chapter III.

Table 2. Direct Detection Analysis Communication Link Parameters (24:57)

Altitude(m)	Aircraft Speed (m/s)	Data Rate (bps)
3048	218.639	20000
3048	218.639	40000
3048	244.361	20000
6096	218.639	20000
6069	218.639	40000
6069	244.361	20000
9144	218.639	20000
9144	218.639	40000
9144	244.361	20000

2.5 Direct Detection System Bit Error Rate Development

As discussed in Section 2.3.3, coherent detection systems offer SNR improvements of 10 to 20 dB over direct detection systems. However, in the presence of atmospheric turbulence, coherent detection systems are affected by both the amplitude and phase fluctuations of the turbulence, while direct detection systems are primarily affected by the amplitude fluctuations. Thus, the SNR improvements coherent detection offers over direct detection may be less in the presence of turbulence.

Kanavos calculated the BERs for a direct detection (noncoherent) air-to-air optical communication link for various path lengths, altitudes, and data rates. He calculated maximum reliable path lengths for optical links both with and without turbulence for a BER of 10^{-5} (24:58,63). Using the parameters listed in Tables 2, 3 and 4, Kanavos calculated the maximum reliable path lengths summarized in Table 5.

It should be noted here that, although Kanavos does present his results in a manner similar to this research effort, a direct comparison cannot be made between his results and this effort's results. This is because Kanavos, in his research methodology, requires parameters not addressed in this effort. This research, likewise, requires parameters not addressed by Kanavos.

Table 3. Direct Detection Analysis Transmitter and Receiver Characteristics (24:57)

Transmitter Output Power:	50 W
Transmitter Optics Efficiency:	0.9
Transmitter and Receiver Aperture Diameters:	0.127 m
Receiver Optics Efficiency:	0.8
Receiver Gain:	40

Table 4. Direct Detection C_n^2 Summary (24:77)

Altitude (m)	C_n^2 $(m^{-2/3})$
3048	6.4×10^{-17}
6096	1.617×10^{-17}
9144	1.947×10^{-18}

Table 5. Direct Detection Analysis Results Summary (24:73)

	Maximum Reliable Path Lengths	
Altitude (m)	Baseline Link (km)	Turbulence Link (km)
3048	95	42
6096	208	77
9144	239	134

2.6 Summary

The literature indicates that optical communication is possible through the atmosphere. However, the atmosphere does degrade the performance of the optical communication system.

Tatarski's work in wave propagation through turbulence laid the foundation for determining the effects of atmospheric turbulence on an optical wave propagating through the atmosphere. Subsequent literature refined Tatarski's results, particularly in the area of the amplitude fluctuation PDF of the optical wave.

The effects of the turbulence also affect the detection of the optical wave. Without turbulence, the literature agrees that coherent detection offers better receiver sensitivity (or SNR) than direct detection. However, although both coherent and direct detection systems are affected by the random amplitude fluctuations of the optical wave, the coherent detection system is further affected by the phase fluctuations.

Bit error rate calculations for direct detection systems indicate path lengths of approximately 40 to 134 km are possible (for a BER of 10^{-5}) in the presence of turbulence.

III. Theory and Methodology

This chapter addresses three topics: general SNR equation development, optimum aperture dimensions, and uniformly weighted aperture SNR and BER equations development. Specifically, this chapter presents the development of the SNR equation for coherent optical communications in the presence of turbulence. Second, a closed-form solution for the SNR is obtained by making assumptions about the aperture weighting functions (Gaussian) and cross-correlation function (Gaussian). From this closed-form solution, an analysis of SNR versus aperture dimensions is made. Third, making new assumptions about the aperture weighting functions (uniform), an integral expression for the SNR is developed. This integral expression is solved using numerical integration methods. This chapter concludes with a short summary.

3.1 General Signal-to-Noise Ratio Development

In this section, the general SNR for coherent optical communications in the presence of turbulence is developed. First, the Huygens-Fresnel principle is presented for vacuum propagation. Using the work of Lutomirski and Yura, the Huygens-Fresnel principle is then extended to the application of propagation in a turbulent medium. Second, the MCF for optical propagation in a turbulent medium is developed. This development includes the development of the cross-correlation function, $H(\underline{p}, \underline{r}, z)$. Finally, the general SNR equation is developed.

3.1.1 **Huygens-Fresnel Principle** Before discussing the Huygens-Fresnel principle for vacuum propagation, a brief review of optical propagation for monochromatic light is presented. First, let the function $u(P,t)$ represent "...the scalar amplitude of one polarization component of the electric or magnetic field associated with a monochromatic optical disturbance" where P is some point in space and t is some

instant in time (18:117). An analytic signal representation associated with $u(P,t)$ can be written as (18:117)

$$\underline{u}(P,t) = \underline{U}(P)\exp(-ikct) \tag{5}$$

where

$\underline{U}(P)$ = phasor amplitude

k = optical wave number (m)

c = speed of light = 3×10^8 m/s

t = time (s)

Referring to Figure 4, the effect of the wave, $\underline{u}(P,t)$, on an infinite surface Σ, as well as the effect of the wave at some point beyond Σ, can be examined. Let $\underline{u}(P,t)$ be incident on Σ from the left. To determine the phasor amplitude, $\underline{U}(P)$, at some point to the right of Σ, say P_o, in terms of the field on Σ, the Huygens-Fresnel principle can be applied. Note that, in Figure 4, θ is the angle between the normal to Σ and the line joining P_1 and P_o, and z is the distance between P_1 and P_o (18:117).

The Huygens-Fresnel principle is based on the theory that, given a spherical wavefront of an optical disturbance, if each point on that wavefront were taken to be a "secondary" spherical disturbance, then the total wavefront at any later instant in time could be constructed from the envelope of the "secondary" wavelets (17:31). Mathematically (and refering to Figure 4), the Huygens-Fresnel principle can be expressed, for $z \gg \lambda$, as (18:117)

$$\underline{U}(P_o) = -\frac{i}{\lambda}\int\int_{\Sigma}\underline{U}(P_1)\frac{\exp(ikz)}{z}\chi(\theta)\,dS \tag{6}$$

where

λ = wavelength (m)

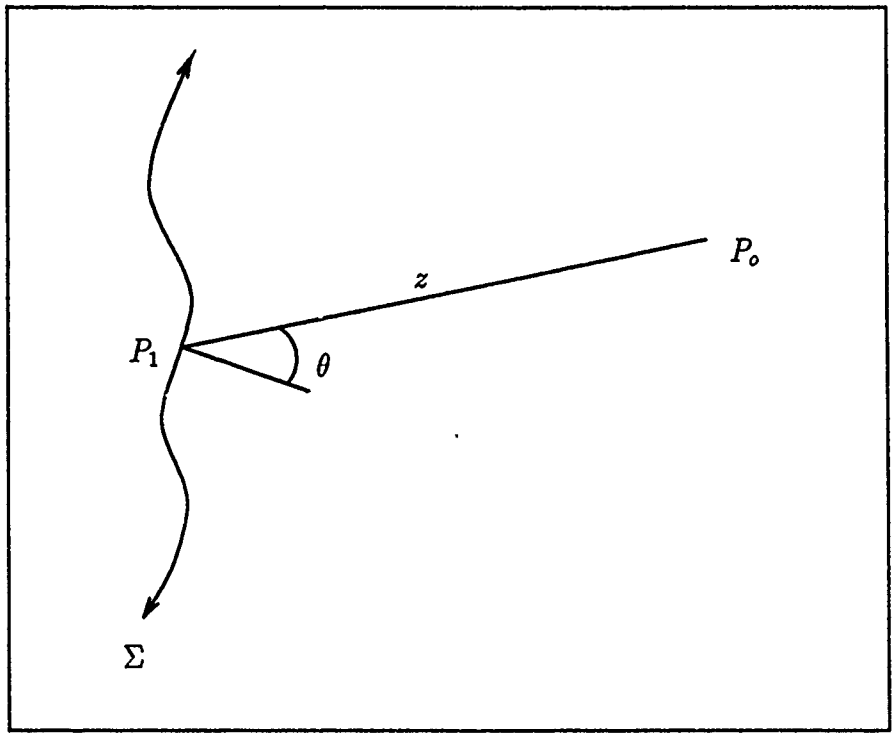

Figure 4. Propagation Geometry (18:118)

Σ = infinite surface on which the wave is incident

z = distance between P_1 and P_o (m)

θ = angle between the normal to Σ and the line joining P_o and P_1

$\chi(\theta)$ = obliquity factor

dS = elemental surface area on Σ

Lutomirski and Yura extended the Huygens-Fresnel principle for vacuum propagation to optical propagation in a weakly inhomogeneous medium (such as atmospheric turbulence) (29:1653). In addition, they considered the disturbance as specified over some finite aperture, as opposed to infinite plane waves, infinite spherical waves or infinite Gaussian disturbances (29:1652).

Under the consideration of a finite aperture, a new parameter, $\underline{r}$, is introduced to denote a point in the transmitter plane, while the parameter $\underline{p}$ will now denote

a point in the observation, or receiver, plane. The transmitter and receiver planes are assumed to be parallel and lie in an x-y orientation (where z is the axis of propagation).

Assuming the scattering angles are sufficiently small (that is, $\theta \approx 0$ so that $\chi(\theta) \approx 1$), the aperture lies in a plane normal to the z axis (axis of propagation), and the quantity $k\left|\underline{p}-\underline{r}\right| \gg 1$, Lutomirski and Yura show (29:1653):

$$\underline{U}(\underline{p}) = \frac{ik}{4\pi}\int \underline{U}(\underline{r})\frac{\exp\left[ik\left|\underline{p}-\underline{r}\right|+\psi(\underline{r},\underline{p})\right]}{\left|\underline{p}-\underline{r}\right|} \times\left[\underline{e}_s\cdot\underline{e}_z-\underline{e}_n\cdot\underline{e}_z+\frac{\nabla\psi(\underline{p},\underline{r})}{ik}\cdot\underline{e}_z\right]d^2\underline{r} \tag{7}$$

where

$\psi\left(\underline{p},\underline{r}\right)$ describes the turbulence-induced phase perturbations on a spherical wave propagating from a point $\underline{r}$ to a point $\underline{p}$ (rad)(37:1401)

$\underline{e}_s$ = unit vector from $\underline{r}$ to $\underline{p}$

$\underline{e}_n$ = unit vector in direction normal to the wavefront in the transmitter plane

$\underline{e}_z$ = unit vector in direction along the z axis

$d^2\underline{r}$ = elemental area at the point $\underline{r}$ in the aperture

When the distance of propagation is large with respect to the aperture size (paraxial approximation), then $\underline{U}\left(\underline{p}\right)$ reduces to (29:1654)

$$\underline{U}\left(\underline{p}\right) = \left[-\frac{i}{2\lambda z_o}\left(1+\cos\theta_o\right)\right]\int\frac{\exp\left[ikz+\psi\left(\underline{p},\underline{r}\right)\right]}{z}\underline{U}(\underline{r})\,d^2\underline{r} \tag{8}$$

where

z = distance between the points $\underline{r}$ (in transmitter plane) and $\underline{p}$ (in receiver plane)
$= |\underline{r}-\underline{p}|$ (m)

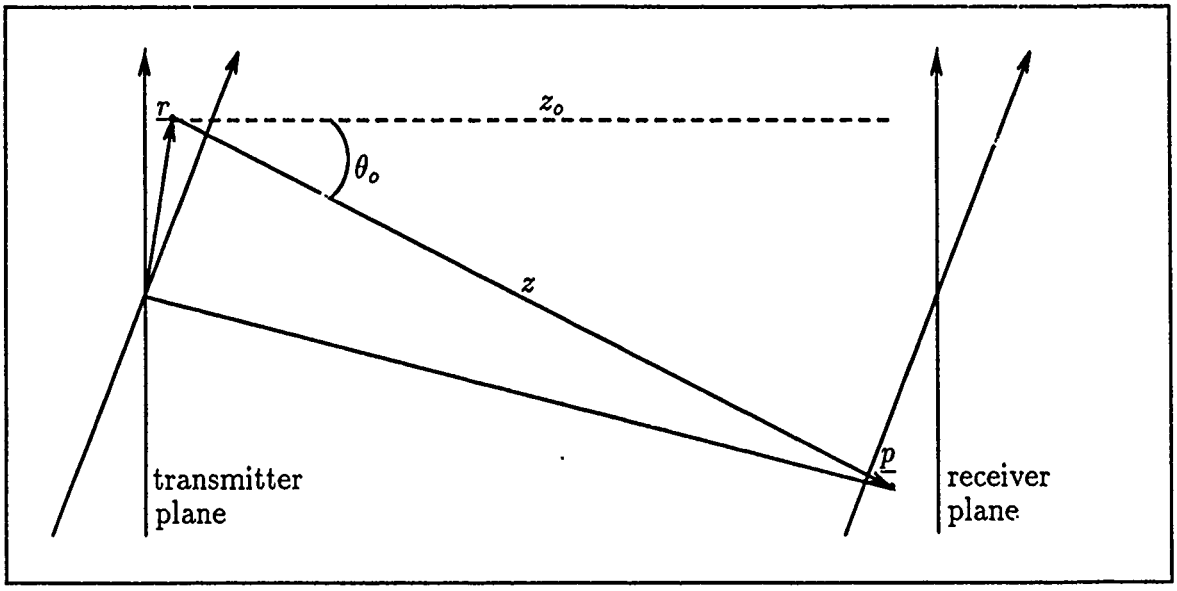

Figure 5. Propagation Geometry for Long Propagation Paths

z_o = perpendicular distance between the transmitter and receiver planes

θ_o = angle between the normal to the transmitter plane and $\underline{r} - \underline{p}$

The geometry is illustrated in Figure 5.

Equation (8) can be reduced and rewritten using the following definitions and assumptions (37:1400):

1. Define $U_A(\underline{r})$ to be the arbitrary complex disturbance at $\underline{r}$, where the subscript A implies the disturbance defined in the transmitter plane.
2. Assume $\theta_o \approx 0$.
3. Define the field at $\underline{p}$ due to a spherical wave propagating in the refractive medium from $\underline{r}$ as

$$G\left(\underline{p},\underline{r}\right) = \frac{\exp\left[ik\left|\underline{p}-\underline{r}\right| + \psi\left(\underline{p},\underline{r}\right)\right]}{\left|\underline{p}-\underline{r}\right|} \tag{9}$$

Note that $G\left(\underline{p},\underline{r}\right)$ is simply one representation of a Green's function.

Now Equation (8) becomes (37:1400)

$$\underline{U}\left(\underline{p}\right) = -\frac{ik}{2\pi}\int G\left(\underline{p},\underline{r}\right) U_A\left(\underline{r}\right) d^2\underline{r} \tag{10}$$

where the integration is carried out over the transmitter aperture (37:1400).

3.1.2 **Mutual Coherence Function Development** In this section, the field amplitude equation developed in Section 3.1.1 is used to determine the MCF of the optical waves in the presence of atmospheric turbulence. The MCF is then manipulated to "pull out" the atmospheric effects in terms of a cross-correlation function $H(\underline{p},\underline{r},z)$. Recall that $H(\underline{p},\underline{r},z)$ was defined to be the two point correlation function (28:2154). The relationship between $H(\underline{p},\underline{r},z)$ and the phase structure function, D_S, is then presented.

The MCF, which represents a cross-correlation of the propagating optical wave at points $\underline{p}_1$ and $\underline{p}_2$ is defined to be (18:174)

$$MCF \triangleq \left\langle \underline{U}\left(\underline{p}_1\right) \underline{U}^*\left(\underline{p}_2\right)\right\rangle \tag{11}$$

where $< \cdot >$ represents the ensemble average. Assuming $U(\underline{p}_i)$ is the field due to a transmitting aperture with field distribution $U_A(\underline{r}_i)$, Equation 10 is substituted into Equation 11 to yield

$$MCF = \left(\frac{k}{2\pi}\right)^2 \int\int \left\langle G\left(\underline{p}_1,\underline{r}_1\right) U_A\left(\underline{r}_1\right) G^*\left(\underline{p}_2,\underline{r}_2\right) U_A^*\left(\underline{r}_2\right)\right\rangle d^2\underline{r}_1 d^2\underline{r}_2 \tag{12}$$

Note that $< U_A\left(\underline{r}_1\right) U_A^*\left(\underline{r}_2\right) >= U_A\left(\underline{r}_1\right) U_A^*\left(\underline{r}_2\right)$, thus the quantity can come out of the ensemble average, which yields the MCF derived by Yura (37:1400):

$$MCF = \left(\frac{k}{2\pi}\right)^2 \int\int \left\langle G\left(\underline{p}_1,\underline{r}_1\right) G^*\left(\underline{p}_2,\underline{r}_2\right)\right\rangle U_A\left(\underline{r}_1\right) U_A^*\left(\underline{r}_2\right) d^2\underline{r}_1 d^2\underline{r}_2 \tag{13}$$

Lutomirski and Yura proved that the reciprocity theorem holds for $G\left(\underline{p},\underline{r}\right)$ (29:1658), that is the field at $\underline{p}$ due to a point source at $\underline{r}$ is identical to the field at $\underline{r}$ due to a point source at $\underline{p}$, thus (37:1401)

$$G\left(\underline{p}_1,\underline{r}_1\right)G^*\left(\underline{p}_2,\underline{r}_2\right) = G\left(\underline{r}_1,\underline{p}_1\right)G^*\left(\underline{r}_2,\underline{p}_2\right) \tag{14}$$

In developing the expression for the MCF as a function of a cross-correlation function, $H(\underline{p},\underline{r},z)$ (as defined by Yura (37:1401)), the importance of the role that the reciprocity theorem plays becomes evident. Recalling Equation (9), then (37:1401)

$$\begin{aligned}\left\langle G\left(\underline{r}_1,\underline{p}_1\right)G^*\left(\underline{r}_2,\underline{p}_2\right)\right\rangle &= \left\{\frac{\exp\left[ik\left(\left|\underline{r}_1-\underline{p}_1\right|-\left|\underline{r}_2-\underline{p}_2\right|\right)\right]}{\left|\underline{r}_1-\underline{p}_1\right|\left|\underline{r}_2-\underline{p}_2\right|}\right\} \\ &\quad\times H\left(\underline{p}_1,\underline{r}_1,\underline{p}_2,\underline{r}_2,z\right)\end{aligned} \tag{15}$$

where

$$H\left(\underline{p}_1,\underline{r}_1,\underline{p}_2,\underline{r}_2,z\right) = \left\langle\exp\left[\psi\left(\underline{r}_1,\underline{p}_1\right)+\psi^*\left(\underline{r}_2,\underline{p}_2\right)\right]\right\rangle \tag{16}$$

Thus adherence by the MCF to the reciprocity theorem allows the phase perturbations, $\psi(\underline{r}_i,\underline{p}_i)$, to be expressed in a form consistent with Yura's (37:1401) definition of $H\left(\underline{p}_1,\underline{r}_1,\underline{p}_2,\underline{r}_2,z\right)$. (That is, if reciprocity did not hold, $\psi(\underline{r}_i,\underline{p}_i)$ would not necessarily equal $\psi(\underline{p}_i,\underline{r}_i)$. The cross-correlation function, $H\left(\underline{p}_1,\underline{r}_1,\underline{p}_2,\underline{r}_2,z\right)$, as defined by Yura, could not then be used in the MCF defined here.)

Recalling the assumption that z, the distance of propagation, is large compared to the aperture size (known as the paraxial approximation), then the $\left|\underline{r}_1-\underline{p}_1\right|$ and $\left|\underline{r}_2-\underline{p}_2\right|$ terms in the denominator of Equation (15) can be replaced by z to yield

$$\begin{aligned}\left\langle G\left(\underline{r}_1,\underline{p}_1\right)G^*\left(\underline{r}_2,\underline{p}_2\right)\right\rangle &= \frac{1}{z^2}\exp\left[ik\left(\left|\underline{r}_1-\underline{p}_1\right|-\left|\underline{r}_2-\underline{p}_2\right|\right)\right] \\ &\quad\times H\left(\underline{p}_1,\underline{r}_1,\underline{p}_2,\underline{r}_2,z\right)\end{aligned} \tag{17}$$

Yura shows that, again using the paraxial approximation (37:1401),

$$\begin{aligned}\left|\underline{r}_1-\underline{p}_1\right|-\left|\underline{r}_2-\underline{p}_2\right| &\cong \frac{1}{2z}\left[\underline{r}_1^2-\underline{r}_2^2+\underline{p}_1^2-\underline{p}_2^2+2\left(\underline{r}_2\cdot\underline{p}_2-\underline{r}_1\cdot\underline{p}_1\right)\right] \\ &\cong \frac{1}{2z}\left[\left|\underline{r}_1-\underline{p}_1\right|^2-\left|\underline{r}_2-\underline{p}_2\right|^2\right] \end{aligned} \tag{18}$$

which now yields

$$\begin{aligned}\left\langle G\left(\underline{r}_1,\underline{p}_1\right)G^*\left(\underline{r}_2,\underline{p}_2\right)\right\rangle &= \frac{1}{z^2}\exp\left\{\frac{ik}{2z}\left[\left|\underline{r}_1-\underline{p}_1\right|^2-\left|\underline{r}_2-\underline{p}_2\right|^2\right]\right\} \\ &\quad\times H(\underline{p}_1,\underline{r}_1,\underline{p}_2,\underline{r}_2,z)\end{aligned} \tag{19}$$

Now an expression for the MCF can be derived by substituting Equation (19) into (13) to yield

$$\begin{aligned}MCF &= \left(\frac{k}{2\pi z}\right)^2\int\int exp\left\{\frac{ik}{2z}\left[\left|\underline{p}_1-\underline{r}_1\right|^2-\left|\underline{p}_2-\underline{r}_2\right|^2\right]\right\} \\ &\quad\times H\left(\underline{p}_1,\underline{r}_1,\underline{p}_2,\underline{r}_2,z\right)U_A\left(\underline{r}_1\right)U_A^*\left(\underline{r}_2\right)d^2\underline{r}_1d^2\underline{r}_2\end{aligned} \tag{20}$$

where the terms are previously defined. For isotropic and homogeneous turbulence, $H\left(\underline{p}_1,\underline{r}_1,\underline{p}_2,\underline{r}_2,z\right)$ is only a function of the difference coordinates so that (28:2154):

$$\begin{aligned}MCF &= \left(\frac{k}{2\pi z}\right)^2\int\int \exp\left\{\frac{ik}{2z}\left[\left|\underline{p}_1-\underline{r}_1\right|^2-\left|\underline{p}_2-\underline{r}_2\right|^2\right]\right\} \\ &\quad\times H\left(\underline{p}_1-\underline{p}_2,\underline{r}_1-\underline{r}_2,z\right)U_A\left(\underline{r}_1\right)U_A^*\left(\underline{r}_2\right)d^2\underline{r}_1d^2\underline{r}_2\end{aligned} \tag{21}$$

Now that a general expression for the MCF has been derived, the function $H\left(\underline{p}_1-\underline{p}_2,\underline{r}_1-\underline{r}_2,z\right)$ can be investigated. Recall Equation (16) which states

$$H\left(\underline{p}_1-\underline{p}_2,\underline{r}_1-\underline{r}_2,z\right)=\left\langle\exp\left[\psi\left(\underline{r}_1,\underline{p}_1\right)+\psi^*\left(\underline{r}_2,\underline{p}_2\right)\right]\right\rangle \tag{22}$$

Yura solved Equation (22) through second order in n_1 where $\psi(\underline{r}_i,\underline{p}_i)$ is related to n_1

via the path integral of n_1 along the optical path from $\underline{p}_i$ to $\underline{r}_i$. Recall that $\psi(\underline{r}_i, \underline{p}_i)$ describes the turbulence-induced phase perturbations of the wave, and that n_1 is a measure of the refractive index fluctuations about the free-space value (where the free-space value is approximately unity). Without presenting the details of Yura's work here, Yura determined that the general form of $H\left(\underline{p}_1 - \underline{p}_2, \underline{r}_1 - \underline{r}_2, z\right)$ can be expressed as (37:1406)

$$H\left(\underline{p}_1 - \underline{p}_2, \underline{r}_1 - \underline{r}_2, z\right) = \exp\left\{-\left[\langle|\psi_1\rangle|^2 - \left\langle\psi_1\left(\underline{r}_1, \underline{p}_1\right)\psi_1^*\left(\underline{r}_2, \underline{p}_2\right)\right\rangle\right]\right\} \tag{23}$$

where

$$\left\langle|\psi_1|^2\right\rangle = 2\pi k^2 z \int \Phi_n(\kappa)\, d\kappa \tag{24}$$

Yura shows that Equation (24) is correct through second order in n_1, but also points out that, given the experimental evidence and various theoretical arguments showing ψ to be a Gaussian random variable, Equation (24) may be correct to all orders in n_1 (37:1401).

Note that, for simplicity, the implicit dependence of $H\left(\underline{p}_1 - \underline{p}_2, \underline{r}_1 - \underline{r}_2, z\right)$ on z is dropped for the remainder of this study.

3.1.3 **Signal-to-Noise Ratio Dependence** In this section, the relationship between the MCF and the signal power, S, is presented. The signal power is averaged and then divided by the noise power, N, to obtain a SNR. This SNR is then normalized by the effective cw transmitter output power, W_A. The section concludes with an expression for the general normalized SNR.

Lutomirski and Buser show that the MCF, as defined by $\text{MCF} = \left\langle \underline{U}(\underline{p}_1)\underline{U}^*(\underline{p}_2)\right\rangle$, is related to the signal power, S, by (28:2157)

$$S = \frac{1}{2}\left(\eta A_R g\right)^2 R\left|\int \underline{U}(\underline{p}) F\left(\underline{p}\right) d^2\underline{p}\right|^2 \tag{25}$$

where

η = quantum efficiency of the receiver photodetector

A_R = amplitude of the receiver local oscillator signal

g = gain of the receiver current amplifier

R = resistance of the receiver load

$F(\underline{p})$ = receiver aperture weighting function

Substituting Equation (21) into (25) and taking the ensemble average yields (28:2157)

$$\begin{aligned}\langle S \rangle &= \frac{1}{2}\left(\frac{k\eta A_R g}{2\pi z}\right)^2 R \int\int\int\int U_A(\underline{r}_1)\, U_A^*(\underline{r}_2)\, F(\underline{p}_1)\, F^*(\underline{p}_2) \\ &\quad \times \exp\left\{\frac{ik}{2z}\left[\left|\underline{p}_1 - \underline{r}_1\right|^2 - \left|\underline{p}_2 - \underline{r}_2\right|^2\right]\right\} \\ &\quad \times H(\underline{p}_1 - \underline{p}_2, \underline{r}_1 - \underline{r}_2)\, d^2\underline{r}_1 d^2\underline{r}_2 d^2\underline{p}_1 d^2\underline{p}_2 \end{aligned} \tag{26}$$

Lutomirski and Buser (assuming circular apertures) stated that, for large current amplifier gains, g, the noise affecting the system will be dominated by shot noise (since A_R is much larger than the received signal amplitude), thus (28:2158)

$$N = eg^2\eta\,(\pi/4)\, D_R^2 A_R^2 R \tag{27}$$

where

N = noise power at the receiver per unit bandwidth $(W \cdot m^2/Hz)$

e = charge on an electron = 1.602×10^{-19} $(coul)$

D_R = receiver diameter (m)

Lutomirski and Buser also pointed out that, for the problem of cw lasers (as in this analysis), multiplying the noise, N, by the effective cw transmitter output

power, W_A, will result in a final SNR normalized to 1 watt of cw transmitter output power. They defined W_A to be (28:2158)

$$W_A = \int |U_A(\underline{r})|^2 \, d^2\underline{r} \tag{28}$$

They then went one step further to define a constant B such that

$$W_A = BD_T^2 \tag{29}$$

where

B = a constant for a given aperture field $U_A(\underline{r})$

D_T = transmitter diameter (m)

Thus, combining Equations (26), (27) and (28) yields the final result of this section, the general SNR (28:2158):

$$\begin{aligned} \frac{\langle S \rangle}{NW_A} = & \frac{2}{\pi^2}\left(\frac{\eta}{e}\right)\frac{k^2}{D_T^2 D_R^2 z^2}\int\int\int\int U_A'(\underline{r}_1)\, U_A'^*(\underline{r}_2)\, F\left(\underline{p}_1\right) F^*\left(\underline{p}_2\right) \\ & \times \exp\left\{\frac{ik}{2z}\left[\left|\underline{p}_1 - \underline{r}_1\right|^2 - \left|\underline{p}_2 - \underline{r}_2\right|^2\right]\right\} \\ & \times H\left(\underline{p}_1 - \underline{p}_2, \underline{r}_1 - \underline{r}_2\right) d^2\underline{r}_1 d^2\underline{r}_2 d^2\underline{p}_1 d^2\underline{p}_2 \end{aligned} \tag{30}$$

where

$$U_A'(\underline{r}_1)\, U_A'^*(\underline{r}_2) = \frac{\pi D_T^2}{4W_A} U_A(\underline{r}_1)\, U_A^*(\underline{r}_2) \tag{31}$$

Lutomirski and Buser (28) solved the general SNR expression, Equation (30), while assuming infinite Gaussian weighting functions for circular transmitter and receiver apertures. Although convenient in that they provide for a closed form solution of the general SNR equation, the infinite Gaussian weighting functions are not realizable due to their infinite extent. Fried accomplished his analysis of optical heterodyne detection in the presence of atmospheric turbulence while assuming uni-

formly weighted, circular receiving apertures (11:58). However, Fried assumed an infinite plane wave incident on the receiver. For this research effort a finite wave is assumed since a finite transmitter aperture is used. The finite aperture is a realizable scenario, unlike Fried's infinite plane wave assumption.

Unfortunately, as discussed in Appendix B, uniformly weighted circular apertures, when used in the general SNR equation, Equation (30), result in a SNR expression consisting of a single four-fold integral. The problem with the four-fold integral is that it cannot easily be reduced analytically. To use numerical methods to solve the SNR equation, the SNR must be reduced to an expression consisting of fewer than four integrals (due to the limited processing capability of the computer's available). Thus, in order to solve the SNR for the purposes of this feasibility study, square apertures have been assumed. As will be shown, square apertures result in a SNR expression consisting of 2 two-fold integrals.

The dimensions of the apertures, to this point, have been with respect to the diameter of a circular aperture. To make meaningful comparisons from a feasibility standpoint, the dimension of the square aperture will be calculated by considering a circular aperture diameter, and then determining the associated square aperture dimension by equating the areas of the uniformly weighted apertures.

The following sections solve Equation (30) for two cases. First, Lutomirski and Buser's approach (infinite Gaussian weighting functions for the circular transmitter and receiver apertures) is developed. This development is accomplished for two purposes: (1) it provides a baseline for the SNR work that has been accomplished in the past, and (2) it provides a simple, closed form solution to the general SNR expression. This closed form solution can then be evaluated to determine trends upon which the following approach can be compared.

The second approach involves extending the results of the general SNR expression to uniformly weighted, finite, square apertures. This derivation, as discussed above, provides for a more realistic optical communication system than either Fried's

(11) or Lutomirski and Buser's (28) scenarios. In addition, this square aperture SNR will provide the basis for the feasibility evaluation.

It should again be recalled that this study is limited in that it only addresses the losses due to propagation path length and turbulence-induced phase perturbations.

3.2 Effective Aperture Sizes Development

In this section, a closed form solution for the general SNR expression, Equation (30), is derived. From this SNR expression, the relationship between the SNR and the phase coherence length, ρ_o, is evaluated. The results of this evaluation are used in a trends analysis of the SNR versus aperture dimensions. This data is also used in a preliminary investigation of the effect of wavelength on the SNR. Recall that ρ_o describes the separation distance at which the correlation between two points of a propagating optical wave is reduced by e^{-1}.

As developed in Section 3.1, the SNR normalized to 1 watt of cw output power can be written

$$\begin{aligned}\frac{<S>}{NW_A} &= \frac{8}{\pi}\left(\frac{\eta}{e}\right)\frac{k^2}{D_R^2 z^2 W_A}\int\int\int\int U_A(\underline{r}_1)\,U_A^*(\underline{r}_2)\,F(\underline{p}_1)\,F^*(\underline{p}_2) \\ &\quad \times \exp\left\{\frac{ik}{2z}\left[\left|\underline{p}_1-\underline{r}_1\right|^2-\left|\underline{p}_2-\underline{r}_2\right|^2\right]\right\} \\ &\quad \times H(\underline{p}_1-\underline{p}_2,\underline{r}_1-\underline{r}_2)\,d^2\underline{r}_1 d^2\underline{r}_2 d^2\underline{p}_1 d^2\underline{p}_2 \end{aligned} \tag{32}$$

where

η = quantum efficiency of the photodetector (receiver)

e = charge on an electron (*coulombs*)

k = wavenumber = $\frac{2\pi}{\lambda}$ (m^{-1})

$W_A = \int |U_A(\underline{r})|^2 d^2\underline{r}$ $(W \cdot m^2)$

D_R = receiver aperture diameter (m)

z = propagation path length (m)

$\underline{r}_i$ = vector in the source plane (transmitter) (m)

$\underline{p}_i$ = vector in the observation plane (receiver) (m)

$U_A(\underline{r})$ = transmitter aperture field distribution

$F(\underline{p})$ = receiver aperture distribution

$H(\underline{p}_1 - \underline{p}_2, \underline{r}_1 - \underline{r}_2)$ = cross-correlation function (as defined by Equation (23))

Assuming nontruncated Gaussian weighting functions for the circular transmitter and receiver apertures, $U_A(\underline{r})$ and $F(\underline{p})$ can be written

$$\begin{aligned} U_A(\underline{r}) &= U_o \exp\left(\frac{-r^2}{2a^2}\right) \\ F(\underline{p}) &= \exp\left(\frac{-p^2}{2b^2}\right) \end{aligned} \tag{33}$$

where

U_o = field at the center of the transmitting aperture

a = effective transmitter aperture diameter (m)

b = effective receiver aperture diameter (m)

This results in

$$W_A = \int\int_{-\infty}^{\infty} U_o^2 \left[\exp\left(\frac{-r^2}{2a^2}\right)\right]^2 d^2\underline{r} \tag{34}$$

Using the fact that $\underline{r} = r_x\hat{x} + r_y\hat{y}$, and the definite integral relation (20:307)

$$\int_{-\infty}^{\infty} \exp\left(-p^2x^2\right) dx = \frac{\sqrt{\pi}}{p} \tag{35}$$

then

$$W_A = \pi U_o^2 a^2 \tag{36}$$

With respect to $H\left(\underline{p}_1 - \underline{p}_2, \underline{r}_1 - \underline{r}_2\right)$, Lutomirski and Buser state that, when the spherical wave coherence function is Gaussian, the corresponding cross-correlation function is given by (28:2158)

$$H\left(\underline{p}_1 - \underline{p}_2, \underline{r}_1 - \underline{r}_2\right) = \exp\left[-\frac{1}{\rho_o^2}\left|(\underline{p}_1 - \underline{p}_2) - (\underline{r}_1 - \underline{r}_2)\right|^2\right] \tag{37}$$

where ρ_o = phase coherence length (m). The use of a Gaussian distribution for $H\left(\underline{p}_1 - \underline{p}_2, \underline{r}_1 - \underline{r}_2\right)$ is discussed in more detail in Section 3.3.2.

Substituting Equations (33), (36) and (37) into (32) and integrating the quadruple integral over $(-\infty, \infty)$ yields (28:2159)

$$\begin{aligned}\frac{<S>}{NW_A} &= \left(\frac{C}{z^2}\right) a^2 b^2 \\ &\quad \times \left[1 + \frac{k^2\left(a^2+b^2\right)^2}{z^2} + \frac{4\left(a^2+b^2\right)}{\rho_o^2}\left(1 + \frac{3k^2a^2b^2}{z^2}\right) + \frac{12a^2b^2}{\rho_o^4}\right]^{-1}\end{aligned} \tag{38}$$

where $C = 8\left(\frac{\pi}{e}\right)\frac{k^2b^2}{D_R^2}$.

Equation (38) can be reduced further by assuming equal effective transmitter and receiver aperture diameters ($a = b = d$). Thus Equation (38) is reduced to

$$\begin{aligned}\frac{<S>}{NW_A} &= \left(\frac{C}{z^2}\right) d^4 \\ &\quad \times \left[1 + \frac{4k^2d^4}{z^2} + \frac{8d^2}{\rho_o^2}\left(1 + \frac{3k^2d^4}{z^2}\right) + \frac{12d^4}{\rho_o^4}\right]^{-1}\end{aligned} \tag{39}$$

where d = effective transmitter/receiver aperture diameter (m).

3.3 Signal-to-Noise Ratio and Bit Error Rate Development

In this section, a SNR expression for uniformly weighted, finite apertures is derived. First, the expressions for the noise power, N, and the normalization factor, W_A, are derived. (Note that the noise power, N, will differ slightly from that presented in Section 3.1.3 (Equation (27)) due to the square apertures.) Sec-

ond, the SNR equation for square apertures is presented. Following this presentation of the SNR, an assumption is made regarding the cross-correlation function, $H(\underline{p}_1 - \underline{p}_2, \underline{r}_1 - \underline{r}_2)$, and variable substitutions are made in order to reduce the SNR to an expression which allows numerical integration methods to be used to solve the given expression. After the SNR equation is derived, the BER equation is developed.

3.3.1 **Noise Power and Normalization Factor** Under the assumption of uniformly weighted, square apertures, the receiver and transmitter aperture distributions can be written

$$U_A(\underline{r}) = U_o W(\underline{r}) \tag{40}$$

$$F(\underline{p}) = W(\underline{p}) \tag{41}$$

where

U_o = amplitude of the transmitting aperture field

$W(\underline{v}_i)$ is defined as

$$W(\underline{v}_i) = \begin{cases} 1 & \left|\underline{v}_x, \underline{v}_y\right| \leq \frac{D}{2} \\ 0 & \left|\underline{v}_x, \underline{v}_y\right| < \frac{D}{2} \end{cases}$$

where v represents either r or p and i represents the x and y coordinates.

Under the assumption of square apertures, minor adjustments must be made to the noise equation, Equation (27) in Section 3.1.3, which assumed circular apertures. Thus, Equation (27) becomes

$$N = eg^2 \eta D_{Rx} D_{Ry} A_R^2 R \tag{42}$$

where

D_{Rx} = receiver aperture length in the x-direction (m)

D_{Ry} = receiver aperture length in the y-direction (m)

Equation (28) in Section 3.1.3 can now be evaluated as follows:

$$\begin{aligned} W_A &= \int_{-D_{Tx}/2}^{D_{Tx}/2} \int_{-D_{Ty}/2}^{D_{Ty}/2} U_o^2 d\underline{r}_x d\underline{r}_y \\ &= U_o^2 D_{Tx} D_{Ty} \end{aligned} \tag{43}$$

where

D_{Tx} = transmitter aperture length in the x-direction (m)

D_{Ty} = transmitter aperture length in the y-direction (m)

Since square apertures are being assumed, Equations (42) and (43) can further be refined as

$$N = eg^2 \eta D_R^2 A_R^2 R \tag{44}$$

$$W_A = U_o^2 D_T^2 \tag{45}$$

where

$D_R = D_{Rx} = D_{Ry}$

$D_T = D_{Tx} = D_{Ty}$

3.3.2 **Square Aperture Signal-to-Noise Ratio Development** The SNR equation for square apertures can be derived by combining Equations (30), (44) and (45) to yield

$$\begin{aligned} \frac{< S >}{N W_A} &= \frac{k^2}{8\pi^2 z^2} \left(\frac{\eta}{e}\right) \frac{1}{D_T^2 D_R^2} \int\int\int\int W(\underline{r}_1) W^*(\underline{r}_2) W(\underline{p}_1) W^*(\underline{p}_2) \\ &\quad \times \exp\left\{\frac{ik}{2z}\left[\left|\underline{p}_1 - \underline{r}_1\right|^2 - \left|\underline{p}_2 - \underline{r}_2\right|^2\right]\right\} \\ &\quad \times H(\underline{p}_1 - \underline{p}_2, \underline{r}_1 - \underline{r}_2)\, d^2\underline{p}_1 d^2\underline{p}_2 d^2\underline{r}_1 d^2\underline{r}_2 \end{aligned} \tag{46}$$

To solve this expression, a closed form solution for $H(\underline{p}_1 - \underline{p}_2, \underline{r}_1 - \underline{r}_2)$ must first be determined. Several authors present solutions for $H(\underline{p}_1 - \underline{p}_2, \underline{r}_1 - \underline{r}_2)$, but these solutions do not all agree. For example, Yura solved the general expression for $H(\underline{p}, \underline{r})$, Equation (23), by assuming a Kolmogorov spectrum for $\Phi_n(\kappa)$. His resulting expression is (37:1402)

$$H(\underline{p}_1 - \underline{p}_2, \underline{r}_1 - \underline{r}_2) = \exp\left\{-\frac{2.91}{2}k^2 C_n^2 z\left[\left(\frac{3}{8}\right)\frac{\left(\left|\underline{p}_1 - \underline{p}_2\right|^{\frac{8}{3}} - \left|\underline{r}_1 - \underline{r}_2\right|^{\frac{8}{3}}\right)}{\left|(\underline{p}_1 - \underline{p}_2) - (\underline{r}_1 - \underline{r}_2)\right|}\right]\right\} \quad (47)$$

Barakat and Beletic, on the other hand, dispute the use of the Kolmogorov spectrum for $\Phi_n(\kappa)$ (1). According to Barakat and Beletic (as well as sources they cite in their paper), the Kolmogorov approach "...does not satisfy the necessary differentiability conditions at $s = 0$ and thus cannot represent a spatially stationary, isotropic surface" (1:669), where s is defined to be $[(p_1 - p_2)^2 + (r_1 - r_2)^2]^{1/2}$ (1:658). They chose to approximate the phase structure function with a Gaussian distribution. To quote a statement they attribute to another paper by Barakat, (noting that their variable $W_s(\xi, \eta)$ is equivalent to $D_S(\underline{p}, \underline{r})$)

> In view of the fact that no one has really been able to specify the statistical properties of $W_s(\xi, \eta)$ by theory or by experiment, it helps to make some plausible assumptions of the statistical behavior of $W_s(\xi, \eta)$ consistent with the physics of the situation. $W_s(\xi, \eta)$ is taken to possess an underlying Gaussian probability structure. This is purely a working hypothesis backed in part by a central limit theorem argument. (1:654)

As a result of Barakat and Beletic's assertions, as well as the fact that Yura'a expression for $H(\underline{p}_1 - \underline{p}_2, \underline{r}_1 - \underline{r}_2)$ is not separable due to the $\left|(\underline{p}_1 - \underline{p}_2) - (\underline{r}_1 - \underline{r}_2)\right|$ term in the denominator of the exponential function (Equation (47)), a Gaussian cross-correlation function is assumed for this study. It should be noted here that the use of a Gaussian representation for the cross-correlation function is common practice. For example, Lutomirski and Buser, as shown in Section 3.2, assumed a

Table 6. Five-Thirds Versus Gaussian Cross-Correlation Function Parameters

$\lambda(nm)$	$C_n^2(m^{-2/3})$	$z(km)$
1.5	1.2×10^{-15}	100
830	1.2×10^{-15}	100
904	1.2×10^{-15}	100

Gaussian cross-correlation function when deriving the closed form solution to Equation (30). For this study, assuming a Gaussian cross-correlation function allows the SNR of Equation (46) to be reduced to an expression consisting of 2 two-fold integrals (as stated earlier).

The Gaussian cross-correlation function can be written (28:2158)

$$H\left(\underline{p}_1 - \underline{p}_2, \underline{r}_1 - \underline{r}_2\right) = \exp\left[-\frac{1}{\rho_o^2}\left|\left(\underline{p}_1 - \underline{p}_2\right) - \left(\underline{r}_1 - \underline{r}_2\right)\right|^2\right] \tag{48}$$

where ρ_o is the phase coherence length and is defined by Equation (4). (See Appendix A for a discussion of the phase coherence length.)

Note that the assumption of square apertures is adequate from a feasibility standpoint. That is, in the analysis of the feasibility of coherent optical communications in an air-to-air role, the shape of the aperture will not affect the analysis. Note also that the Gaussian cross-correlation function assumption closely approximates Yura's five-thirds cross-correlation function in most cases. Figures 6 through 8 illustrate examples of the two cross-correlation functions for wavelengths of 1.5, 830 and 904 nm, respectively, with the specific parameters used to plot the functions listed in Table 6. In all cases, the difference $\underline{r}_1 - \underline{r}_2$ is assumed to be zero.

With the Gaussian cross-correlation function, the SNR equation can now be written

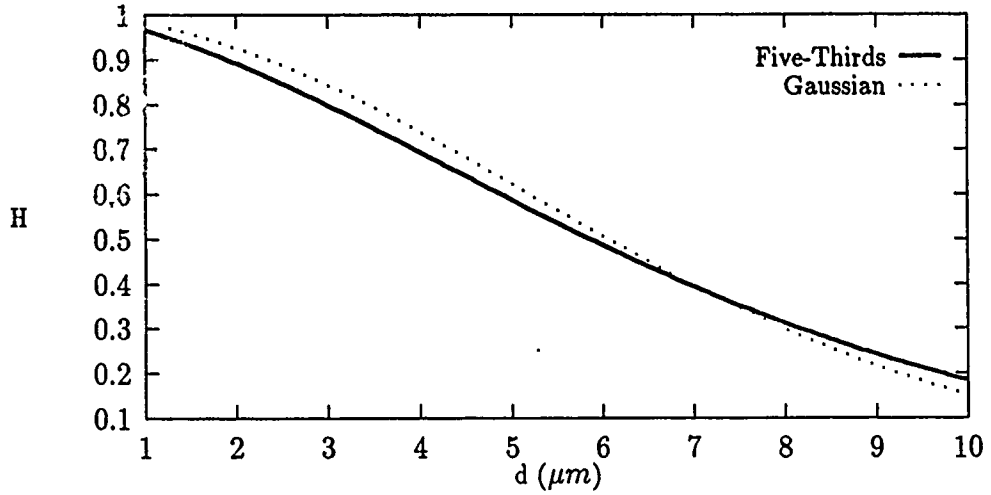

Figure 6. Comparisons of the Five-Thirds and Gaussian Cross-Correlation Functions: $\lambda = 1.5\ nm$

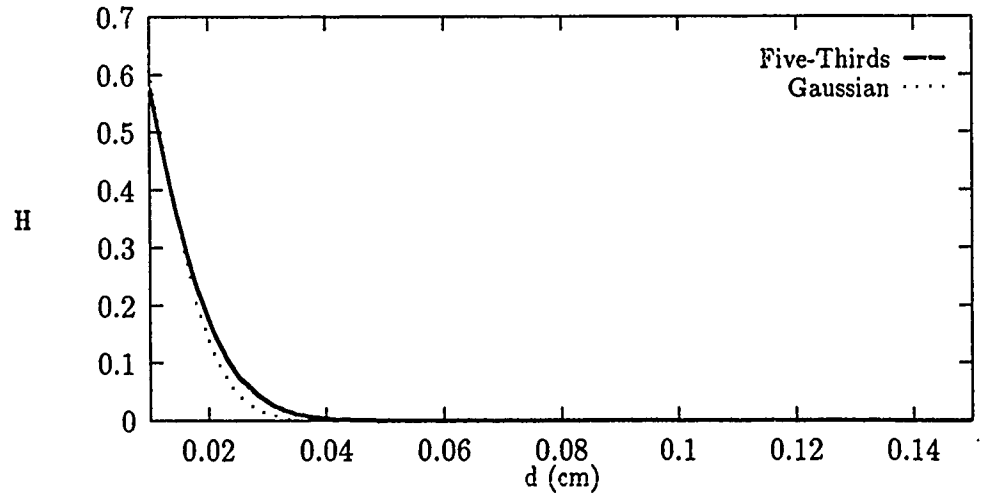

Figure 7. Comparisons of the Five-Thirds and Gaussian Cross-Correlation Functions: λ =830 nm

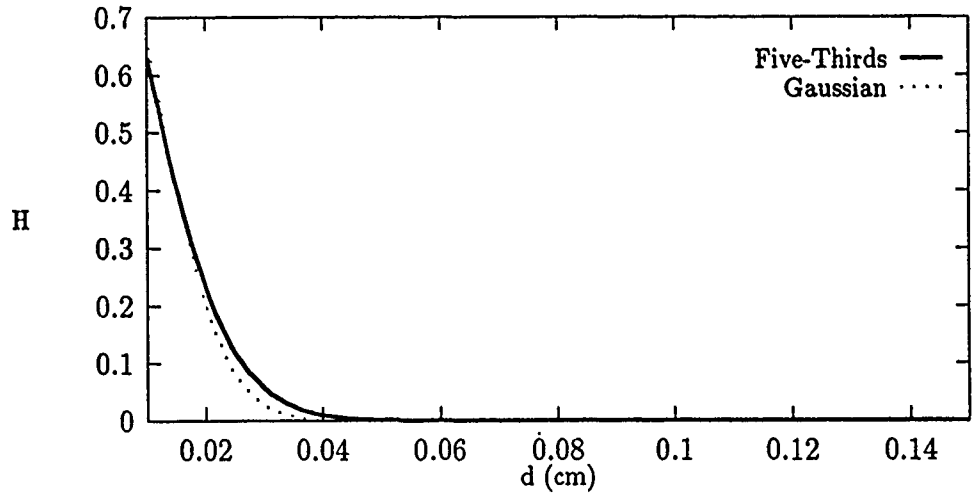

Figure 8. Comparisons of the Five-Thirds and Gaussian Cross-Correlation Functions: λ =904 nm

$$\frac{< S >}{NW_A} = \frac{k^2}{8\pi^2 z^2}\left(\frac{\eta}{e}\right)\frac{1}{D_T^2 D_R^2} \int\int\int\int W(\underline{r}_1)\, W^*(\underline{r}_2)\, W(\underline{p}_1)\, W^*(\underline{p}_2) \times \exp\left\{\frac{ik}{2z}\left[\left|\underline{p}_1 - \underline{r}_1\right|^2 - \left|\underline{p}_2 - \underline{r}_2\right|^2\right]\right\} \times \exp\left[-\frac{1}{\rho_o^2}\left|\left(\underline{p}_1 - \underline{p}_2\right) - \left(\underline{r}_1 - \underline{r}_2\right)\right|^2\right] d^2\underline{p}_1 d^2\underline{p}_2 d^2\underline{r}_1 d^2\underline{r}_2 \qquad (49)$$

where

$\rho_o = (0.545k^2 C_n^2 z)^{-\frac{3}{5}}$ (m)

C_n^2 = refractive index structure constant $(m^{-2/3})$

Note that the structure constant, C_n^2, is generally a function of altitude and is often expressed analytically using the Hufnagel model (23:6-14):

$$C_n^2 = 8.2 \times 10^{-56} V^2 h^{10} \exp\left(-\frac{h}{1000}\right) + 2.7 \times 10^{-16} \exp\left(-\frac{h}{1500}\right) \qquad (50)$$

where

h = altitude above sea level (m)

V = relative rms wind speed (aircraft velocity) (m/s)

In order to reduce Equation (49), sum and difference variable substitutions are made as follows:

$$\begin{aligned} \underline{\Delta x}_i &= \underline{p}_i - \underline{r}_i \\ \underline{\Sigma x}_i &= \frac{1}{2}\left(\underline{p}_i + \underline{r}_i\right) \end{aligned} \tag{51}$$

so that

$$\begin{aligned} \underline{p}_i &= \underline{\Sigma x}_i + \frac{1}{2}\underline{\Delta x}_i \\ \underline{r}_i &= \underline{\Sigma x}_i - \frac{1}{2}\underline{\Delta x}_i \end{aligned} \tag{52}$$

The Jacobian for this transformation is unity.

Substituting Equations (51) and (52) into (49), and rearranging the integrals yields

$$\begin{aligned} \frac{<S>}{NW_A} = & \frac{k^2}{8\pi^2 z^2}\left(\frac{\eta}{e}\right)\frac{1}{D_T^2 D_R^2} \\ & \times \int\int \exp\left[\frac{ik}{2z}\left(|\underline{\Delta x}_1|^2 - |\underline{\Delta x}_2|^2\right)\right] \exp\left\{-\frac{1}{\rho_o^2}\left[|\underline{\Delta x}_1 - \underline{\Delta x}_2|^2\right]\right\} \\ & \times \left\{\int\int W\left(\underline{\Sigma x}_1 - \frac{1}{2}\underline{\Delta x}_1\right) W\left(\underline{\Sigma x}_2 - \frac{1}{2}\underline{\Delta x}_2\right)\right. \\ & \times \left. W\left(\underline{\Sigma x}_1 + \frac{1}{2}\underline{\Delta x}_1\right) W\left(\underline{\Sigma x}_2 + \frac{1}{2}\underline{\Delta x}_2\right) d^2\underline{\Sigma x}_1 d^2\underline{\Sigma x}_2\right\} \\ & \times d^2\underline{\Delta x}_1 d^2\underline{\Delta x}_2 \end{aligned} \tag{53}$$

Rewriting the vectors in terms of their x and y components

$$\begin{aligned} \underline{\Delta x}_i &= \Delta x_{xi}\hat{x} + \Delta x_{yi}\hat{y} \\ \underline{\Sigma x}_i &= \Sigma x_{xi}\hat{x} + \Sigma x_{yi}\hat{y} \end{aligned} \tag{54}$$

The inner integrals of Equation (53) can be solved using a geometric approach. Assuming equal sized, square transmitter and receiver apertures, a new variable, D, can be defined such that $D = D_T = D_R$. Note that this assumption follows from use of the reciprocity theorem. Recall that, as stated explicitly by Lytomirski and Buser, "...a necessary and sufficient condition for instantaneous reciprocity is that the transmitter aperture field and the receiver weighting be *identical*" (28:2157). That is, the transmitter and receiver apertures must be equal in size and have the same form of aperture weighting (in this case, uniform weighting).

Figure 9 shows the geometry used to solve

$$\begin{aligned} Area = \int\int & W\left[\left(\Sigma x_{xi} - \frac{1}{2}\Delta x_{xi}\right)\hat{x} + \left(\Sigma x_{yi} - \frac{1}{2}\Delta x_{yi}\right)\hat{y}\right] \\ & \times W\left[\left(\Sigma x_{xi} + \frac{1}{2}\Delta x_{xi}\right)\hat{x} + \left(\Sigma x_{yi} + \frac{1}{2}\Delta x_{yi}\right)\hat{y}\right] \\ & \times d\Sigma x_{xi} d\Sigma x_{yi} \end{aligned} \tag{55}$$

As shown in Figure 9, the area of overlap is

$$Area = (D - |\Delta x_{xi}|)(D - |\Delta x_{yi}|) \tag{56}$$

where

$$\begin{aligned} -D &\leq \Delta x_{xi} \leq D \\ -D &\leq \Delta x_{yi} \leq D \end{aligned} \tag{57}$$

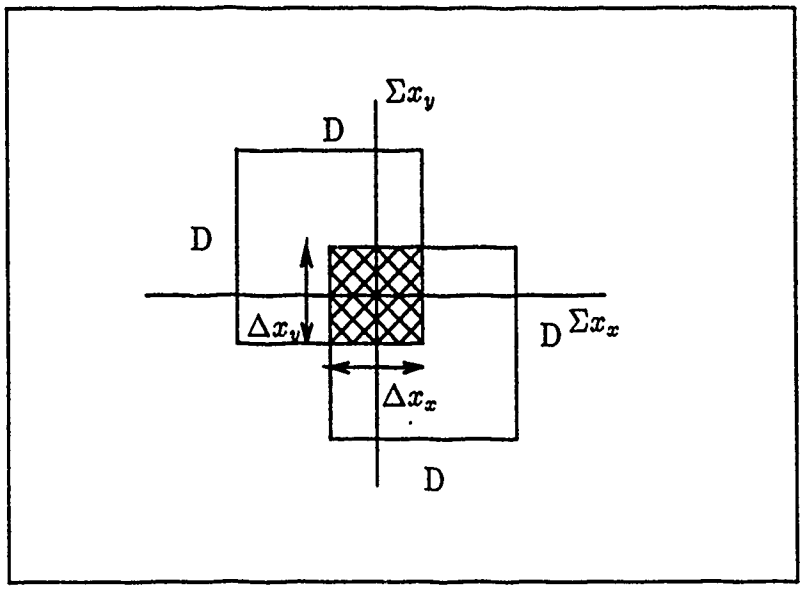

Figure 9. Sum Integral Geometry

Thus, the SNR now becomes

$$\begin{aligned}\frac{<S>}{NW_A} &= \frac{k^2}{8\pi^2 z^2}\left(\frac{\eta}{e}\right)\frac{1}{D^4}\int_{-D}^{D}\int_{-D}^{D}\left(D-|\Delta x_{x1}|\right)\left(D-|\Delta x_{x2}|\right) \\ &\quad\times\exp\left[\frac{ik}{2z}\left(\Delta x_{x1}^2-\Delta x_{x2}^2\right)\right] \\ &\quad\times\exp\left[-\frac{1}{\rho_o^2}\left(\Delta x_{x2}-\Delta x_{x1}\right)^2\right]d\Delta x_{x1}d\Delta x_{x2} \\ &\quad\times\int_{-D}^{D}\int_{-D}^{D}\left(D-|\Delta x_{y1}|\right)\left(D-|\Delta x_{y2}|\right)\exp\left[\frac{ik}{2z}\left(\Delta x_{y1}^2-\Delta x_{y2}^2\right)\right] \\ &\quad\times\exp\left[-\frac{1}{\rho_o^2}\left(\Delta x_{y2}-\Delta x_{y1}\right)^2\right]d\Delta x_{y1}d\Delta x_{y2} \qquad (58)\end{aligned}$$

The above SNR can now be solved using numerical methods. Appendix C discusses the numerical methods used to solve the SNR equation and the resulting computer code.

3.3.3 **Bit Error Rate Development** In this section, the BER equation will be developed. First, the BER will be defined for optical communication systems.

Then the relationship between the BER and the SNR will be discussed. The section will conclude with the BER expression used for this analysis.

The BER, for binary systems, is equivalent to the probability of error, $P(e)$. Assuming the number of ones and zeros transmitted are the same, then the probability of error becomes (33:430)

$$P(e) = \frac{1}{2}\left[P(0/1) + P(1/0)\right] \tag{59}$$

where

$P(0/1)$ = probability of a "0" being received when a "1" is transmitted

$P(1/0)$ = probability of a "1" being received when a "0" is transmitted

For this research effort, a binary phase shift keying (BPSK) modulation scheme will be assumed due to the coherent optical detection. In addition, antipodal signals will be assumed. The $P(e)$ for antipodal BPSK is written (34:158)

$$P(e) = Q\left[\left(\frac{2E_b}{N_o}\right)^{\frac{1}{2}}\right] \tag{60}$$

where

$Q(\cdot)$ = complementary error function = $\frac{1}{\sqrt{2\pi}}\int_x^\infty \exp\left(-\frac{u^2}{2}\right) du$

E_b = signal energy per binary symbol (J)

N_o = additive white Gaussian noise (AWGN) energy (J)

For coherent optical systems, the noise is dominated by shot noise (which has Poisson statistics) rather than thermal noise (which has Gaussian statistics) (28:2158); nevertheless, a Gaussian distribution can be assumed for the noise (33:431).

The quantity E_b/N_o is related to the SNR by (34:158)

$$\frac{E_b}{N_o} = \frac{S}{N_T}\frac{B_s}{R} \tag{61}$$

where

S/N_T = total SNR

S = average signal power $(W \cdot m^2)$

N_T = average noise power $(W \cdot m^2)$

B_s = signal bandwidth (Hz)

R = bit rate (bps)

The total SNR, S/N_T, must now be related to the normalized SNR derived in Section 3.3.2 (Equation (58)). First, the average noise power, N_T, is related to N (noise per unit bandwidth) by

$$N_T = N \times B_s \tag{62}$$

Second, the relationship between the average signal power, S, and the average signal power per watt of cw output power, $\frac{<S>}{W_A}$, can be expressed as

$$S = \frac{< S >}{W_A} P_t \tag{63}$$

where P_t is the output power of the transmitter laser. The transmitter (laser) power, P_t, is related to the effective cw output power by

$$P_t = \frac{W_A}{D_T^2} \tag{64}$$

Examining the expression for $< S >$, Equation (26), from a dimensional analysis viewpoint, it can be seen that $< S >$ is expressed in units of $W \cdot m^4$. Noting that N_T is expressed in units of $W \cdot m^2$, then $\frac{<S>}{N_T}$ is expressed in units of m^2. Thus,

this expression for the average SNR must be normalized by m^{-2}. Recall that W_A, the normalization factor used in developing the normalized SNR for this study, is defined as the intensity of the transmitter field integrated over the transmitter aperture (that is, W_A is a power density) (28:2158). Dividing the average SNR by the aperture dimension will then restore the dimensionless integrity of the SNR. That is,

$$\frac{S}{N_T} = \frac{< S > W_A}{N_T W_A D_T^2} \tag{65}$$

Equations (62) and (65) can be combined to yield

$$\frac{S}{N_T} = \frac{< S >}{N W_A} \frac{W_A}{B_s D_T^2} \tag{66}$$

so that substituting Equations (61) and (66) into Equation (60) results in the BER equation to be evaluated for this feasibility study:

$$P(e) = Q\left[\left(2\frac{< S >}{N W_A}\frac{W_A}{R D_T^2}\right)^{\frac{1}{2}}\right] \tag{67}$$

3.4 Summary

In this chapter, the general SNR was developed. Under the assumptions of uniformly weighted apertures and a Gaussian cross-correlation function for the turbulence, an expression for a closed form solution to the general SNR was obtained. Also, under the assumption of square apertures, a different solution to the SNR was obtained, this one being solved using numerical integration methods. Finally, an expression for the BER was derived based on the BERs relationship to the SNR.

IV. Analysis and Evaluation

This chapter addresses the analysis and evaluation of the SNR and BER data gathered during this research effort. Specifically, this chapter addresses five topics: trends analysis of SNR versus aperture sizes, SNR efficiency factor, SNR versus altitude and aperture sizes, C_n^2 comparison, and BER feasibility analysis. The trends analysis of the SNR versus aperture dimensions investigates the relationship between the SNR and the effective transmitter and receiver diameters when assuming infinite Gaussian weighting functions. In addition, the relationship between the SNR and the phase coherence length, ρ_o, is investigated. The SNR efficiency factor analysis discusses the SNR degradation due to turbulence. The SNR versus altitude and aperture sizes analysis compares the SNRs for various altitudes as well as the SNRs for various aperture sizes. The C_n^2 comparison compares the SNRs determined with the Hufnagel model (23) with Feldmann's (10) experimentally derived C_n^2 data. The BER feasibility analysis discusses the BER data and presents the evaluation of the feasibility analysis.

4.1 Signal-to-Noise Ratio Versus Aperture Size Trends Analysis

In this section, the results of Lutomirski and Buser's closed form solution for the SNR is investigated. Recall that the closed form solution was obtained by assuming infinite, circularly symmetric, Gaussian transmitter and receiver aperture weighting functions.

The reason for investigating the infinite Gaussian weighting functions SNR is two fold. First, the general behavior of the SNR with respect to varying the diameter of the apertures is evaluated. This behavior will assist in determining the expected behavior of the square aperture SNR. Second, the effect of wavelength on the SNR is analyzed.

4.1.1 **Expected Results** The behavior of the infinite Gaussian weighting functions SNR was investigated by Lutomirski and Buser. In their investigation, they found that the SNR improves with increasing transmitter and receiver aperture diameters until each diameter is on the order of the phase coherence length, ρ_o. Once the aperture diameters exceeded ρ_o, the SNR degraded so that any further increase in the aperture diameters does not result in a corresponding increase in the SNR (28:2159). In other words, the SNR will saturate once the aperture diameters increase beyond ρ_o. (Recall Fried's and Chen's saturation discussion from Section 2.3.4.)

The other result expected from this section concerns the behavior of the SNR with respect to the wavelength, λ. Lutomirski and Buser pointed out that, while the SNR for propagation in a vacuum is independent of wavelength, the turbulence affected SNR is not. They discussed the fact that, since ρ_o increases with wavelength, potentially better performance can be expected for longer wavelengths (28:2159).

4.1.2 **Varying Aperture Sizes Results** Table 7 lists the parameters used for this particular analysis. In addition, the phase coherence length, ρ_o, is provided for comparative purposes. Figures 10 through 12 illustrate the results of Equation (39). (Note that, for these figures, the physical receiver aperture diameter is assumed to equal the effective receiver aperture diameter, and W represents W_A.)

Figures 10 through 12 show the normalized SNR, in dB, with respect to the effective aperture diameter, d. Figure 10 illustrates the case where the SNR has reached saturation for all aperture diameters since, from Table 7, ρ_o is on the order of micrometers. Figures 11 and 12 show similar results for the $z = 100\ km$ and $z = 160\ km$ data points (in which ρ_o is slightly less than 1 cm). However, for the $z = 40\ km$ data points, ρ_o is equal to, or slightly greater than, 1 cm. In this case, it can be seen that the SNR saturates at approximately 3 dB above the SNR for $d = 1\ cm$. This is in agreement with Fried's and Chen's findings as discussed in

Table 7. Infinite Gaussian Aperture Signal-to-Noise Ratio Parameters

Figure	$\lambda(nm)$	$C_n^2(m^{-2/3})$	$z(km)$	$\rho_o(cm)$
10	1.5	1.625E-15	40	5.30E-4
			100	3.03E-4
			160	2.31E-4
11	830	1.625E-15	40	1.0
			100	0.7
			160	0.5
12	904	1.625E-15	40	1.1
			100	0.7
			160	0.5

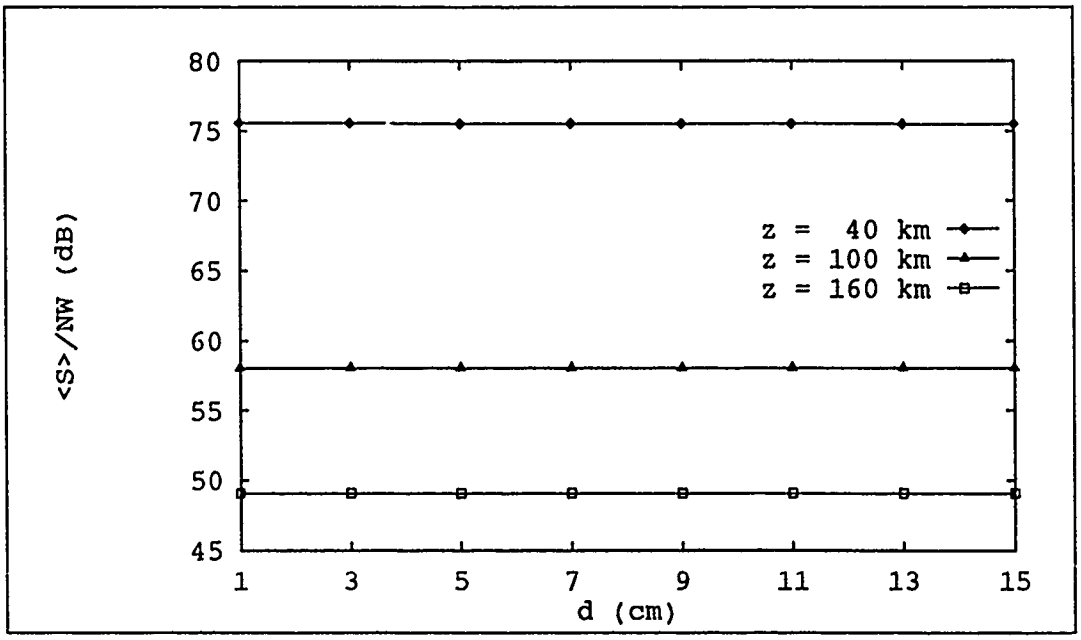

Figure 10. Infinite Gaussian Aperture Signal-to-Noise Ratio: $\lambda = 1.5\ nm$

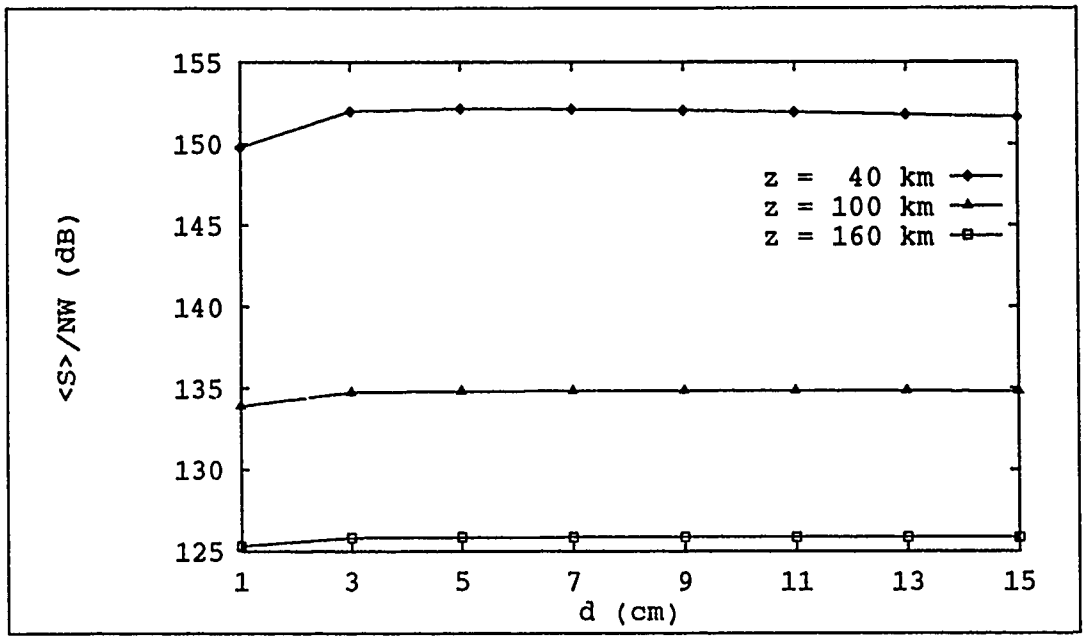

Figure 11. Infinite Gaussian Aperture Signal-to-Noise Ratio: $\lambda = 830\ nm$

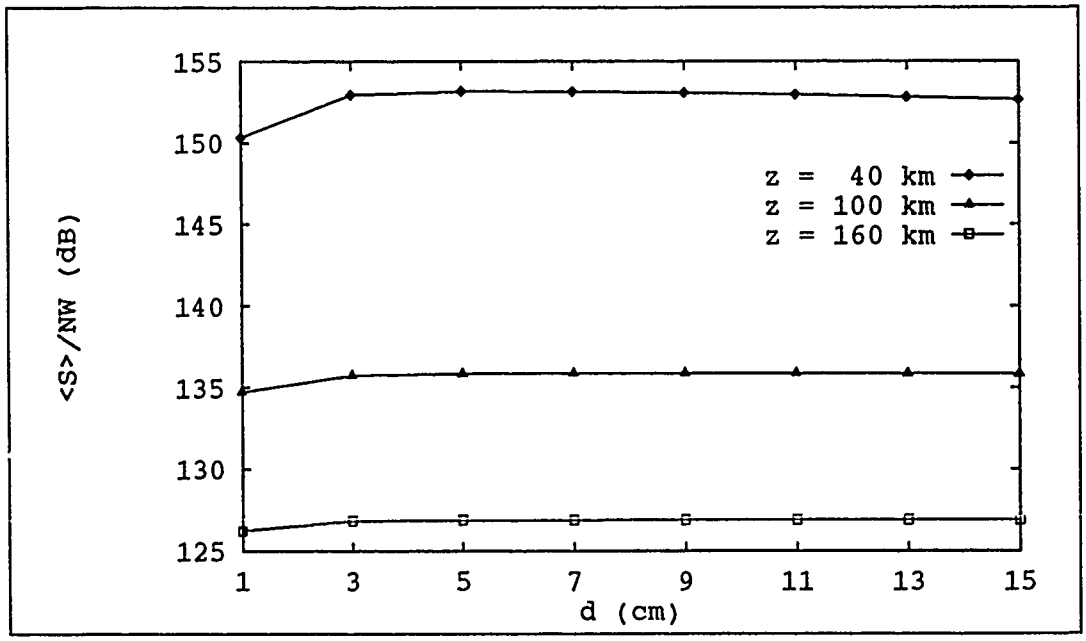

Figure 12. Infinite Gaussian Aperture Signal-to-Noise Ratio: $\lambda = 904\ nm$

Section 2.3.4. Thus, with respect to varying aperture sizes, the results obtained are as expected.

4.1.3 **Wavelength Evaluation Results** Referring to Figures 10 through 12, the results with respect to wavelength are also as expected. Specifically, Figures 10 and 11 depict the significantly better performance of $\lambda = 830\ nm$ and $\lambda = 904\ nm$ than the $\lambda = 1.5\ nm$ performance depicted by Figure 10. As a consequence of these results, and noting that the performance of the 904 nm wavelength is slightly better than 830 nm, only the 904 nm wavelength will be considered for the remainder of this study.

4.1.4 **Summary** The behavior of the infinite Gaussian weighting functions SNR, as derived by Lutomirski and Buser, was investigated. It was shown that the derived SNR performed as expected with respect to increasing aperture sizes, saturation behavior and wavelength.

4.2 Signal-to-Noise Ratio Efficiency Factor Analysis

The remainder of this chapter addresses the SNR expression that was derived with the assumptions of uniformly weighted, finite, square apertures. In this section, a SNR performance measure is analyzed. Specifically, a SNR efficiency factor, α, is defined to be the ratio of the SNR with turbulence effects considered to the SNR without turbulence effects considered. This factor, α, is thus one measure of the SNR degradation due to turbulence. The SNR efficiency analysis is performed to verify that the derived SNR expression using uniformly weighted, finite, square apertures behaves in a manner consistent with Fried's (infinite plane wave incident on a finite receiver aperture) and Lutomirski and Buser's (infinite Gaussian transmitter and receiver aperture weighting functions) results.

In particular, this section will briefly address the overall efficiency of the uniformly weighted, finite, square apertures SNR. This overall efficiency is interesting

Table 8. Best, Medium and Worst Case Signal-to-Noise Ratio Efficiencies Parameters

	$\lambda(nm)$	$D(cm)$	$V(m/s)$	$h(m)$
best	904	1	218	5000
medium	904	7.5	218	7500
worst	904	15	218	10000

primarily in that it provides a baseline for the remaining discussions. The behavior of α with respect to varying aperture sizes and altitudes is then examined. Finally, the relationship between α and the normalized SNR is discussed.

4.2.1 **Expected Results** As briefly discussed in Section 4.1.1, the SNR performance is expected to degrade when a circular aperture diameter exceeds the phase coherence length, ρ_o. This behavior can easily be extended to the case of square apertures. That is, the SNR performance is expected to degrade when the square aperture side length exceeds ρ_o. Also, consistent with Fried's and Chen's saturation discussion, it is expected that, as α decreases, the SNR approaches the saturation limit (for the particular parameters used).

4.2.2 **Overall Efficiency** Figure 13 shows the best, medium and worst efficiencies calculated for a wavelength of 904 nm. As can be seen, by varying the aperture dimension, D, and the altitude, h, the efficiency, α, ranges from 0.16 to 67.2 percent. Table 8 contains the parameters used in plotting Figure 13.

The importance of Figure 13 is best understood when compared to the applicable phase coherence lengths. Table 9 shows the value of ρ_o for various altitudes and path lengths. By comparing these values with Figure 13, it becomes apparent why the best case ($D = 1$ cm) results in such a significantly better α than the other two cases ($D = 7.5$ cm, $D = 15$ cm). The phase coherence lengths are less than 1 cm for the medium and worst case efficiencies; whereas, the phase coherence length

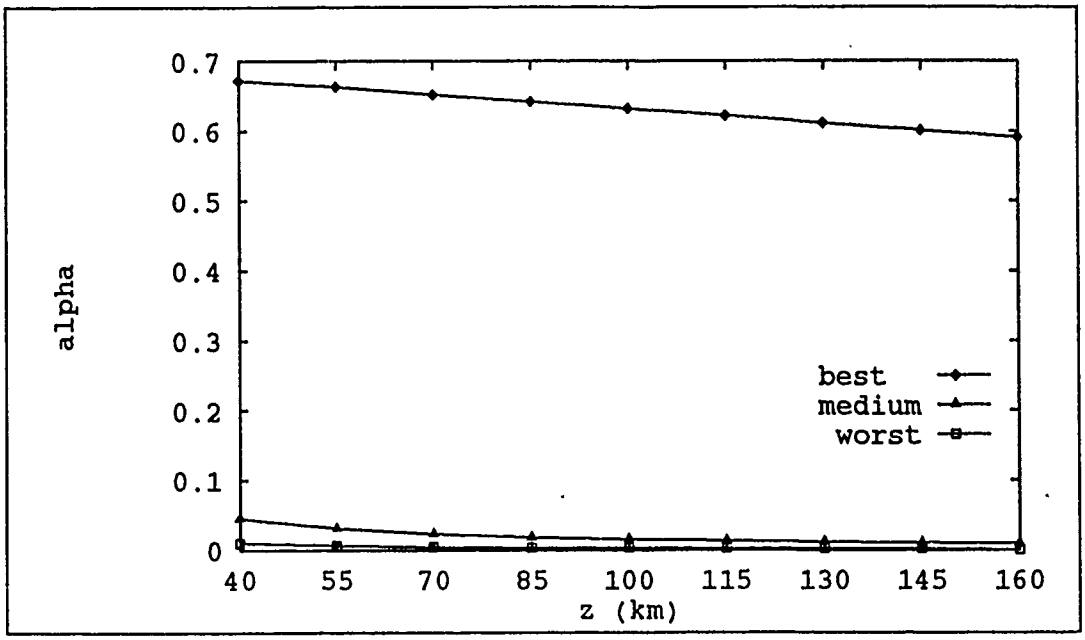

Figure 13. Best, Medium and Worst Case SNR Efficiencies: $\lambda = 904\ nm$

for the best case is 3.40 cm.

Thus, the behavior of α is as predicted in Section 4.2.1. It is seen that, the more the square aperture side length exceeds ρ_o, the worst the efficiency, α.

4.2.3 **Alpha Versus Varying Parameters** This section examines the behavior of α while varying different parameters as detailed in Table 10. The results

Table 9. Phase Coherence Lengths: $\lambda = 904\ nm$, $V = 218\ m/s$

$h(m)$	5000	7500	10000	12500
$z(km)$	$\rho_o(cm)$	$\rho_o(cm)$	$\rho_o(cm)$	$\rho_o(cm)$
40	3.40	1.37	1.09	1.28
60	2.67	1.07	0.86	1.01
80	2.24	0.90	0.72	0.85
100	1.96	0.79	0.63	0.74
120	1.76	0.71	0.56	0.66
140	1.60	0.64	0.51	0.60
160	1.48	0.60	0.48	0.56

Table 10. Alpha Versus Varying Parameters Cases

Figure	$D(cm)$	$h(m)$	$z(km)$
14	varying	5000	40-160
15	varying	8750	40-160
16	varying	12500	40-160
17	varying	5000-12500	40
18	varying	5000-12500	100
19	varying	5000-12500	160
20	1	varying	40-160
21	7.5	varying	40-160
22	15	varying	40-160

are presented graphically in Figures 14 through 22. First, the behavior of α with respect to aperture size is examined. Figures 14 through 19 illustrate this behavior for both increasing path length (Figures 14 through 16) and increasing altitude (Figures 17 through 19).

As can be seen from Figures 14 through 16, and recalling the ρ_o values defined in Table 9, α decreases with increasing aperture side length, as expected. However, it is interesting to note that the relative decrease in α is less at the longer path lengths, z. This is due to the dependence of ρ_o on z (37:1403):

$$\rho_o = \left(0.545k^2C_n^2z\right)^{-\frac{3}{5}} \tag{68}$$

That is, as z increases, ρ_o decreases.

Figures 17 through 19 also illustrate the behavior of α with increasing aperture side length. What is interesting to note here, however, is the behavior of α with respect to increasing altitude, h (for any given aperture side length). It is seen that α does not continually decrease as h increases, but rather reaches a minimum at about 10000 m and then starts increasing again. This behavior, however, is as expected when considering the behavior of the turbulence strength, C_n^2. For all of these figures, C_n^2 was modeled using the Hufnagel model. As illustrated in Figure 23,

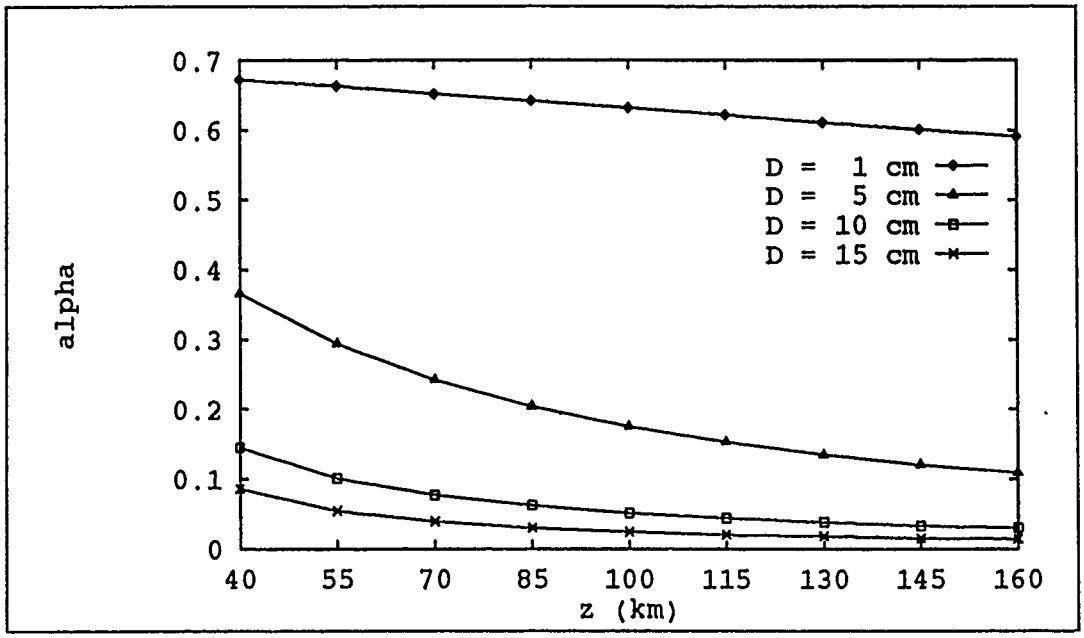

Figure 14. Alpha Versus Path Length with Varying Aperture Size:$h = 5000\ m$

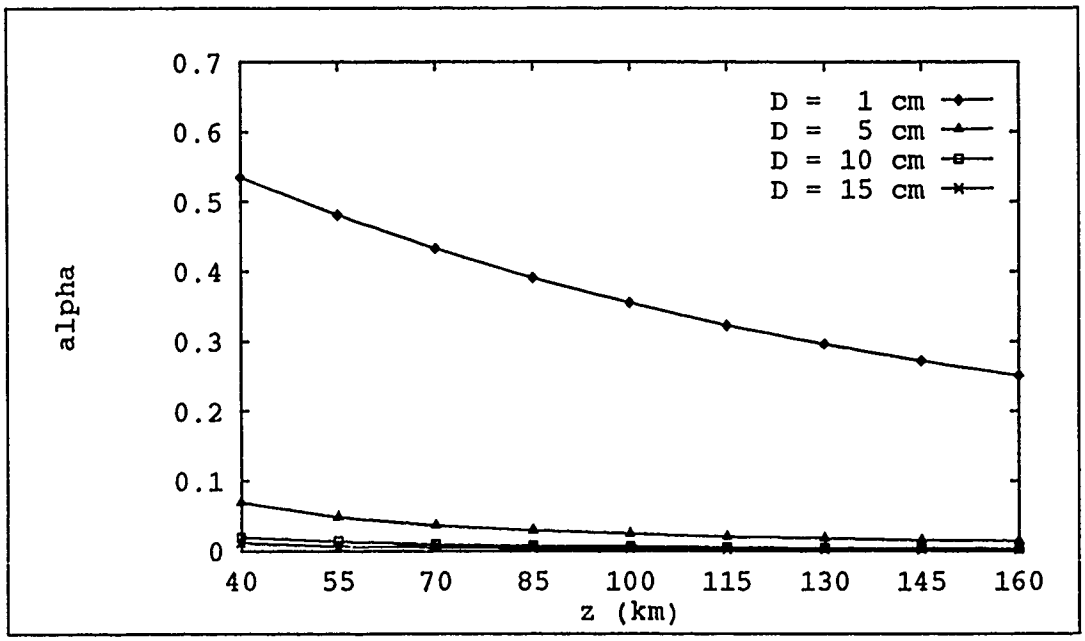

Figure 15. Alpha Versus Path Length with Varying Aperture Size:$h = 8750\ m$

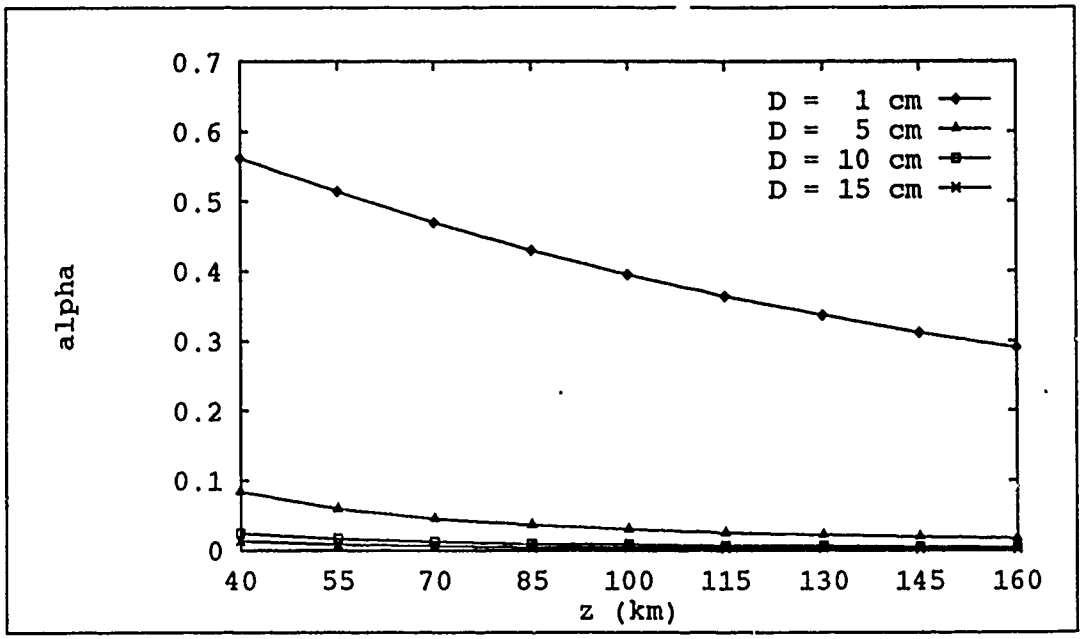

Figure 16. Alpha Versus Path Length with Varying Aperture Size:$h = 12500\ m$

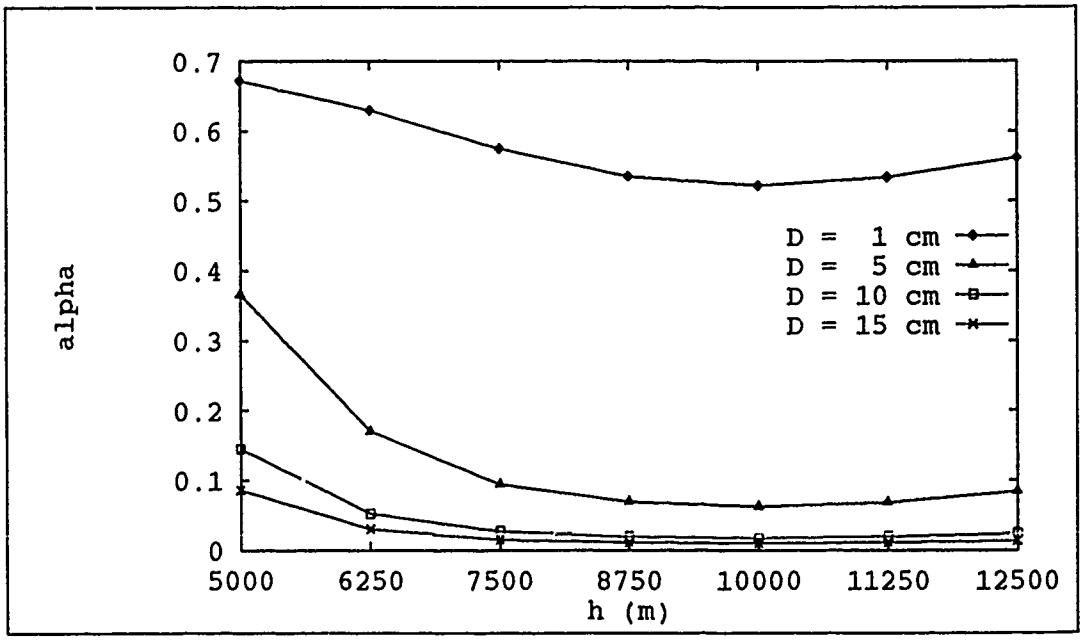

Figure 17. Alpha Versus Altitude with Varying Aperture Size:$z = 40\ km$

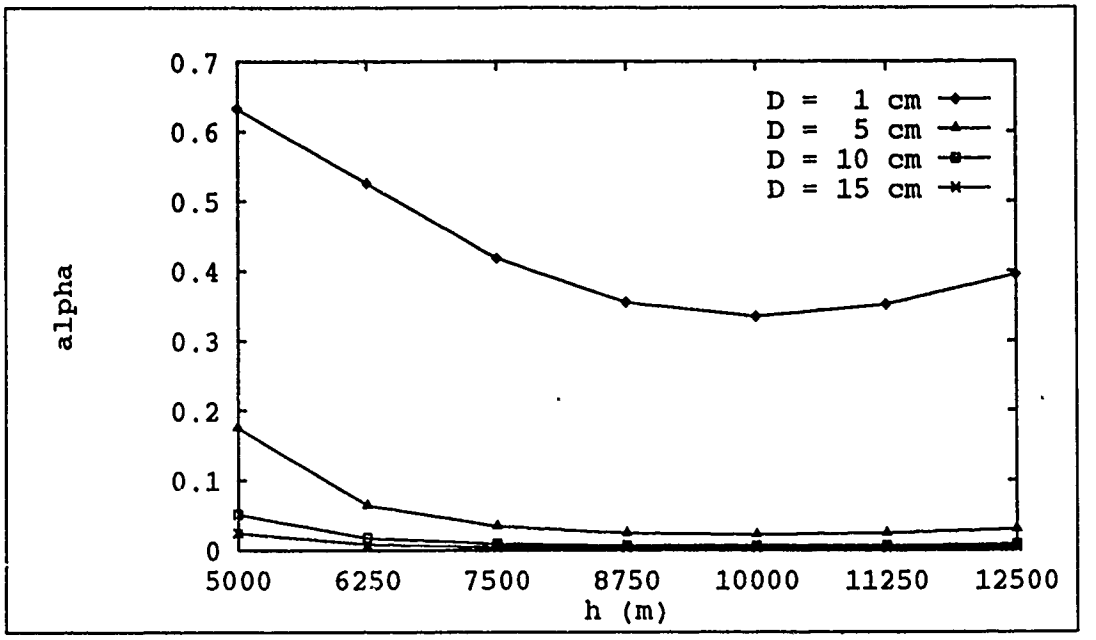

Figure 18. Alpha Versus Altitude with Varying Aperture Size:$z = 100\ km$

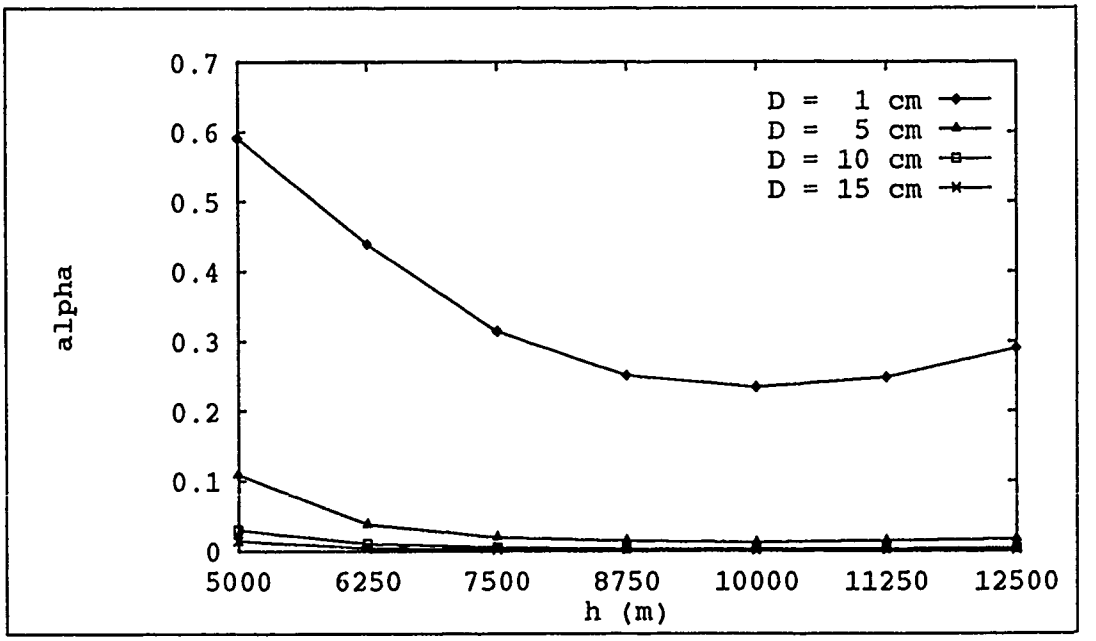

Figure 19. Alpha Versus Altitude with Varying Aperture Size:$z = 160\ km$

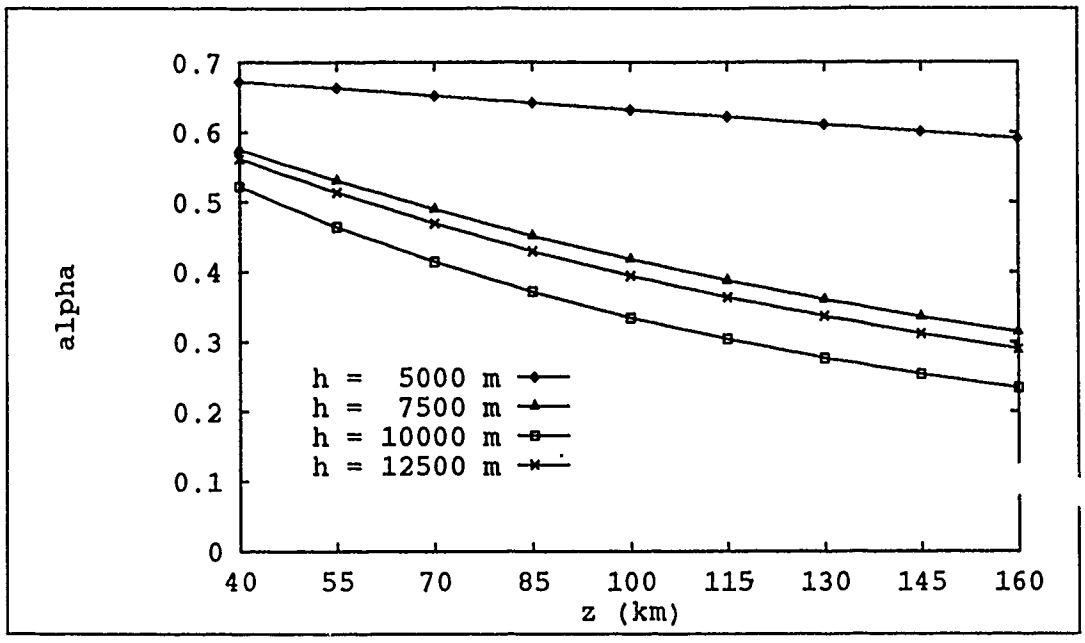

Figure 20. Alpha Versus Path Length with Varying Altitude: $D = 1\ cm$

the Hufnagel model characterizes the turbulence strength as increasing over 5000 m to about 10000 m, then decreasing to 12500 m. (A good discussion on the behavior of C_n^2 can be found in the *Infrared Handbook* (23), Chapter 6.)

The behavior of α with respect to varying altitude is further illustrated in Figures 20 through 22. Again, this behavior is as expected.

4.2.4 **Alpha Versus Turbulence Affected Signal-to-Noise Ratio** As a final evaluation of the behavior of α, this section examines the relationship between α and the normalized, turbulence affected SNR. To reiterate, the purpose for this evaluation is to verify that the uniformly weighted, square aperture SNR derived in this study produces results consistent with previous studies. Table 11 presents the values of α and the normalized SNR for varying aperture dimensions and altitudes, while maintaining a constant path length. Specifically, Table 11 investigates the case for $\lambda = 904\ nm$, $V = 218\ m/s$, and $z = 100\ km$.

As can be seen, Table 11 illustrates the expected behavior of both α and the normalized SNR with respect to ρ_o. That is, as the aperture side length, D, is

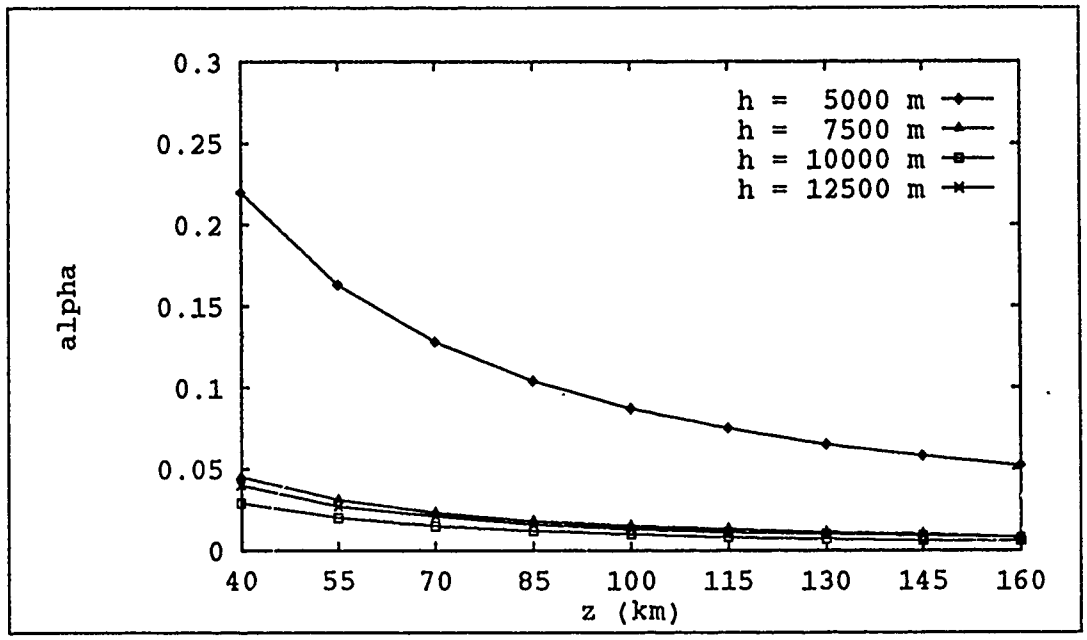

Figure 21. Alpha Versus Path Length with Varying Altitude: $D = 7.5\ cm$

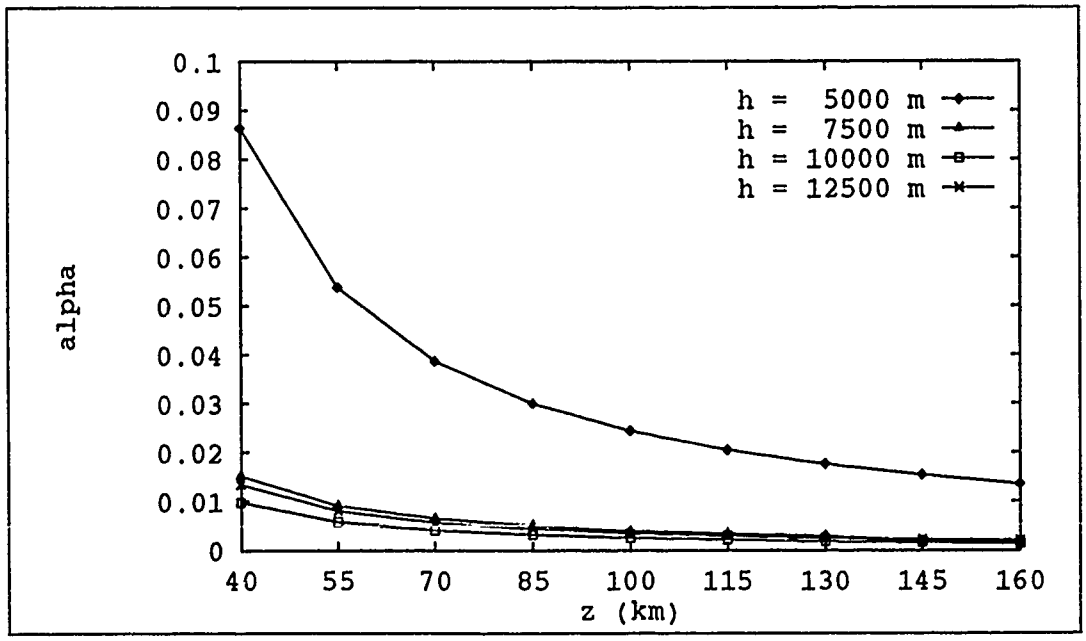

Figure 22. Alpha Versus Path Length with Varying Altitude: $D = 15\ cm$

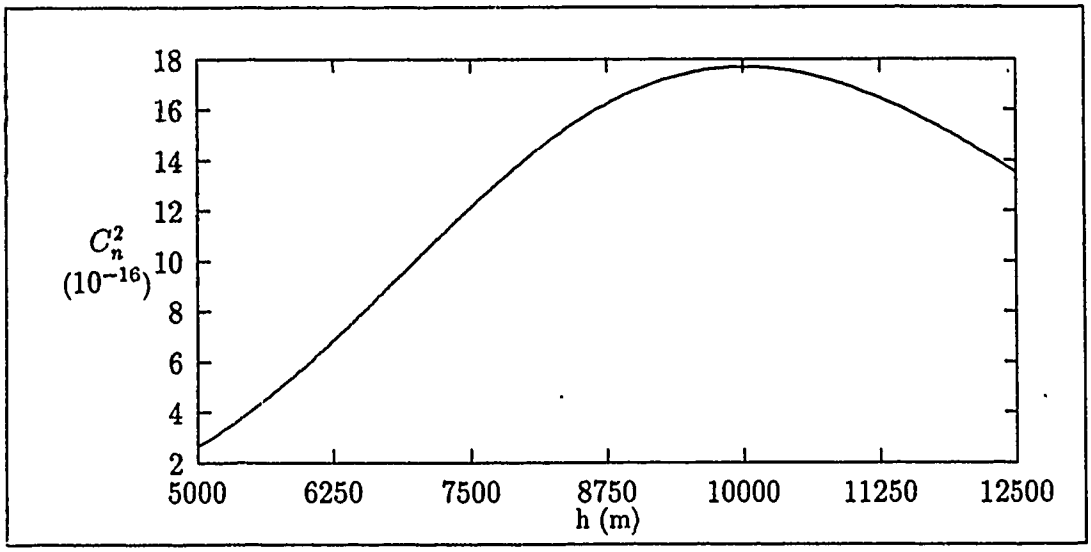

Figure 23. Plot of Turbulence Strength Characteristics Using the Hufnagel Model

Table 11. Alpha Versus Signal-to-Noise Ratio: $\lambda = 904\ nm$, $V = 218\ m/s$, $z = 100\ km$

$h(m)$	$\rho_o(cm)$	$D(cm)$	α	$< S > /NW_A\ (dB)$
5000	1.96	1	6.318E-1	163.83
		5	1.749E-1	172.22
		10	5.136E-2	172.88
		15	2.440E-2	173.01
7500	0.79	1	4.186E-1	162.04
		5	3.355E-2	165.05
		10	8.684E-3	165.17
		15	4.029E-3	165.19
10000	0.63	1	3.353E-1	161.08
		5	2.165E-2	163.15
		10	5.552E-3	163.22
		15	2.571E-3	163.24
12500	0.74	1	3.954E-1	161.79
		5	2.963E-2	164.51
		10	7.648E-3	164.61
		15	3.546E-3	164.63

increased beyond the phase coherence length, ρ_o, α decreases while the normalized SNR begins to saturate. Note that, if the normalized SNR data were extrapolated for the case of $D = \rho_o$, it appears that the saturated SNR is about 3 dB greater (as predicted by Chen (5)).

4.2.5 **Summary** The behavior of the SNR efficiency factor, α, was examined. It was shown that α behaved as expected in all respects. It was further shown that the behavior of α versus the normalized SNR supports the findings of Fried (11) and Chen (5) with respect to a SNR saturation limit.

4.3 Signal-to-Noise Ratio Versus Altitude and Aperture Sizes

In the previous section, α versus varying altitudes and aperture sizes was examined. In this section, attention is focused on the behavior of the turbulence affected SNR while varying the altitude and aperture sizes. This investigation of the turbulence affected SNR is accomplished for the purpose of again verifying the consistency of this study's results with previous results (such as Fried's (11) and Lutomirski and Buser's (28)).

4.3.1 **Expected Results** The results expected from the uniformly weighted, square aperture SNR versus altitude and aperture size are the same as the expected results of Section 4.2.1. To reiterate, as the aperture side length, D, is increased beyond the phase coherence length, ρ_o, the SNR is expected to reach a saturation limit (which is about 3 dB greater than the SNR achieved for $D = \rho_o$). In addition, as the altitude is increased, the SNR is expected to behave in a manner inversely related to the turbulence strength, C_n^2.

4.3.2 **Signal-to-Noise Ratio Versus Altitude** First, the behavior of the SNR with respect to altitude is examined. Table 12 lists the parameters used for Figures 24 through 27. These figures illustrate the behavior of the turbulence affected

Table 12. Signal-to-Noise Ratio Versus Altitude Parameters

Figure	$\lambda(nm)$	$V(m/s)$	$D(cm)$	$z(km)$	$W_A(mW)$
24	904	218	1	Varying	1
25	904	218	10	Varying	1
26	904	218	Varying	40	1
27	904	218	Varying	100	1

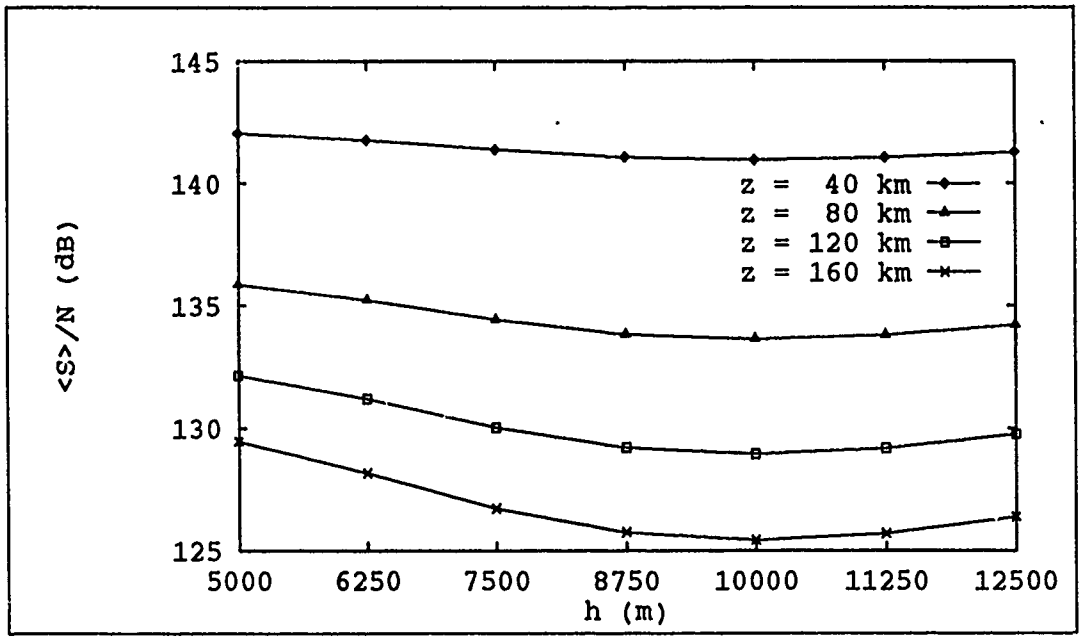

Figure 24. Signal-to-Noise Ratio Versus Altitude with Varying Path Length - $D = 1\ cm$

SNR with respect to altitude. As discussed in Section 4.2.2, the behavior shown in Figures 24 through 27 is as expected. That is, as the altitude increases from 5000 m to 10000 m, the SNR decreases; whereas, as the altitude increases further to 12500 m, the SNR increases. Note that this is true regardless of path length and aperture size.

4.3.3 **Signal-to-Noise Ratio Versus Aperture Size** The behavior of the SNR with respect to aperture size is examined here. Figures 26 through 27 also illustrate the behavior of the turbulence affected SNR with respect to aperture size.

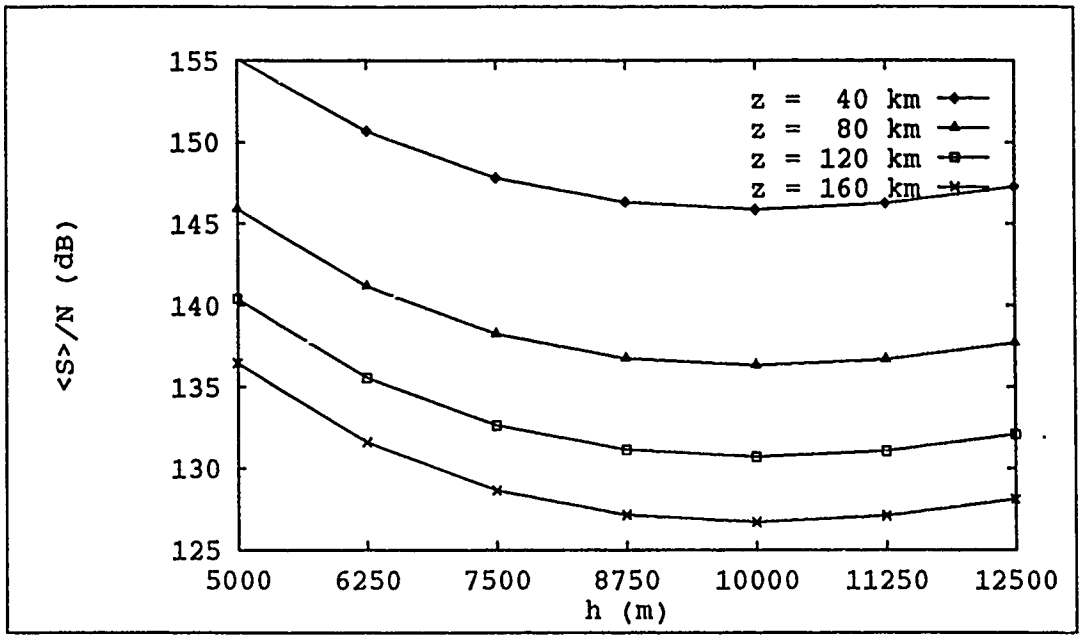

Figure 25. Signal-to-Noise Ratio Versus Altitude with Varying Path Length - $D = 10\ cm$

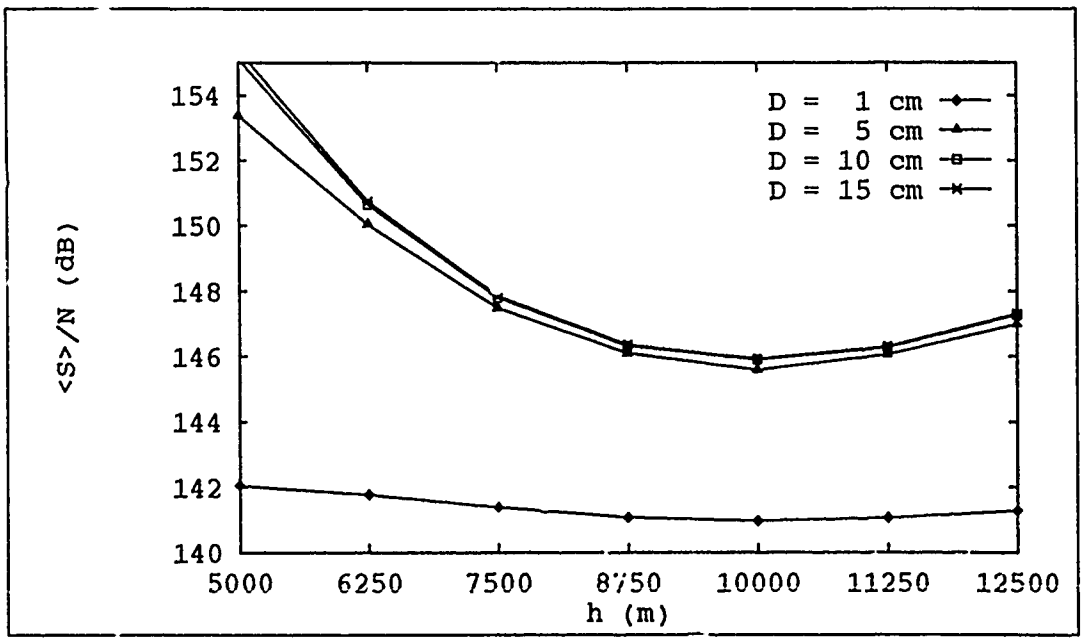

Figure 26. Signal-to-Noise Ratio Versus Altitude with Varying Aperture Size - $z = 40\ km$

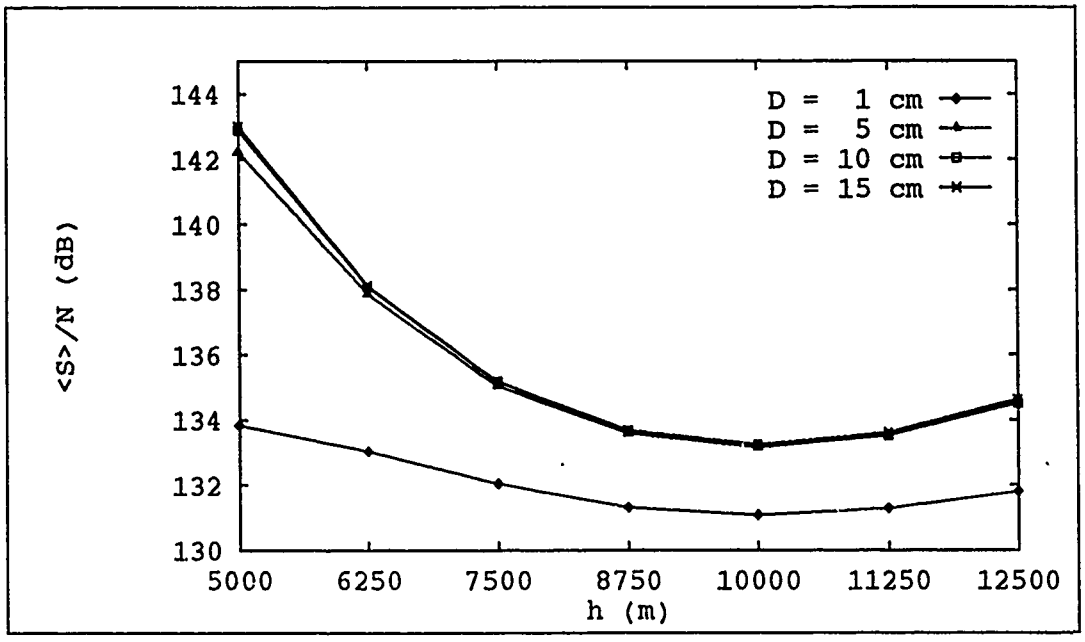

Figure 27. Signal-to-Noise Ratio Versus Altitude with Varying Aperture Size - $z = 100\ km$

As can be seen, these figures support the findings of Section 4.2.2. It is also interesting to observe the behavior of the SNR with respect to aperture side length in a format similar to Fried's and Chen's saturation limit figure, Figure 3. Figure 28 shows the normalized SNR versus D/ρ_o for $\lambda = 904\ nm$, $h = 7500\ m$, $z = 100\ km$, and $\rho_o = 0.79\ cm$. As can be seen, Figure 28 presents a very close approximation to Figure 3.

4.3.4 **Summary** The behavior of the turbulence affected SNR for uniformly weighted, finite, square apertures was examined. It was shown that the SNR performed as expected for both cases considered: varying altitude and varying aperture sizes.

4.4 Signal-to-Noise Ratio Versus C_n^2 Comparison

In this section, the SNRs determined using the Hufnagel model (23) for C_n^2 are compared to the SNRs determined using Feldmann's experimentally derived C_n^2 (10).

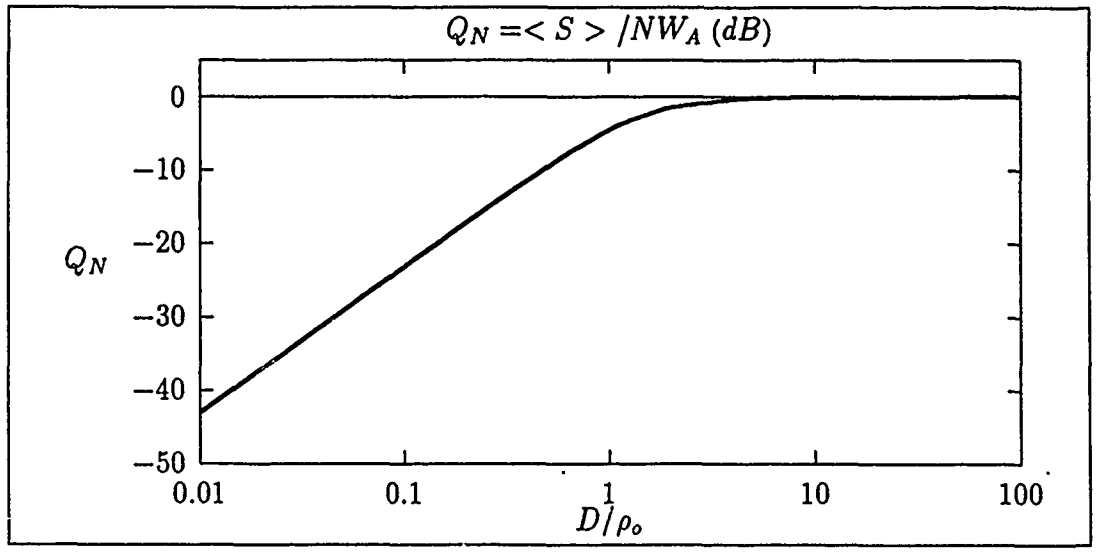

Figure 28. Normalized Signal-to-Noise Ratio Versus Normalized Aperture Size

Table 13. C_n^2 Comparison (10:55,58)

Constants	$D = 10.01cm$	$W_A = 1.0mW$	$\lambda = 904nm$	$C_n^2\ (m^{-2/3})$		$< S > /N\ (dB)$	
Run	$h(m)$	$z(m)$	$V(m/s)$	Feldmann	Hufnagel	Feldmann	Hufnagel
1	9754	46300	180.0	5.0E-13	1.2E-15	114.55	145.86
2	9144	46300	198.1	5.0E-13	1.4E-15	114.55	145.06
3	3048	46300	141.0	2.5E-13	4.1E-17	118.15	159.54
4	3353	24076	154.3	5.0E-14	4.1E-17	135.62	166.28
5	6096	46300	170.0	5.0E-14	3.8E-16	126.53	151.54
6	12497	46300	159.5	5.0E-14	7.2E-16	126.53	148.41

This comparison is made in an effort to determine the impact on the SNR when a theoretical model is used to determine C_n^2 as opposed to experimentally derived C_n^2. Table 13 lists the parameters used and presents the resulting SNRs. As can be see Feldmann's C_n^2 values are 100 to 1000 times greater than the C_n^2 predicted by . Hufnagel model; that is, Feldmann predicts much stronger turbulence for all altitudes than the Hufnagel model. As a result, the SNRs determined with Feldmann's C_n^2 are much smaller.

Several factors should be considered when evaluating the C_n^2 comparison results. First, the Hufnagel model is just that, a model. It does not accurately match the observed fine structure of the turbulence, but it is more accurate than other

models used to predict C_n^2 (23:6-15). Second, C_n^2 is a continuously varying feature of turbulence. For example, wind sheer, time of day and temperature inversions all affect the turbulence strength (23:6-13 - 6-14). Finally, Feldmann's data is based on a "best-fit" approach. As stated by Feldmann, "...values of C_n^2 were consistently larger than predicted by the Hufnagel model but, for the most part remained within the accepted range of variability" (10:62).

4.5 Bit Error Rate Analysis

In this section, the heart of this study is discussed: feasibility. First, the BER data collected is analyzed with respect to effective cw output power and data rate. Then, the feasibility of an air-to-air optical heterodyne communication system is evaluated. However, before this analysis is presented, several concerns need to be addressed. First, it should be emphasized again that this analysis only considers the losses due to propagation path length and the turbulence-induced phase perturbations. As will be discussed in more detail shortly, the losses due to beam steering, beam spreading, and scintillation are ignored. Also, the transmitter and receiver, as well as receiver tracking, are assumed to be ideal. Further, as was shown in Section 4.4, the Hufnagel model for C_n^2 predicts SNRs consistently larger (on the order of 30 dB) than Feldmann's experimentally derived C_n^2 data. All of these concerns serve to reduce the required effective cw output power, and thus the transmitter (laser) power, necessary to achieve the desired BERs. This will be addressed further in Section 4.5.3.

4.5.1 **Expected Results** Consistent with the SNR results, the BERs are expected to "saturate" for aperture side lengths, D, greater than ρ_o. That is, the ranges at which some defined BER is achieved should not increase appreciably as D increases for $D > \rho_o$.

4.5.2 **Bit Error Rate Data Analysis** The BER data will follow the same trends as the turbulence affected SNR. This is obvious upon examination of the relationship between the BER and SNR:

$$BER = Q\left(\left[\frac{SNR}{R}\right]^{\frac{1}{2}}\right) \tag{69}$$

where

$Q(\cdot)$ = complementary error function

R = data rate (bps)

It is also obvious from Equation (69) that as the data rate, R, increases, the BER decreases.

Tables 14 through 17 present examples of these trends. In these tables, the data points presented represent the range (km) at which the appropriate data rate is obtained.

4.5.3 **Air-to-Air Optical Heterodyne Communication System Feasibility** The results of this analysis demonstrate that an air-to-air optical heterodyne communication system is feasible. However, this study did not consider many of the additional losses that would affect the communication link and the system, such as beam steering, beam spreading, scintillation and the receiver and transmitter performance characteristics. All of these considerations will, of course, reduce the overall SNR and consequently the BER. Further reductions in the SNR and BER may be realized when more accurate turbulence strength, C_n^2, factors are considered. The question becomes, when the additional loss considerations are taken into account, will acceptable BERs still be obtained for the ranges presented in this study.

To answer this question, the effective cw transmitter output powers, W_A, used to generate Tables 14 through 17 need to be examined. Recall that W_A is related to

Table 14. Bit Error Rate Trends - R = 20000 bps: "+" - Range greater than 160 *km*; "-" - Range less than 40 *km*

BER			10^{-5}				10^{-10}			
	$h(m)$		5000	7500	10000	12500	5000	7500	10000	12500
$D(cm)$	$W_A(nW)$	$P_t(nW)$								
1	0.1	1000	+	+	+	+	+	+	152	+
	0.5	5000	+	+	+	+	+	+	+	+
	1.0	10000	+	+	+	+	+	+	+	+
	5.0	50000	+	+	+	+	+	+	+	+
7.5	0.1	17.78	+	+	+	+	+	+	+	+
	0.5	88.89	+	+	+	+	+	+	+	+
	1.0	177.78	+	+	+	+	+	+	+	+
	5.0	888.89	+	+	+	+	+	+	+	+
15	0.1	4.44	+	+	+	+	+	+	+	+
	0.5	22.22	+	+	+	+	+	+	+	+
	1.0	44.44	+	+	+	+	+	+	+	+
	5.0	222.22	+	+	+	+	+	+	+	+

Table 15. Bit Error Rate Trends - R = 40000 bps: "+" - Range greater than 160 *km*; "-" - Range less than 40 *km*

BER			10^{-5}				10^{-10}			
	$h(m)$		5000	7500	10000	12500	5000	7500	10000	12500
$D(cm)$	$W_A(nW)$	$P_t(nW)$								
1	0.1	1000	+	+	158	+	+	130	118	127
	0.5	5000	+	+	+	+	+	+	+	+
	1.0	10000	+	+	+	+	+	+	+	+
	5.0	50000	+	+	+	+	+	+	+	+
7.5	0.1	17.78	+	+	+	+	+	155	135	149
	0.5	88.89	+	+	+	+	+	+	+	+
	1.0	177.78	+	+	+	+	+	+	+	+
	5.0	888.89	+	+	+	+	+	+	+	+
15	0.1	4.44	+	+	+	+	+	155	135	149
	0.5	22.22	+	+	+	+	+	+	+	+
	1.0	44.44	+	+	+	+	+	+	+	+
	5.0	222.22	+	+	+	+	+	+	+	+

Table 16. Bit Error Rate Trends - R = 100000 bps: "+" - Range greater than 160 *km*; "-" - Range less than 40 *km*

BER			10^{-5}				10^{-10}			
	$h(m)$		5000	7500	10000	12500	5000	7500	10000	12500
$D(cm)$	$W_A(nW)$	$P_t(nW)$								
1	0.1	1000	158	125	114	122	109	91	84	89
	0.5	5000	+	+	+	+	+	+	152	+
	1.0	10000	+	+	+	+	+	+	+	+
	5.0	50000	+	+	+	+	+	+	+	+
7.5	0.1	17.78	+	149	130	144	+	116	101	112
	0.5	88.89	+	+	+	+	+	+	+	+
	1.0	177.78	+	+	+	+	+	+	+	+
	5.0	888.89	+	+	+	+	+	+	+	+
15	0.1	4.44	+	150	130	144	+	117	101	112
	0.5	22.22	+	+	+	+	+	+	+	+
	1.0	44.44	+	+	+	+	+	+	+	+
	5.0	222.22	+	+	+	+	+	+	+	+

Table 17. Bit Error Rate Trends - R = 1000000 bps: "+" - Range greater than 160 *km*; "-" - Range less than 40 *km*

BER			10^{-5}				10^{-10}			
	$h(m)$		5000	7500	10000	12500	5000	7500	10000	12500
$D(cm)$	$W_A(nW)$	$P_t(nW)$								
1	0.1	1000	53	48	46	47	-	-	-	-
	0.5	5000	114	95	88	93	78	68	64	67
	1.0	10000	158	125	114	122	109	91	84	89
	5.0	50000	+	+	+	+	+	+	152	+
7.5	0.1	17.78	126	72	63	70	97	56	49	54
	0.5	88.89	+	120	104	115	+	93	81	89
	1.0	177.78	+	149	130	144	+	116	101	112
	5.0	888.89	+	+	+	+	+	+	+	+
15	0.1	4.44	128	73	63	70	100	56	49	54
	0.5	22.22	+	121	105	116	+	94	81	90
	1.0	44.44	+	150	130	144	+	117	101	112
	5.0	222.22	+	+	+	+	+	+	+	+

Table 18. Transmitter Powers

$P_t\ (nW)$		$W_A\ (nW)$			
		0.1	0.5	1.0	5.0
$D\ (cm)$	1	1000	5000	10000	50000
	7.5	17.78	88.89	177.78	888.89
	15	4.44	22.22	44.44	222.22

the transmitter power, P_t, by

$$W_A = P_t D_T^2$$

(where transmitter power refers to the intensity of the transmitter field incident on the transmitting aperture). Table 18 consolidates the associated transmitter powers for the effective cw transmitter output powers used to generate Tables 14 through 17.

The transmitter powers presented here are much lower than one would expect for the application at hand. Transmitter (laser) powers on the order of hundreds of milliwatts would seem more reasonable. But, again, this analysis was accomplished while only considering the losses due to propagation path length and turbulence induced phase perturbations. The SNR efficiency analysis in Section 4.2 showed that the turbulence induced phase perturbations caused the SNR efficiency to be reduced as much as 99.9 percent. If the losses due to beam steering, beam spreading, and scintillation also produced significant reductions to the SNR efficiency, plus taking into account less than ideal transmitter and receiver performance (including tracking by the receiver) as well as stronger turbulence (that is, greater C_n^2), it becomes evident that the overall efficiency of the optical communication system may decrease significantly. Thus, the transmitter power would need to be increased considerably to account for the additional losses. For example, assume the additional losses combine to reduce the efficiency by another 99.9 percent and the combined non-ideal transmitter and receiver performance (including tracking) contributes another

99.9 percent efficiency loss. The transmitter (laser) power would then need to be increased on the order of 10^4 to get similar results to those presented in Tables 14 through 17.

4.6 Summary

This chapter presented the analysis and evaluation of the SNR and BER data gathered during this study. It was shown that the SNR efficiency ranged from 0.16 to 67.2 percent for the parameters considered in this study. The behavior of the SNR efficiency factor, α, was examined with respect to altitude, path length and aperture size. As expected, α decreases with increasing path length and increasing aperture size ($D > \rho_o$), and is inversely related to the turbulence strength, C_n^2. The turbulence affected SNR was then investigated. It also exhibited the expected behavior for increasing path length (SNR decreased), aperture size (SNR saturated for $D > \rho_o$) and turbulence strength (SNR inversely related). A comparison of the C_n^2 model used for this study was compared to experimentally derived C_n^2 data from a SNR standpoint. From this comparison it was shown that the model predicts weaker turbulence than the experimentally derived data, thus the SNRs were higher for the model. Finally, the BER performance was presented with respect to data rate and path length (ranges). This analysis illustrated that BERs up to 10^{-10} could be achieved at ranges of 160 *km* under certain conditions. The final result of the BER analysis was that air-to-air optical heterodyne communication systems are feasible.

V. Conclusions and Recommendations

This chapter presents the conclusions of this research effort. Specifically, the findings of the BER feasibility study are presented. Following the conclusions, recommendations for further research are discussed.

5.1 Conclusions

The foremost question to be answered by this thesis effort was "is an air-to-air optical heterodyne communcation system feasible?". From a BER standpoint, the answer is a resounding "yes"! The analysis in Section 4.5 illustrates that (depending on the system parameters) communications can be conducted at ranges in excess of 160 km for BERs of 10^{-10} and data rates of 20 to 1000 $kbps$. Of course, even longer ranges are possible for a BER of 10^{-5}.

In addition, it was shown that aperture dimensions, D, greater than the phase coherence length, ρ_o, result in a saturation of the SNR. This saturation is approximately 4.5 dB greater than the SNR achieved when $D = \rho_o$. Therefore, the best choice for the aperture dimensions are on the order of the phase coherence length.

5.2 Recommendations

Given that air-to-air optical communication systems are feasible, the question now becomes, as discussed in Section 4.5, what transmitter (laser) powers are required to achieve these results. As discussed throughout this study, this analysis assumed nearly ideal conditions. That is, this study only considered the losses due to path length propagation and turbulence induced phase perturbations. This leads to several possible research topics in this area of air-to-air optical heterodyne communication systems.

1. Investigate the effects of additional losses on the system, to include beam steering, beam spreading, scintillation, transmitter characteristics (such as laser phase noise) and receiver characteristics (such as quantum efficiency, shot noise and tracking capability).

2. Compare this system to a direct detection system. As discussed in Chapter II, the coherent detection system performs better when turbulence is not a factor (that is, in a vacuum). How much more the turbulence degrades the coherent detection system than the direct detection system, and the overall impact on the absolute performance would better enable the Air Force in determining which system is more feasible from a cost versus performance standpoint.

3. Experientally verify the results of the research, or at least some portion of the results. This, of course, is the ideal method to proving feasibility, but also the most costly. It may be possible to verify portions of the research which, in turn, would lead to better theoretical results.

4. Investigate the use of adaptive optics schemes to compensate for the wave front tilt induced by the turbulence. Included in this effort may be an investigation into tracking techniques by the receiver.

5. Investigate the use of an array of small receivers, each on the order of the phase coherence length, as a means of increasing the efficiency of the communication system.

Appendix A. Phase Coherence Length Discussion

In this appendix, various representations for the phase coherence length are briefly discussed. Specifically, five different nomenclature and mathematical definitions used to represent the phase coherence length are presented. It is then demonstrated that each of these representations produce approximately the same values.

A.1 Phase Coherence Length Nomenclature and Definitions

In this section, the nomenclatures and mathematical definitions of five separate papers are presented: Fried (11), Lutomirski and Buser (28), Yura (37), Greenwood and Fried (21), and Wilkins (36).

Fried refers to the phase coherence length as the "efficiency saturation dimension" and denotes it r_o. He stated that, for horizontal propagation, r_o can be defined as (11:57,63)

$$r_o = (0.1089k^2 C_n^2 z)^{-3/5} \tag{70}$$

where

k = optical wave number (equal to $\frac{2\pi}{\lambda}$) (m^{-1})

z = propagation path length (m)

C_n^2 = turbulence strength $(m^{-2/3})$

Lutomirski and Buser refer to the phase coherence length as both a "turbulence-induced coherence length" (28:2153) and a "transverse coherence length" (28:2159). They denote the phase coherence length by ρ_o and define it to be (28:2157)

$$\rho_o = \left(0.5k^2 C_n^2 z\right)^{-3/5} \tag{71}$$

Yura refers to the phase coherence length, ρ_o, as "...the MCF of a point source located in the plane of observation and observed in the aperture plane" (37:1403). He then defines ρ_o for homogeneous turbulence by (37:1403)

$$\rho_o = (0.545k^2C_n^2z)^{-3/5} \tag{72}$$

Greenwood and Fried refer to the phase coherence length as "Fried's coherence length" and denote it r_o. They define r_o by (21:200)

$$r_o = \left(0.423k^2C_n^2z\right)^{-3/5} s^{-1} \tag{73}$$

where

$$s = \begin{cases} 1 & \text{for plane waves} \\ \frac{z'}{z} & \text{for spherical waves} \end{cases}$$

and where z' is defined to be an observation point along the propagation path such that $0 \leq \frac{z'}{z} \leq 1$.

Finally, Wilkins refers to the phase coherence length as the "atmospheric phase coherence length" and denotes it r_o. He also stated that r_o is known as "the diffraction limited aperture of the atmosphere" or as "Fried's parameter" (36:1). Wilkins defines r_o by the expression (36:1)

$$r_o = \left[0.423k^2 \int_0^z C_n^2(L)dL\right]^{-3/5} \tag{74}$$

where L defines the propagation path integral (m). By modeling C_n^2 using the Hufnagel model, C_n^2 is not a function of the path length z. Thus, Equation (74) can be rewritten as

$$r_o = \left(0.423k^2C_n^2z\right)^{-3/5} \tag{75}$$

which is equivalent to Equation (73) for $s = 1$.

Table 19. Phase Coherence Length Comparison Parameters

Example	$\lambda(nm)$	$C_n^2(m^{-2/3})$	$z(km)$
1	1.5	1.353×10^{-15}	40
2	830	1.625×10^{-15}	100
3	904	2.661×10^{-16}	160

Table 20. Phase Coherence Length Comparison

Example	Fried $r_o(cm)$	Lutomirski/Buser $\rho_o(cm)$	Yura $\rho_o(cm)$	Greenwood/Fried $r_o(cm)$	Wilkins $r_o(cm)$
1	7.09×10^{-4}	6.22×10^{-4}	5.91×10^{-4}	6.88×10^{-4}	6.88×10^{-4}
2	0.72	0.63	0.60	0.70	0.70
3	1.77	1.58	1.48	1.72	1.72

A.2 Phase Coherence Length Comparisons

In this section, the different phase coherence length representations are compared. It is seen that these representations all predict approximately the same values for the phase coherence length.

Table 19 presents the parameters used to determine the phase coherence lengths as defined by Equations (70) through (75). The phase coherence lengths are presented in Table 20.

Appendix B. **Signal-to-Noise Ratio for Circular Apertures**

In this appendix, the SNR for uniformly weighted, circular apertures will be developed. Starting with the general SNR equation developed in Chapter III, a Gaussian cross-correlation function will be assumed. Sum and difference variable substitutions will then be made, followed by reduction of the integral equation to a four-fold expression.

The uniformly weighted, circular aperture SNR, denoted SNR_c, is derived from the general SNR, Equation (30). Restated here for convenience, the general SNR is written

$$\begin{aligned}\frac{<S>}{NW_A} &= \frac{2}{\pi^2}\left(\frac{\eta}{e}\right)\frac{k^2}{D_R^2 D_T^2 z^2}\int\int\int\int U_A'(\underline{r}_1)\,U_A'^{*}(\underline{r}_2)\,F\left(\underline{p}_1\right)F^{*}\left(\underline{p}_2\right)\\ &\quad\times\exp\left\{\frac{ik}{2z}\left[\left|\underline{p}_1-\underline{r}_1\right|^2-\left|\underline{p}_2-\underline{r}_2\right|^2\right]\right\}\\ &\quad\times H\left(\underline{p}_1-\underline{p}_2,\underline{r}_1-\underline{r}_2\right)d^2\underline{r}_1 d^2\underline{r}_2 d^2\underline{p}_1 d^2\underline{p}_2 \qquad (76)\end{aligned}$$

where

$$U_A'(\underline{r}_1)\,U_A'^{*}(\underline{r}_2)=\frac{\pi D_T^2}{4W_A}U_A(\underline{r}_1)\,U_A^{*}(\underline{r}_2) \qquad (77)$$

and where the terms are defined in Chapter III.

For uniformly weighted, circular apertures, the complex disturbance at $\underline{r}$, $U_A(\underline{r})$, can be written

$$U_A(\underline{r})=U_o W(\underline{r}) \qquad (78)$$

and the receiver weighting factor, $F\left(\underline{p}\right)$, can be written

$$F\left(\underline{p}\right)=W\left(\underline{p}\right) \qquad (79)$$

where

$$W(\underline{x}) = \begin{cases} 1 & |\underline{x}| \leq \frac{D}{2} \\ 0 & |\underline{x}| > \frac{D}{2} \end{cases} \tag{80}$$

and where D = aperture diameter.

Recall that W_A, the normalization factor is defined to be

$$W_A = \int |U_A(\underline{r})|^2 \, d^2\underline{r} \tag{81}$$

Substituting Equations (78) and (80) into (81) then yields

$$\begin{aligned} W_A &= \int\int U_o^2 W(\underline{r}_1) W^*(\underline{r}_2) \, d\underline{r}_1 d\underline{r}_2 \\ &= \int\int_{-D_T/2}^{D_T/2} U_o^2 d\underline{r}_1 d\underline{r}_2 \\ &= U_o^2 D_T^2 \end{aligned} \tag{82}$$

where D_T = transmitter aperture diameter.

The uniformly weighted, circular aperture SNR, SNR_c, can now be written by substituting Equations (77), (78), (79) and (82) into (76):

$$\begin{aligned} SNR_c = \frac{k^2}{2\pi D_T^2 D_R^2 z^2} &\int\int\int\int W(\underline{r}_1) W(\underline{r}_2) W(\underline{p}_1) W(\underline{p}_2) \\ &\times \exp\left\{\frac{ik}{2z}\left[|\underline{p}_1 - \underline{r}_1|^2 - |\underline{p}_2 - \underline{r}_2|^2\right]\right\} \\ &\times H(\underline{p}_1 - \underline{p}_2, \underline{r}_1 - \underline{r}_2) \, d^2\underline{r}_1 d^2\underline{r}_2 d^2\underline{p}_1 d^2\underline{p}_2 \end{aligned} \tag{83}$$

To be consistent with the development of the uniformly weighted, square apertures SNR development of Chapter III, a Gaussian cross-correlation function is again assumed. Thus, SNR_c can now be written

$$
\begin{aligned}
SNR_c &= \frac{k^2}{2\pi D_T^2 D_R^2 z^2} \int\int\int\int W(\underline{r}_1)\, W(\underline{r}_2)\, W\left(\underline{p}_1\right) W\left(\underline{p}_2\right) \\
&\quad \times \exp\left\{\frac{ik}{2z}\left[\left|\underline{p}_1 - \underline{r}_1\right|^2 - \left|\underline{p}_2 - \underline{r}_2\right|^2\right]\right\} \\
&\quad \times \exp\left\{-\frac{1}{\rho_o^2}\left[\left|\left(\underline{p}_1 - \underline{p}_2\right) - \left(\underline{r}_1 - \underline{r}_2\right)\right|^2\right]\right\} d^2\underline{r}_1 d^2\underline{r}_2 d^2\underline{p}_1 d^2\underline{p}_2
\end{aligned} \tag{84}
$$

Note that $\left|\left(\underline{p}_1 - \underline{p}_2\right) - \left(\underline{r}_1 - \underline{r}_2\right)\right|^2$ can also be written $\left|\left(\underline{p}_1 - \underline{r}_1\right) - \left(\underline{p}_2 - \underline{r}_2\right)\right|^2$.

In order to reduce Equation (84), sum and difference variable substitutions are made as follows:

$$
\begin{aligned}
\underline{\Delta x}_i &= \underline{p}_i - \underline{r}_i \\
\underline{\Sigma x}_i &= \frac{1}{2}\left(\underline{p}_i + \underline{r}_i\right)
\end{aligned} \tag{85}
$$

so that

$$
\begin{aligned}
\underline{p}_i &= \underline{\Sigma x}_i + \frac{1}{2}\underline{\Delta x}_i \\
\underline{r}_i &= \underline{\Sigma x}_i - \frac{1}{2}\underline{\Delta x}_i
\end{aligned} \tag{86}
$$

Substituting Equations (85) and (86) into (84), and rearranging the integrals then yields

$$
\begin{aligned}
SNR_c &= \frac{k^2}{2\pi D_T^2 D_R^2 z^2} \int\int \exp\left\{\frac{ik}{2z}\left[\left|\underline{\Delta x}_1\right|^2 - \left|\underline{\Delta x}_2\right|^2\right]\right\} \\
&\quad \times \exp\left\{-\frac{1}{\rho^2}\left[\left|\underline{\Delta x}_1 - \underline{\Delta x}_2\right|^2\right]\right\} \\
&\quad \times \left\{\int\int W\left(\underline{\Sigma x}_1 - \frac{1}{2}\underline{\Delta x}_1\right) W\left(\underline{\Sigma x}_2 - \frac{1}{2}\underline{\Delta x}_2\right)\right. \\
&\quad \left. \times\, W\left(\underline{\Sigma x}_1 + \frac{1}{2}\underline{\Delta x}_1\right) W\left(\underline{\Sigma x}_2 + \frac{1}{2}\underline{\Delta x}_2\right) d^2\underline{\Sigma x}_1 d^2\underline{\Sigma x}_2\right\} \\
&\quad \times d^2\underline{\Delta x}_1 d^2\underline{\Delta x}_2
\end{aligned} \tag{87}
$$

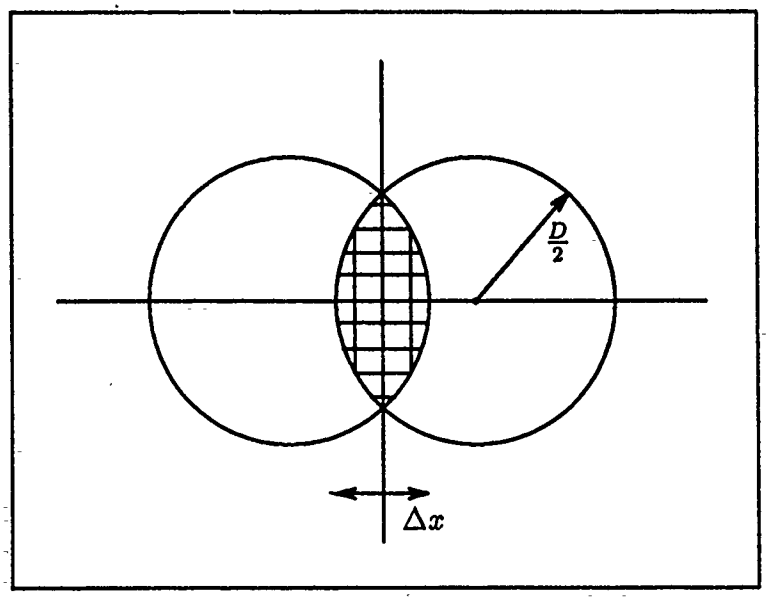

Figure 29. Circular Aperture Geometry (21:205)

Looking at the inner integrals:

$$\begin{aligned} Area &= \int W\left(\underline{\Sigma x}_1 - \frac{1}{2}\underline{\Delta x}_1\right) W\left(\underline{\Sigma x}_1 + \frac{1}{2}\underline{\Delta x}_1\right) d^2\underline{\Sigma x}_1 \\ &\quad \times \int W\left(\underline{\Sigma x}_2 - \frac{1}{2}\underline{\Delta x}_2\right) W\left(\underline{\Sigma x}_2 + \frac{1}{2}\underline{\Delta x}_2\right) d^2\underline{\Sigma x}_2 \end{aligned} \tag{88}$$

This area is illustrated in Figure 29. The limits of integration are described by the area of overlap of the circles. By defining a new variable $\mathcal{I}$ to be (21:196)

$$\mathcal{I}_i(1) = \frac{1}{A_R A_T} \int W\left(\underline{\Sigma x}_i - \frac{1}{2}\underline{\Delta x}_i\right) W\left(\underline{\Sigma x}_i + \frac{1}{2}\underline{\Delta x}_i\right) d^2\underline{\Sigma x}_i \tag{89}$$

where

A_R = area of receiver aperture

A_T = area of transmitter aperture

the inner integrals can now be written by substituting Equation (89) into (88) to yield

$$Area = A_R^2 A_T^2 \mathcal{I}_1(1)\mathcal{I}_2(1) \tag{90}$$

Greenwood solves the integral $\mathcal{I}_i$, Equation (89), with the result (21:196)

$$\mathcal{I}_i(1) = \begin{cases} \cos^{-1}(\Delta x_i/D_T) - (\Delta x_i/D_T)\left[1-(\Delta x_i/D_T)^2\right]^{1/2} & 0 \le \Delta x_i \le D_T \\ 0 & D_T \le \Delta x_i \end{cases} \tag{91}$$

Thus, Equation (88) can now be rewritten

$$\begin{aligned} Area &= \frac{4A_R^2}{\pi^2}\left\{\cos^{-1}(\Delta x_1/D_T) - (\Delta x_1/D_T)\left[1-(\Delta x_1/D_T)^2\right]^{1/2}\right\} \\ &\quad \times \left\{\cos^{-1}(\Delta x_2/D_T) - (\Delta x_2/D_T)\left[1-(\Delta x_2/D_T)^2\right]^{1/2}\right\} \end{aligned} \tag{92}$$

The final form of the uniformly weighted, circular aperture SNR can now be written by substituting Equation (92) into (87) and by making use of the relation $A_R = \pi D_R^2/4$:

$$\begin{aligned} SNR_c &= \frac{k^2 D_R^2}{8\pi D_T^2 z^2}\int\int \exp\left\{\frac{ik}{2z}\left[|\underline{\Delta x}_1|^2 - |\underline{\Delta x}_2|^2\right]\right\} \\ &\quad \times \exp\left\{-\frac{1}{\rho_o^2}\left[|\underline{\Delta x}_1 - \underline{\Delta x}_2|^2\right]\right\} \\ &\quad \times \left\{\cos^{-1}(\Delta x_1/D_T) - (\Delta x_1/D_T)\left[1-(\Delta x_1/D_T)^2\right]^{1/2}\right\} \\ &\quad \times \left\{\cos^{-1}(\Delta x_2/D_T) - (\Delta x_2/D_T)\left[1-(\Delta x_2/D_T)^2\right]^{1/2}\right\} \\ &\quad \times d^2\underline{\Delta x}_1 d^2\underline{\Delta x}_2 \end{aligned} \tag{93}$$

Note that Equation (93) can not be separated due to the cross term introduced by $\exp\left\{-\frac{1}{\rho_o^2}\left[|\underline{\Delta x}_1 - \underline{\Delta x}_2|^2\right]\right\}$.

Appendix C. Signal-to-Noise Ratio Computer Code Development

The signal-to-noise ratio (SNR) developed in Chapter III (Equation (58)) must be solved using numerical methods. This appendix details the development of the numerical methods used, the manipulation of the SNR equation into a codable format and a listing of the FORTRAN 77 computer code.

C.1 Numerical Integration Methods

The development of the numerical method to be used is based on the approach of "...adding up the value of the integrand of a sequence of abscissas within the range of integration" (31:103). Figure 30 illustrates the geometry of the approach. Mathematically, the geometry of Figure 30 can be expressed as

$$x_i = x_o + ih \tag{94}$$

$$f(x_i) \equiv f_i \tag{95}$$

where

$i = 0, 1, 2, ..., N+1$

$f(\cdot) =$ integrand

$h =$ constant step size within the abscissa sequence

A method to solve such a sequence is the trapezoidal rule. The trapezoidal rule can be written as (31:105)

$$\int_{x_1}^{x_2} f(x)dx = h\left[\frac{1}{2}f_1 + \frac{1}{2}f_2\right] + O\left(h^3 f''\right) \tag{96}$$

where

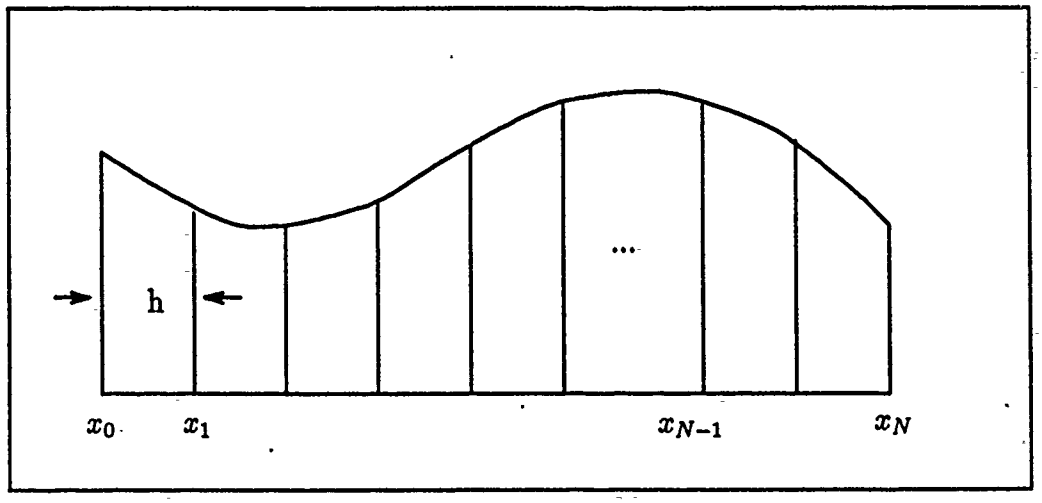

Figure 30. Numerical Integration Geometry. Numerical methods formulas with equally spaced abscissas compute the integral of a function between x_o and x_{N+1}. Closed formulas evaluate the function on the boundary points, while open formulas refrain from doing so (useful if the evaluation algorithm breaks down on the boundary points). (31:104)

f'' = second derivative of the function $f(x)$

$O(\cdot)$ = error term

The error term, $O(\cdot)$, is undetermined, otherwise the integral would be solvable in a closed form.

Equation (96) is a two-point formula. Press and others show that this can be extended to a three-point formula by use of Simpson's rule. Simpson's rule can be written (31:105)

$$\int_{x_1}^{x_3} f(x)dx = h\left[\frac{1}{3}f_1 + \frac{4}{3}f_2 + \frac{1}{3}f_3\right] + O\left(h^5 f^{(4)}\right) \tag{97}$$

Press and others further show that, by using Equation (96) $N-1$ times (that is, for each of the intervals) and adding up the results, an extended trapezoidal rule

can be obtained. The extended trapezoidal rule is written (31:107)

$$\int_{x_1}^{x_N} f(x)dx = h\left[\frac{1}{2}f_1 + f_2 + f_3 + \cdots + f_{N-1} + \frac{1}{2}f_N\right] + O\left(\frac{h^3 f''}{N^2}\right) \quad (98)$$

By applying the extended trapezoidal rule, Equation (98), to Simpson's rule, Equation (97), the extended Simpson's rule results. The extended Simpson's rule can be written (31:108)

$$\int_{x_1}^{x_N} f(x)dx = h\left[\frac{1}{3}f_1 + \frac{4}{3}f_2 + \frac{2}{3}f_3 + \frac{4}{3}f_4 + \cdots + \frac{2}{3}f_{N-2} + \frac{4}{3}f_{N-1} + \frac{1}{3}f_N\right] + O\left(\frac{1}{N^4}\right) \quad (99)$$

Press and others use the extended Simpson's rule, along with the extended trapezoidal rule, to write subroutines to calculate an integral numerically. These subroutines (QSIMP and TRAPZD) are used to numerically solve the inner integrals of the two-fold integrals of the SNR equation. The outer integrals are then solved numerically by again applying the extended Simpson's rule.

Once the SNR is calculated, the BER is determined. As discussed in Chapter III, the BER uses the complimentary error function, $Q(\cdot)$. Another form of the complimentary error function, erfc, is written

$$erfc(x) = \frac{2}{\sqrt{\pi}} \int_x^\infty exp\left(-u^2\right) du \quad (100)$$

where (34:743)

$$Q(x) = \frac{1}{2} erfc\left(\frac{x}{\sqrt{2}}\right)$$

Press and others write an erfc routine, which in turn uses other routines, which are also employed in this code. The routines are ERFC, GAMMP, GAMMQ, GAMMLN,

GSER, and GCF (31:157-164).

C.2 Signal-to-Noise Ratio Equation Manipulation into a Codable Format

The SNR equation to be modeled, Equation (58), presents itself in an easily codable format with two exceptions. The first "problem" concerns the imaginary term in the exponential:

$$\exp\left[\frac{ik}{2z}\left(\Delta x_{q1}^2 - \Delta x_{q2}^2\right)\right]$$

where q denotes either x or y. The second "problem" arises due to the nature of the three functions being integrated:

$$D - |\Delta x_{qi}|$$

$$\exp\left[\frac{ik}{2z}\left(\Delta x_{q1}^2 - \Delta x_{q2}^2\right)\right]$$

$$\exp\left[-\frac{1}{\rho^2}\left(\Delta x_{q1} - \Delta x_{q2}\right)^2\right]$$

A solution to the imaginary term "problem" is straight forward. First, separate the variable terms, then apply Euler's identities. Thus

$$\exp\left[\frac{ik}{2z}\left(\Delta x_{q1}^2 - \Delta x_{q2}^2\right)\right] = \exp\left[\frac{ik}{2z}\Delta x_{q1}^2\right]\exp\left[-\frac{ik}{2z}\Delta x_{q2}^2\right]$$

and

$$\exp\left[\pm\frac{ik}{2z}\Delta x_q^2\right] = \cos\left(\frac{k}{2z}\Delta x_q^2\right) \pm i\sin\left(\frac{k}{2z}\Delta x_q^2\right)$$

In this form, it can easily be verified that the imaginary terms cancel out since the integration limits on Δx_{q1} and Δx_{q2} are the same. The result of this manipulation is

$$\exp\left[\frac{ik}{2z}\left(\Delta x_{q1}^2 - \Delta x_{q2}^2\right)\right] \Rightarrow \cos\left(\frac{k}{2z}\Delta x_{q1}^2\right)\cos\left(\frac{k}{2z}\Delta x_{q2}^2\right) + \sin\left(\frac{k}{2z}\Delta x_{q1}^2\right)\sin\left(\frac{k}{2z}\Delta x_{q2}^2\right)$$

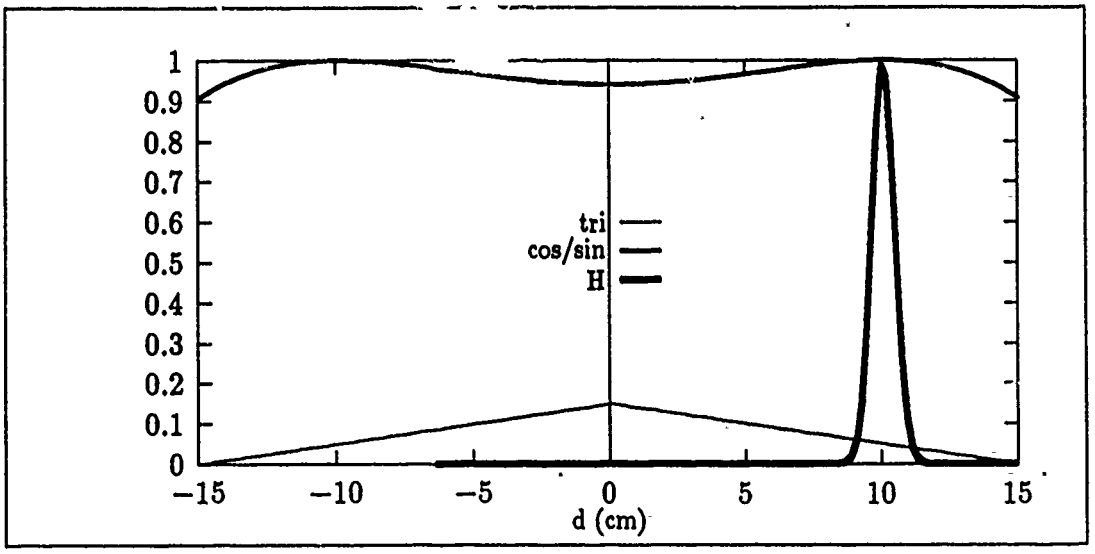

Figure 31. Integration Terms

The second problem requires an understanding of the behavior of the three terms being integrated. Figure 31 illustrates the case for $\Delta x_{q1} = 0.10$ while varying Δx_{q2} over the range of integration. For the figure, $\lambda = 904\ nm$, $z = 100\ km$ and $\rho_o = 0.6\ cm$. Note that

$$\begin{aligned} tri &\rightarrow D - |\Delta x_{q1}| \\ cos/sin &\rightarrow \cos\left(\frac{k}{2z}\Delta x_{q1}^2\right)\cos\left(\frac{k}{2z}\Delta x_{q2}^2\right) + \sin\left(\frac{k}{2z}\Delta x_{q1}^2\right)\sin\left(\frac{k}{2z}\Delta x_{q2}^2\right) \\ H &\rightarrow \exp\left[-\frac{1}{\rho_o^2}(\Delta x_{q1} - \Delta x_{q2})^2\right] \end{aligned}$$

As can be seen from Figure 31, the H term significantly limits the area of integration. To compensate for this, the limits of integration for the model are set to 5σ where σ is defined as the variance for the Gaussian function:

$$\sigma = \sqrt{\frac{\rho_o^2}{2}}$$

C.3 FORTRAN 77 Code

The following is the listing of the computer code used to determine the SNR along with the associated BER. The code is written in the FORTRAN 77 computer language.

```
C     PROGRAM: snr.f
C     AUTHOR: Capt Rebecca N. Seeger, GE-90D

C     This program calculates the Signal-to-Noise Ratio for
C     an optical heterodyne communication system in the
C     presence of atmospheric turbulence.  The only losses
C     considered are those associated with the path length
C     and those associated with the phase perturbations
C     resulting from propagation through an inhomogeneous
C     medium (i.e. turbulence).

C     This code calculates the SNR assuming both transmitter
C     and receiver are at the same altitude (> 3000 m).  The
C     SNR is run for path lengths of 40, 45, ... 160 km.

C     Variable Definitions:
C        STEP - the number of segments that the outer integral
C               is broken up into when applying Simpson's rule.
C        DIST - the number of path lengths considered.
C        IAREA# - inner integral function to be integrated
C               using the routine QSIMP.
C        S# - the value of the integration returned from QSIMP.
C        OAREA# - outer integral function to be integrated
C               using the routine INTEGRATE.
C        SO# - the value of the integration returned from
C               INTEGRATE.
C        X# - the integration variables (representing transmitter
C               and receiver square aperture dimensions).
C        LIM# - the limits of integration for the turbulence
C               affected SNR.
C        Z,Z0 - path length.
C        RHO,RHO0 - phase coherence length.
C        C - constant in front of the integrals.
C        CN2 - turbulence strength as defined by the Hufnagel
C               model.
C        CN21,CN22 - the two terms in the Hufnagel model.
C        D1 - transmitter aperture dimension.
C        D2 - receiver aperture dimension.
C        LAMBDA - wavelength.
C        ETA - quantum efficiency of the receiver.
C        K - optical wave number (equal to 2*PI/LAMBDA).
C        E - charge on an electron (equal to 1.602e-19).
```

```
C       PI - 3.14159265359
C       V - velocity of the aircraft (relative wind speed).
C       H - altitude of the aircraft.
C       SIGMA - standard deviation of the cross-correlation
C               term in the integration.  This defines the
C               limits of integration for the turbulence
C               affected SNR.
C       W - effective cw output power (or power density).
C       R - data rate.
C       SNRTRB - turbulence affected SNR for purpose of
C               determining ALPHA.  Does not contain terms
C               in common with SNRCLN.
C       SNRCLN - non-turbulence affected SNR (see above
C               with respect to SNRTRB).
C       ERROR - argument of the erfc routine used to determine
C               the BER.
C       BER - bit error rate.
C       ALPHA - ratio of SNRTRB to SNRCLN.
C       SNR - actual turbulence affected SNR.  Output
C               value is expressed as a ratio (not in dB).
C       I#,J# - do loop counters.
C       NINT,NREAL - number of integration steps used in the
C               INTEGRATE routine.
C       RESULTS - File results will be written to.

C ************************************************************

C     Variable declarations.

      INTEGER STEP, DIST
      PARAMETER (STEP=401)
      PARAMETER (DIST=25)

C     Integration variables.

      REAL IAREA1, IAREA2, S1, S2, IAREA3, IAREA4, S3, S4
      REAL OAREA1(1:STEP), OAREA2(1:STEP), OAREA(1:STEP)
      REAL OAREA3(1:STEP), OAREA4(1:STEP)
      REAL SO1, SO2, SO3, SO4, X1, X2, LIM1, LIM2

C     Constant variables.
```

```
      REAL Z(1:DIST), RHO(1:DIST), C
      REAL CN2, CN21, CN22, D1, D2, LAMBDA, ETA
      REAL Z0, RHO0, K, E, PI, V, H, SIGMA, W, R

C     Output variables.

      REAL SNRTRB(1:DIST), BER(1:DIST), ERROR
      REAL SNRCLN(1:DIST), ALPHA(1:DIST),SNR(1:DIST)

C     Other variables.

      INTEGER I1, I2, I3, J1, J2, J3, NINT
      INTEGER J4, J5
      REAL NREAL
      CHARACTER*20 RESULTS

C     Declare data, functions.

      EXTERNAL IAREA1, IAREA2, ERFC, GAMMP, GAMMQ, GAMMLN
      EXTERNAL IAREA3, IAREA4
      INTRINSIC COS, SIN, EXP, ABS, SQRT, MIN, MAX
      DATA PI/3.14159265359/, E/1.602E-19/

C     Declare common variables.
      COMMON/BLOCK1/X1,Z0,RHO0,K,D1,D2,SIGMA
      COMMON/BLOCK2/OAREA

C     Input user defined terms.

      PRINT*,'Enter results filename:'
      READ (*,'(A20)') RESULTS

      PRINT*,'Enter transmitter aperture side length in cm:'
      READ*,D1

      PRINT*,'Enter receiver aperture side length in cm:'
      READ*,D2

      PRINT*,'Enter wavelength in nm:'
      READ*,LAMBDA

      PRINT*,'Enter quantum efficiency:'
```

```
      READ*,ETA

      PRINT*,'Enter aircraft altitude in m:'
      READ*,H

      PRINT*,'Enter relative wind speed in m/s:'
      READ*,V

      PRINT*,'Enter transmitter output power in nW:'
      READ*,W

      PRINT*, 'Enter data rate in bps:'
      READ*, R

C     Calculate the remaining constants.

      D1 = D1 * 1.0E-2
      D2 = D2 * 1.0E-2

      CN21 = 8.2E-30 * (V**2) * (H**5) * (H**5) * EXP(-H/1000.0)
      CN22 = 2.7E-16 * EXP(-H/1500.0)
      CN2 = (CN21 * 1.0E-26) + CN22

      LAMBDA = LAMBDA * 1.0E-9
      K = (2.0 * PI)/LAMBDA

      C = ((K**2)*ETA)/(8.0*(PI**2)*(D2**2)*E)

      W = W * 1.0E-9

C     The SNR is calculated over the path
C     lengths between 40 and 160 km.

      DO 10 I1 = 1,DIST
            Z(I1) = (5.0 * REAL(I1-1) + 40.0) * 1.0E3
            RHO(I1) = (0.545 * (K**2) * CN2 * Z(I1))**(-0.6)
10    CONTINUE

C     Determine the SNR.

      DO 20 I2=1,DIST
            Z0 = Z(I2)
```

```
            RHO0 = RHO(I2)
            SIGMA = (5.0 * RHO0)/SQRT(2.0)
         DO 30 I3=1,STEP
            X1 = -D1+(2.0 * D1 * (REAL(I3-1)/REAL(STEP-1)))
            IF((ABS(D1-ABS(X1)).LT.1.0E-6).OR.(ABS(D2-ABS(X2)).
     +         LT.1.0E-6)) THEN
               S1 = 0.0
               S2 = 0.0
            ELSE
                 LIM1 = MAX(X1-SIGMA,X1-D2)
                 LIM2 = MIN(X1+SIGMA,X1+D2)

C               Calculate the inner integrals over X1.

               CALL QSIMP(IAREA1,LIM1,LIM2,S1)
               CALL QSIMP(IAREA2,LIM1,LIM2,S2)
               CALL QSIMP(IAREA3,-D2,D2,S3)
               CALL QSIMP(IAREA4,-D2,D2,S4)

            END IF
            OAREA1(I3) = S1*(D1-ABS(X1))*COS((K*(X1**2))/(2.0*Z0))
            OAREA2(I3) = S2*(D1-ABS(X1))*SIN((K*(X1**2))/(2.0*Z0))
            OAREA3(I3) = S3*(D1-ABS(X1))*COS((K*(X1**2))/(2.0*Z0))
            OAREA4(I3) = S4*(D1-ABS(X1))*SIN((K*(X1**2))/(2.0*Z0))
30       CONTINUE

C     Now calculate the outer integrals over X2.

      NREAL = REAL(STEP-1)/2.0
      NINT = INT(NREAL)

      DO 40 J1=1,STEP
            OAREA(J1) = OAREA1(J1)
40    CONTINUE
      CALL INTEGRATE(SO1,NINT,-D1,D1)

      DO 45 J2=1,STEP
            OAREA(J2) = OAREA2(J2)
45    CONTINUE
      CALL INTEGRATE(SO2,NINT,-D1,D1)

      DO 47 J4=1,STEP
```

```
            OAREA(J4) = OAREA3(J4)
47      CONTINUE
        CALL INTEGRATE(SO3,NINT,-D1,D1)

        DO 49 J5=1,STEP
            OAREA(J5) = OAREA4(J5)
49      CONTINUE
        CALL INTEGRATE(SO4,NINT,-D1,D1)

C       Determine the SNR values.

        SNRTRB(I2) = (SO1 + SO2)**2
        SNRCLN(I2) = (SO3 + SO4)**2
        ALPHA(I2) = SNRTRB(I2)/SNRCLN(I2)
        SNR(I2) = (W*C*SNRTRB(I2))/((Z(I2)**2)*(D1**2)*(D2**2))

20      CONTINUE

C       Determine the BER using the erfc function, then convert
C       to Q function.

        DO 50 J3=1,DIST
            ERROR = SQRT(SNR(J3)/R)
            BER(J3) = 0.5 * ERFC(ERROR)
50      CONTINUE

C       Print out the results to a user named file.

        OPEN(UNIT=20,FILE=RESULTS,STATUS='NEW',
     +      ACCESS='SEQUENTIAL',FORM='FORMATTED',
     +      ERR=1000)

        DO 72 J3=1,7
            WRITE(20,73,ERR=2000) '  '
73          FORMAT(A)
72      CONTINUE

        WRITE(20,76,ERR=2000)'D1=',D1,'D2=',D2,'LAMBDA=',LAMBDA,
     +                       'H=',H,'C=',C
76      FORMAT(7X,A,F5.3,4X,A,F5.3,4X,A,E11.4,4X,A,F8.0,4X,A,E11.4)

        WRITE(20,88,ERR=2000)'W=',W,'R=',R,'ETA=',ETA,'V=',V,'Cn2=',CN2
```

```
88      FORMAT(7X,A,E11.4,4X,A,F8.0,4X,A,F6.3,4X,A,F8.0,4X,A,E11.4)

        WRITE(20,73,ERR=2000) ' '
        WRITE(20,73,ERR=2000) ' '

        DO 60 J3=1,DIST
              WRITE(20,75,ERR=2000) 'Z=',Z(J3),'SNR(w/)=',SNRTRB(J3),
     +                        'SNR(w/o)=',SNRCLN(J3),'ALPHA=',ALPHA(J3)
     +                        ,'SNR=',SNR(J3),'BER=',BER(J3)
75            FORMAT(7X,A,F8.0,4X,A,E11.4,4X,A,E11.4,4X,A,E11.4,4X,A,
     +              E11.4,4X,A,E11.4)
60      CONTINUE

        ENDFILE 20
        CLOSE(UNIT=20,STATUS='KEEP')
        GO TO 999

1000    PRINT*,'CANNOT OPEN FILE!',ERRSIG
        GO TO 999

2000    PRINT*,'ERROR WRITING TO FILE!',ERRSIG
        GO TO 999

999     END

C       Define the inner integral functions.

        REAL FUNCTION IAREA1(X2)
        COMMON/BLOCK1/X1,Z0,RH00,K,D1,D2,SIGMA
        REAL X1,X2,Z0,RH00,D2,K
        IAREA1 = (D2-ABS(X2)) * COS((K*(X2**2))/(2.0*Z0)) *
     +          EXP((-1.0/RH00**2)*((X1-X2)**2))
        RETURN
        END


        REAL FUNCTION IAREA2(X2)
        REAL X1,X2,D2,K,Z0,RH00
        COMMON/BLOCK1/X1,Z0,RH00,K,D1,D2,SIGMA
         IAREA2 = (D2-ABS(X2)) * SIN((K*(X2**2))/(2.0*Z0)) *
     +           EXP((-1.0/RH00**2)*((X1-X2)**2))
        RETURN
```

```
      END

      REAL FUNCTION IAREA3(X2)
      REAL X2,D2,K,Z0
      COMMON/BLOCK1/X1,Z0,RH00,K,D1,D2,SIGMA
       IAREA3=(D2-ABS(X2))*COS((K*(X2**2))/(2.0*Z0))
      RETURN
      END

      REAL FUNCTION IAREA4(X2)
      REAL X2,D2,K,Z0
      COMMON/BLOCK1/X1,Z0,RH00,K,D1,D2,SIGMA
       IAREA4=(D2-ABS(X2))*SIN((K*(X2**2))/(2.0*Z0))
      RETURN
      END

C     Outer integral routines.

      SUBROUTINE INTEGRATE(AREA,N,A,B)
      COMMON/BLOCK2/OAREA
      REAL AREA, A, B, H1, OAREA(1001)
      INTEGER N, IFACTOR, L
      H1 = (B-A)/(2.0 * REAL(N))
      IFACTOR = 4
      AREA = 0.0
      DO 50 L=2,2*N
            AREA = AREA + REAL(IFACTOR) * OAREA(L)
            IFACTOR = 8/IFACTOR
50    CONTINUE

      AREA = AREA + OAREA(1)
      AREA = AREA + OAREA(2*N+1)
      AREA = AREA * (H1/3.0)

      RETURN
      END

C     Inner integral routines.

      SUBROUTINE QSIMP(FUNC,A,B,S)
      PARAMETER (EPS=5.E-3, JMAX=20)
      OST=-1.E30
```

```
      OS= -1.E30
      DO 11 J=1,JMAX
        CALL TRAPZD(FUNC,A,B,ST,J)
        S=(4.*ST-OST)/3.
        IF (ABS(S-OS).LT.EPS*ABS(OS)) RETURN
        OS=S
        OST=ST
11    CONTINUE
      PAUSE 'Too many steps.'
      END


      SUBROUTINE TRAPZD(FUNC,A,B,S,N)
      IF (N.EQ.1) THEN
        S=0.5*(B-A)*(FUNC(A)+FUNC(B))
        IT=1
      ELSE
        TNM=IT
        DEL=(B-A)/TNM
        X=A+0.5*DEL
        SUM=0.
        DO 11 J=1,IT
          SUM=SUM+FUNC(X)
          X=X+DEL
11      CONTINUE
        S=0.5*(S+(B-A)*SUM/TNM)
        IT=2*IT
      ENDIF
      RETURN
      END

C     BER routines.

      FUNCTION ERFC(X)
      IF(X.LT.0.)THEN
        ERFC=1.+GAMMP(.5,X**2)
      ELSE
        ERFC=GAMMQ(.5,X**2)
      ENDIF
      RETURN
      END
```

```
      FUNCTION GAMMP(A,X)
      IF(X.LT.0..OR.A.LE.0.)PAUSE
      IF(X.LT.A+1.)THEN
        CALL GSER(GAMSER,A,X,GLN)
        GAMMP=GAMSER
      ELSE
        CALL GCF(GAMMCF,A,X,GLN)
        GAMMP=1.-GAMMCF
      ENDIF
      RETURN
      END

      FUNCTION GAMMQ(A,X)
      IF(X.LT.0..OR.A.LE.0.)PAUSE
      IF(X.LT.A+1.)THEN
        CALL GSER(GAMSER,A,X,GLN)
        GAMMQ=1.-GAMSER
      ELSE
        CALL GCF(GAMMCF,A,X,GLN)
        GAMMQ=GAMMCF
      ENDIF
      RETURN
      END

      FUNCTION GAMMLN(XX)
      REAL*8 COF(6),STP,HALF,ONE,FPF,X,TMP,SER
      DATA COF,STP/76.18009173D0,-86.50532033D0,24.01409822D0,
     *    -1.231739516D0,.120858003D-2,-.536382D-5,2.50662827465D0/
      DATA HALF,ONE,FPF/0.5D0,1.0D0,5.5D0/
      X=XX-ONE
      TMP=X+FPF
      TMP=(X+HALF)*LOG(TMP)-TMP
      SER=ONE
      DO 11 J=1,6
        X=X+ONE
        SER=SER+COF(J)/X
11    CONTINUE
      GAMMLN=TMP+LOG(STP*SER)
      RETURN
      END

      SUBROUTINE GCF(GAMMCF,A,X,GLN)
```

```
      PARAMETER (ITMAX=100,EPS=3.E-7)
      GLN=GAMMLN(A)
      GOLD=0.
      A0=1.
      A1=X
      B0=0.
      B1=1.
      FAC=1.
      DO 11 N=1,ITMAX
        AN=FLOAT(N)
        ANA=AN-A
        A0=(A1+A0*ANA)*FAC
        B0=(B1+B0*ANA)*FAC
        ANF=AN*FAC
        A1=X*A0+ANF*A1
        B1=X*B0+ANF*B1
        IF(A1.NE.0.)THEN
          FAC=1./A1
          G=B1*FAC
          IF(ABS((G-GOLD)/G).LT.EPS)GO TO 1
          GOLD=G
        ENDIF
11    CONTINUE
      PAUSE 'A too large, ITMAX too small'
1     GAMMCF=EXP(-X+A*ALOG(X)-GLN)*G
      RETURN
      END

      SUBROUTINE GSER(GAMSER,A,X,GLN)
      PARAMETER (ITMAX=100,EPS=3.E-7)
      GLN=GAMMLN(A)
      IF(X.LE.0.)THEN
        IF(X.LT.0.)PAUSE
        GAMSER=0.
        RETURN
      ENDIF
      AP=A
      SUM=1./A
      DEL=SUM
      DO 11 N=1,ITMAX
        AP=AP+1.
        DEL=DEL*X/AP
```

```
        SUM=SUM+DEL
        IF(ABS(DEL).LT.ABS(SUM)*EPS)GO TO 1
11    CONTINUE
      PAUSE 'A too large, ITMAX too small'
1     GAMSER=SUM*EXP(-X+A*LOG(X)-GLN)
      RETURN
      END
```

Bibliography

1. Barakat, Richard and James W. Beletic. "Influence of atmospherically induced random wave fronts on diffraction imagery: a computer simulation model for testing image reconstruction algorithms," *Journal of the Optical Society of America, A, Vol 7, No4:* 653-671 (April 1990).
2. Brookner, Eli. "Atmospheric Propagation and Communication Channel Model for Laser Wavelengths," *IEEE Transactions on Communication Technology, Com-18, No 4:* 396-416 (August 1970).
3. Chase, David M. "Power Loss in Propagation Through a Turbulent Medium for an Optical-Heterodyne System with Angle Tracking," *Journal of the Optical Society of America, Vol 6, No 1:* 33-44 (January 1966).
4. Chen, C.C. and C.S. Gardner. *Comparison of Direct and Heterodyne Detection Optical Intersatellite Communication Links.* PhD dissertation. University of Illinois at Urbana-Champaign, Urbana IL, March 1987 (EOSL No. 87-002).
5. Chen, Chien-Chung. "Performance Analysis of a Noncoherently Combined Large Aperture Optical Heterodyne Receiver," *IEEE Transactions on Communications, Vol 38, No 7:* 1013-1021 (July 1990).
6. Churnside, James H. and Steven F. Clifford. "Log-normal Rician probability-density function of optical scintillations in the turbulent atmosphere," *Journal of the Optical Society of America, Vol 4, No 10:* 1923-1930 (October 1987).
7. Churnside, James H. and R.G. Frehlich. "Experimental evaluation of log-normally modulated Rician and IK models of optical scintillation in the atmosphere," *Journal of the Optical Society of America, Vol 6, No 11:* 1760-1766 (November 1989).
8. Clifford, S.F. "The Classical Theory of Wave Propagation in a Turbulent Medium," *Topics in Applied Physics, Vol 25: Laser Beam Propagation in the Atmosphere,* edited by J.W. Strohbehn. New York: Springer-Verlag, 1978.
9. Davis, J.I. "Consideration of Atmospheric Turbulence in Laser Systems Design," *Applied Optics, Vol 5, No 1:* 139-147 (January 1966).
10. Feldmann, Robert J. *Airborne Laser Communications Scintillation Measurements.* MS thesis, AFIT/GEO/ENG/87J-2. School of Engineering, Air Force Institute of Technology (AU), Wright-Patterson AFB OH, June 1987 (AD-B113375L).
11. Fried, David L. "Optical Heterodyne Detection of an Atmospherically Distorted Signal Wave Front," *Proceedings of the IEEE, Vol 55, No 1:* 57-67 (January 1967).

12. Fried, David L. "Optical Resolution Through a Randomly Inhomogeneous Medium for Very Long and Very Short Exposures," *Journal of the Optical Society of America, Vol 56 , No 10:* 1372-1379 (October 1966).

13. Fried, David L. "Statistics of a Geometric Representation of Wavefront Distortion," *Journal of the Optical Society of America, Vol 55, No 11:* 1427-1435 (November 1965).

14. Gagliardi, Robert M. *Satellite Communications.* London: Lifetime Learning Publications, 1984.

15. Gagliardi, Robert M. and Sherman Karp. *Optical Communications.* New York: John Wiley and Sons, 1976.

16. Gardner, Chester S. and Robert L. Gallawa. "Optical Communications," *Reference Data for Engineers: Radio, Electronics, Computer, and Communications, 7th Ed.* Indianapolis: SAMS, 1985.

17. Goodman, Joseph W. *Introduction to Fourier Optics.* San Francisco: McGraw-Hill Book Company, 1968.

18. Goodman, Joseph W. *Statistical Optics.* New York: John Wiley and Sons, 1985.

19. Gowar, John. *Optical Communication Systems.* London: Prentice/Hall International, 1984.

20. Gradshteyn, I.S. and I.M. Ryzhik. *Tables of Integrals, Series, and Products: Corrected and Enlarged Edition,* prepared by Alan Jeffrey. San Diego: Harcourt Brace Jovanovich, Publishers, 1980.

21. Greenwood, Darryl P. and David L. Fried. "Power spectral requirements for wavefront-compensative systems," *Journal of the Optical Society of America, Vol 66, No 3:* 193-206 (March 1976).

22. GTE Government Systems Corporation. *HAVE LACE: Final Report for Period January 1984 - March 1986.* Report No. AFWAL-TR-86-1102. GTE Government Systems Corporation, Western Division, 2 December 1986.

23. The Infrared Information and Analysis (ARIA) Center. *The Infrared Handbook.* Edited by William L. Wolfe and George J. Zissis. Environmental Research Institute of Michigan for the Office of Naval Research, Dept of the Navy, Washington DC, 1978.

24. Kanavos, Jay N. *The Effects of Atmospheric Turbulence on an Air-to-Air Optical Communication Link.* MS thesis, AFIT/GE/ENG/84D-38. School of Engineering, Air Force Institute of Technology (AU), Wright-Patterson AFB OH, December 1984 (AD-A151840).

25. Kazovsky, Leonid G. "Coherent Optical Receivers: Performance Analysis and Laser Linewidth Requirements," *Proceedings of SPIE's 29th Annual International Technical Symposium, Paper 568-05:* August 1985.

26. Linke, Richard A. "Optical Heterodyne Communications Systems," *IEEE Communications Magazine:* 36-41 (October 1989).

27. Lukin, V.P. and V.V. Pokasov. "Optical Wave Phase Fluctuations," *Applied Optics, Vol 20, No 1:* 121-135 (1 January 1981).

28. Lutomirski, R.F. and R.G. Buser. "Mutual Coherence Function of a Finite Optical Beam and Application to Coherent Detection," *Applied Optics, Vol 12, No 9:* 2153-2160 (September 1973).

29. Lutomirski, R.F. and H.T. Yura. "Wave Structure Function and Mutual Coherence Function of an Optical Wave in a Turbulent Atmosphere," *Journal of the Optical Society of America, Vol 61, No 4:* 482-487 (April 1971).

30. Personick, Stewart D. "Fundamental Limits in Optical Communication," *Proceedings of the IEEE, Vol 69, No 2:* 262-266 (February 1981).

31. Press, William H. and others. *Numerical Recipes: The Art of Scientific Computing.* Cambridge, United Kingdom: Cambridge University Press, 1986.

32. Salz, J. "Modulation and Detection of Coherent Lightwave Communications," *IEEE Communications Magazine, Vol 24, No 6:* 38-49 (June 1986).

33. Senior, John M. *Optical Fiber Communications: Principles and Practices.* London: Prentice/Hall International, 1985.

34. Sklar, Bernard. *Digital Communications: Fundamentals and Applications.* Englewood Cliffs NJ, 1988.

35. Tatarski, V.I. *Wave Propagation in a Turbulent Medium,* translated by R.A. Silverman. New York: McGraw- Hill Book Company, Inc., 1961.

36. Wilkins, Gary D. *Measurement of the Atmospheric Phase Coherence Length, r_o: In-House Report,* Report Number RADC-TR-86-192. Rome Air Development Center, Griffiss AFB NY, December 1986.

37. Yura, H.T. "Mutual Coherence Function of a Finite Cross Section Optical Beam Propagating in a Turbulent Medium," *Applied Optics, Vol 11, No 6:* 1399-1406 (June 1972).

REPORT DOCUMENTATION PAGE

Form Approved
OMB No. 0704-0188

1. AGENCY USE ONLY (Leave blank)	2. REPORT DATE	3. REPORT TYPE AND DATES COVERED
	December 1990	*Master's Thesis*

4. TITLE AND SUBTITLE
Characterization of an Air-to-Air Optical Heterodyne Communication System

5. FUNDING NUMBERS

6. AUTHOR(S)
Rebecca N. Seeger, Capt, USAF

7. PERFORMING ORGANIZATION NAME(S) AND ADDRESS(ES)
Air Force Institute of Technology, WPAFB OH 45433-6583

8. PERFORMING ORGANIZATION REPORT NUMBER
AFIT/GE/ENG/90D-55

9. SPONSORING/MONITORING AGENCY NAME(S) AND ADDRESS(ES)
Robert J. Feldmann WRDC/AAAI-2 WPAFB, OH 513-255-3455

10. SPONSORING/MONITORING AGENCY REPORT NUMBER

11. SUPPLEMENTARY NOTES

12a. DISTRIBUTION/AVAILABILITY STATEMENT
Approved for Public Release; Distribution Unlimited.

12b. DISTRIBUTION CODE

13. ABSTRACT *(Maximum 200 words)*

The primary goal of this research was to determine the feasibility of air-to-air optical communication systems using coherent detection in a turbulent environment. Secondary goals were to determine (1) the signal-to-noise ratio (SNR) degradation due to turbulence and (2) the effect of varying the wavelength (1.5, 830, 904 nm), altitude (5000-12500 m), path length (40-160 km) and aperture side length (1-15 cm) on the turbulence affected SNR. The research was conducted under the following assumptions: (1) ideal transmitter and receiver, (2) equally sized, uniformly weighted, square transmitter and receiver apertures, (3) ideal tracking by the receiver, and (4) zero losses due to beam steering, beam spreading and scintillation. It was shown that the SNR efficiency (defined as the ratio of the turbulence affected SNR to the non-turbulence affected SNR) ranged from 0.16 to 67.2 percent. The 67.2 percent efficiency was achieved for a wavelength of 904 nm, path length of 40 km, altitude of 5000 m and aperture side length of 1 cm. The feasibility analysis showed that, depending on the transmitter power and data rate, path lengths in excess of 160 km could be achieved for bit error rates of both 10^{-5} and 10^{-10}.

14. SUBJECT TERMS
Optical Communications, Atmospheric Turbulence, Optical Coherent Detection

15. NUMBER OF PAGES
124

16. PRICE CODE

17. SECURITY CLASSIFICATION OF REPORT	18. SECURITY CLASSIFICATION OF THIS PAGE	19. SECURITY CLASSIFICATION OF ABSTRACT	20. LIMITATION OF ABSTRACT
UNCLASSIFIED	UNCLASSIFIED	UNCLASSIFIED	UL